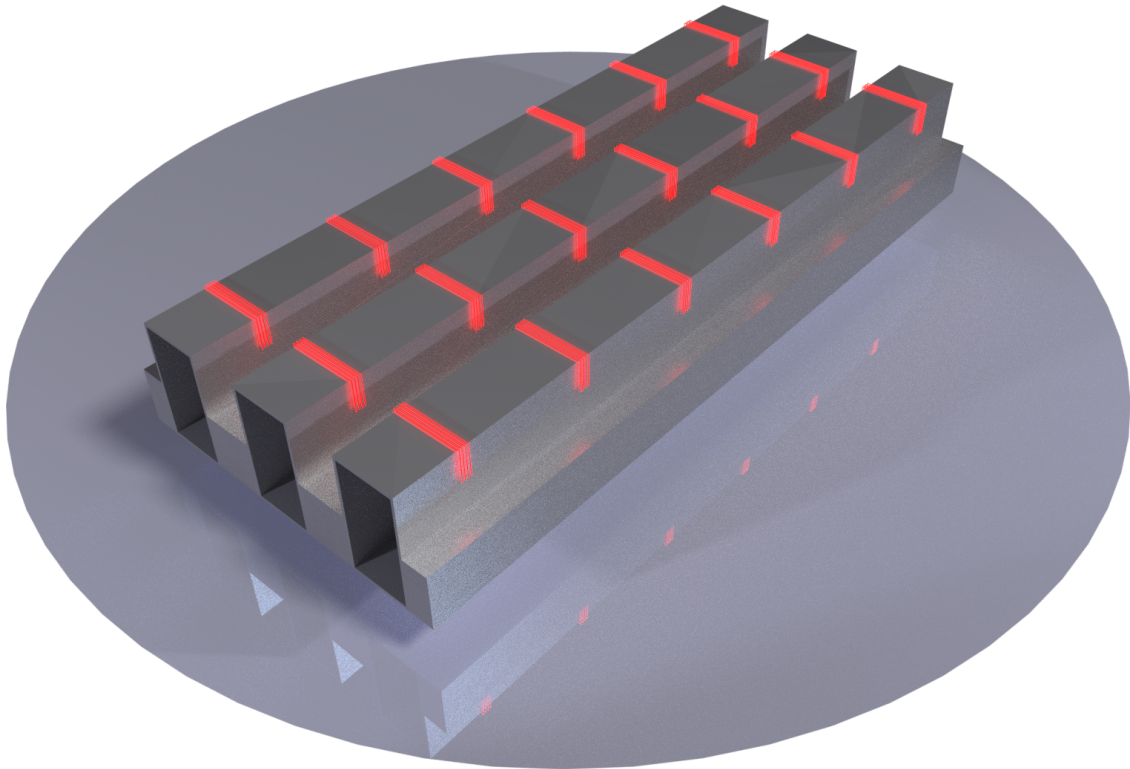




CHALMERS
UNIVERSITY OF TECHNOLOGY



Hybrid Synthesis Method for Narrow Wall Waveguide Arrays

Master's thesis in Wireless, Photonics, and Space Engineering

ERIK SILFVERSWÄRD

MASTER'S THESIS EX081/2017

Hybrid Synthesis Method for Narrow Wall Waveguide Arrays

ERIK SILFVERSWÄRD



Department of Electrical Engineering
Division of Communication and Antenna Systems
Antenna Systems Group
CHALMERS UNIVERSITY OF TECHNOLOGY
Gothenburg, Sweden 2017

Hybrid Synthesis Method for Narrow Wall Waveguide Arrays
ERIK SILFVERSWÄRD

© ERIK SILFVERSWÄRD, 2017.

Supervisor: Johan Wettergren, RUAG Space AB
Examiner: Marianna Ivashina, Department of Signals and Systems

Master's Thesis EX081/2017
Department of Electrical Engineering
Division of Communication and Antenna Systems
Antenna Systems Group
Chalmers University of Technology
SE-412 96 Gothenburg
Telephone +46 31 772 1000

Cover: Example of a Slotted Waveguide Array with Slots Replaced by Equivalent Magnetic Currents.

Typeset in L^AT_EX
Gothenburg, Sweden 2017

Hybrid Synthesis Method for Narrow Wall Waveguide Arrays
ERIK SILFVERSWÄRD
Department of Electrical Engineering
Chalmers University of Technology

Abstract

A novel design method for waveguide slot array antennas is presented. Through the use of domain decomposition and mode matching, a methodology for transferring the simulation problem from full-wave electromagnetic simulations to circuit domain is presented whilst minimizing the number of complete antenna simulations needed.

The method is based on the assumption that the exterior of the antenna does not change, allowing for separation of the complete problem into smaller, individually solvable, problems. The complete solution may then be reconstructed through clever combination of the individual solutions. The assumption that all slots have the same field distribution is made. It is shown that this has small influence on the resulting designs.

Two proofs-of-concept are also presented, implementing the methodology on a linear uniform array of six elements. The elements consist of narrow wall slots on a single rectangular waveguide of dimensions 40 mm x 20 mm, excited by irises on either side of the slots with $\lambda_{wg}/2$ element spacing. It is shown that the theory in this thesis can both predict the waves within, and excitations of, a slotted waveguide as well as optimize a design for a Taylor excitation mask.

Keywords: Waveguide Slot Array Antenna, Domain Decomposition, Mode Matching, Hybrid Antenna Synthesis.

Acknowledgements

I would like to express great appreciation to Dr Johan Wettergren, my supervisor at RUAG SPACE for his constructive feedback to my work and for his assistance of keeping me on the right path. I also wish to gratefully thank Dr Robert Nyquist for being an invaluable sounding board and providing guidance and encouragement through the whole process.

Further, I wish to thank my examiner Professor Marianna Ivashina for her guidance and feedback during my work. I would also like to offer thanks to Per Magnusson for his valuable insights in slotted waveguide antennas. Finally I would like to express my gratitude to ANSYS for providing me with a license to their software ANSYS HFSS for the duration of my thesis.

Erik Silfverswård, Gothenburg, June 2017

Contents

Nomenclature	xi
1 Introduction	1
1.1 Existing Methods	2
2 Background Theory	5
2.1 Maxwell's Equations	5
2.1.1 Boundary Conditions	6
2.2 Waves in Rectangular Waveguides	7
2.3 Mode Matching	9
2.4 Surface Equivalence Theorem	10
2.5 Green's Function	11
2.6 Reflection From a Single Slot in an Infinite Wave-Guide	13
2.7 Radiation Pattern From an Arbitrary Slot in an Infinite Ground Plane	15
2.8 Equivalent RF Circuit of a Slotted Waveguide	17
2.8.1 Equivalent Circuit of N Cascaded Shunts	17
2.8.2 Equivalent Circuit of a General Cascade	18
3 Method Derivation	21
3.1 Domain Decomposition	21
3.1.1 Single Mode Analysis	24
3.1.2 Boundary Conditions	25
3.2 Coupling Between Ports and Slots	26
3.2.1 Proof of Reciprocity	28
3.3 Scattering Parameters of a Single Waveguide Section	30
3.3.1 Transmission Parameters from Scattering Parameters	33
4 Practical work	35
4.1 Slot Excitation	35
4.1.1 Slot Geometry	37
4.1.2 Selecting Iris Parameters	37
4.2 Verifying Assumptions	38
4.2.1 Single Mode at Slot Interface	38
4.2.1.1 Inner Excitation	45
4.2.1.2 Exterior Excitation	46
4.2.2 Single mode in WG between each III domain	53

5	Implementation	57
5.1	Suggested Implementation of Theory	57
5.1.1	Calculating Equation Components in HFSS	58
5.1.1.1	Interior Components	58
5.1.1.2	Exterior Components	59
5.1.2	Reducing Simulation Requirements	60
6	Proof-of-Concept	63
7	Conclusion	71
	Bibliography	73
A	Scattering Parameters	I
A.1	S-Parameters	I
A.2	T-Parameters	II
A.3	Generalized S- and T-Parameters	III

Nomenclature

EM Electromagnetic.

HFSS High Frequency Electromagnetic Field Simulation (originally High Frequency Structural Simulator), a full wave electromagnetic solver by ANSYS. Uses an implementation of the Finite Element Method and adaptive meshing to efficiently finding full field solutions.

MATLAB Matrix Laboratory, a numerical computation software and programming language developed and maintained by Mathworks.

PEC Perfect Electric Conductor, characterized by having an infinite conductivity and thus no electric field within.

RF Radio Frequency, typically when the wavelength of the signals are on the same scale as the dimensions of the structures considered.

S-parameters Wave scattering parameters, a method of representing an N-port's behaviour at a single frequency point. Relate the wave amplitudes leaving each port to those incident on each port when all ports are perfectly matched.

T-parameters Transfer parameters, closely related to the S-parameters, however relate a 2-port's wave amplitudes at one port of to those at the other. Used to efficiently calculate the waves along an RF network of cascaded 2-ports.

TE Transverse Electric, a class of electromagnetic wave modes where the electric field only lies in the plane transverse to the direction of propagation.

Waveguide Structure for guiding electromagnetic waves, typically constructed from low loss metals. Experiences low loss and has a high power capacity. Very common method in RF technology to transferring high power signals with minimal loss and distortion.

1

Introduction

Array antennas are widely used today in a wide variety of applications, including but not limited to, radar, telecommunications, and satellite remote imaging. Their popularity is based mostly in their high level of customizability, simple steering equations, and lack of moving parts, making them powerful and versatile devices. Array antennas use the superposition of radiating fields from several elements (typically identical) to design more advanced far field patterns. By controlling the amplitude and phase of each element's radiation, the far field pattern may be controlled without the need to redesign the actual radiating element. However, having multiple elements leads to complications when designing antennas. Factors such as grating lobes and coupling between elements must be taken into account, complicating the design process.

Waveguide slot arrays are especially attractive for use in radar and imaging systems due their low loss, flat design, and relatively simple and cheap manufacturing process. They do however experience fairly high levels of coupling between elements and additional coupling internally along shared waveguides.

Although the selection of amplitudes and phases of an array's elements are easily found^[1-4], the design of the elements' feeding is not. The coupling effects of the antenna hinders each element to be considered and designed independently. Since each element's radiating field excites other elements as well as change their apparent active admittance, a perturbation of excitation in one element leads to a change in all other element excitations. These changes in turn further affect other elements, creating a domino effect. This makes for a complicated linked system where all elements must be evaluated at the same time. Since array antennas are typically both electrically large and have finely detailed parts, simulating such a design using full wave electromagnetic solvers is often expensive both in regard to time and computational resources^[5]. Robust and quick design tools are always desired within the industry in order to efficiently and accurately evaluate multiple designs iterations in an optimization process.

This master's thesis derives and describes a hybrid method which, through the use of domain decomposition, allows for moving the problem of finding the waves and excitations in a waveguide array from its full wave electromagnetic expression to an equivalent RF network circuit problem. This is done under the assumptions that each slot element's position is fixed and that the fields within them maintain the same distribution and only vary in terms of amplitude and phase. Moving the

simulation from a full wave solver to an RF circuit problem allows for six orders of magnitude faster evaluation. This is especially useful in an optimization process as a large number of iterations are typically required to be evaluated.

The method consists of first splitting the outer and inner domains of the problem followed by further splitting the inner domain into similar unit cells. If the relations of the waves in each adjacent domain is known, each domain may be solved independently and the solutions combined to yield the full solution. As will be shown in this thesis, these relations can be constructed similar to the *Transfer Parameters* used in RF circuit theory. A suggested implementation of this is to initially solve the exterior problem and construct a library of solved interior unit cells by full wave simulations. Then, an antenna consisting of any combination of such unit cells may be quickly simulated in RF circuit domain by reconstruction of the existing solutions. The building of such a library is costly, but the solutions therein may be re-used for any antenna evaluation, reducing the repeatable cost considerably.

Through use of the methodology presented in this master's thesis, each costly full wave solution in an optimization problem may be replaced by a quicker, equivalent, RF circuit evaluation. The run-time of such an optimization may then be reduced to a fraction of its original time as each iteration may be evaluated six orders of magnitude faster.

The thesis first presents some background theory in regard to electromagnetic waves in antennas and the necessary mathematical tools. Second, the methodology's supporting theory is derived for a single mode waveguide and the equations for relating the waves within, and excitations of the antenna are presented. Third, the practical work done in this thesis is presented; selection of slot design, verification of assumptions, and implementation of theory in ANSYS HFSS. Finally, as a proof of concept, the methodology is implemented in a 1x6 slotted waveguide array using ANSYS HFSS and MATLAB to show both its validity and utility in antenna optimization.

1.1 Existing Methods

There exists many examples of methods for solving the complex problem of array element design such that a specific excitation is achieved. Examples of methods for reducing computational requirements or complexity include omitting mutual coupling of elements^[6], only considering the mutual coupling to the nearest neighbouring elements^[7], or assuming uniform infinite arrays^[8].

This master's thesis focuses on the use of the domain decomposition method to separate the complex problem of designing slotted waveguide array elements into smaller, individually solvable, problems. The individual solutions are then such that they may be recombined to accurately form the full solution to the original problem without additional simulations and minimal loss of information.

Enjiu et al.^[9] presented a method for narrow wall slotted waveguide array element

optimization by initial collection of excitation and admittance values for multiple element designs. Simulations were performed assuming the full array used identical elements. The recorded values were then used to select each element design such that an excitation mask and total admittance were achieved.

The domain decomposition method is a common tool for solving many large problems in electromagnetic in order to reduce computational resources. Li et al.^[10] present the method's use for iteratively simulating the electrically large body of a plane in multiple, smaller, domains such that the full solution is yielded from the combination of each sub-domain's solution. Ozgun and Kuzuoglu^[11] show how, through clever use of perfectly matched layers (PML), the domain decomposition method may be implemented non-iteratively for certain geometries. This method is used to reduce the computational requirements for the calculations of large radar cross sections (RCS).

Similarly, the mode matching method may be used to separate domains when asserting that the amplitudes of all (or all significant) modes are equal on either side of an interface. Kim and Eom^[12] presented a method of modelling a single broad side slot in a waveguide through use of mode matching to separate and individually solve the slotted waveguide constituents. Expanding the single slot solution to a full array, ignoring mutual coupling, a full array was evaluated quickly whilst remaining computationally inexpensive.

The method presented herein uses a semi-analytic non-iterative domain decomposition method, using mode matching, allowing for separation of and subsequent easily solved sub-domains. After an initial collection of such solutions, they may be recombined for quick and inexpensive evaluations of waveguide array antennas. No assumptions are made regarding antenna geometry other than that the interfaces between array section may be expanded in a single mode. When exploring existing methods, no such hybrid-method which allows for fast and accurate computation whilst still considering the full coupling effects was found.

2

Background Theory

The theory presented in this chapter includes a quick presentation of Maxwell's equations, their use in waveguide theory, and the additional mathematical tools which will be used throughout this thesis. Further, the radiation pattern of a general slot in an infinite ground plane as well as the scattering due to a general slot in a cylindrical waveguide¹ are presented. These simplified cases give insight to the inner workings in a slotted waveguide antenna and will find analogies in the final theory.

2.1 Maxwell's Equations

Most electromagnetic phenomena can be described through the use of Maxwell's equations, named after James Clerk Maxwell (1831-1879). The equations built upon the work of Gauss, Ampere and Faraday, discoverers of Gauss' Law, Ampere's Law and Faraday's Law, respectively. Maxwell collated their work into one grand theory and connected them by the addition of the electric displacement current, \mathbb{D} ^[13].

Maxwell's equations can be written in both their differential and integral forms as^[1]

Differential Form	Integral Form
$\nabla \times \mathbb{E} = -\mathbb{M}_i - \frac{\partial \mathbb{B}}{\partial t}$	$\oint_{\delta S} \mathbb{E} \cdot d\mathbf{l} = - \iint_S \mathbb{M}_i \cdot d\mathbf{s} - \frac{\partial}{\partial t} \iint_S \mathbb{B} \cdot d\mathbf{s} \quad (2.1a)$

$\nabla \times \mathbb{H} = \mathbb{J}_i - \frac{\partial \mathbb{D}}{\partial t}$	$\oint_{\delta S} \mathbb{H} \cdot d\mathbf{l} = \iint_S \mathbb{J}_i \cdot d\mathbf{s} + \frac{\partial}{\partial t} \iint_S \mathbb{D} \cdot d\mathbf{s} \quad (2.1b)$
--	--

$\nabla \cdot \mathbb{D} = q_e$	$\oiint_S \mathbb{D} \cdot d\mathbf{s} = \iiint_V q_e \quad (2.1c)$
---------------------------------	---

$\nabla \cdot \mathbb{B} = q_m$	$\oiint_S \mathbb{B} \cdot d\mathbf{s} = \iiint_V q_m \quad (2.1d)$
---------------------------------	---

where \mathbb{E} (V/m) is the electric field intensity, \mathbb{H} (A/m) is the magnetic field intensity, \mathbb{B} (Wb/m²) is the magnetic flux density, \mathbb{D} (C/m²) is the electric flux density, \mathbb{M}_i (V/m²) is the impressed magnetic current density, \mathbb{J}_i (A/m²) is the impressed electric current density, q_e (C/m³) is the electric charge density, and q_m (Wb/m³) is the magnetic charge density.

¹A cylindrical waveguide is a waveguide with a general, uniform cross section.

The magnetic current \mathbb{M} and magnetic charge q_m are fictitious sources with powerful mathematical uses (which will be used in this thesis) but no proven base in reality. They are typically added to Maxwell's equation for the sake of completeness. Maxwell's equations originally did not include these sources.

The field intensities are related to the corresponding flux densities, which for linear, isotropic media can be written as^[13]

$$\mathbb{D} = \epsilon \mathbb{E} \quad (2.2a)$$

$$\mathbb{H} = \mu \mathbb{B} \quad (2.2b)$$

where ϵ (F/m) is the permittivity and μ (H/m) is the permeability of the media. ϵ and μ may in turn be written in terms of the free space parameters $\epsilon_0 = 8.854 \times 10^{-12}$ F/m and $\mu_0 = 4\pi \times 10^{-7}$ H/m as^[13]

$$\epsilon = \epsilon_r \epsilon_0$$

$$\mu = \mu_r \mu_0$$

where in free-space clearly $\epsilon_r = \mu_r = 1$. ϵ and μ are related to the speed of light in the medium as $c = \frac{1}{\sqrt{\mu\epsilon}}$.

Through combination, equations (2.1a) and (2.1b) can be used to form the wave equation (Helmholtz Equation). For lossless and source free media it may be stated as

$$\nabla^2 \mathbf{u} = k^2 \frac{\partial^2 \mathbf{u}}{\partial t^2} \quad (2.4)$$

where $k = \omega \sqrt{\mu\epsilon}$ is the wave number, ω is the angular frequency of the wave and \mathbf{u} is either \mathbb{E} or \mathbb{H} ^[13].

2.1.1 Boundary Conditions

The boundary conditions of Maxwell's Equations may be derived by considering either a closed loop or a pillbox on the boundary of two media. By applying equation (2.1a) or equation (2.1b) on the closed loop and taking the limit when the loop only lies along the boundary, the boundary conditions for the tangential components of the \mathbb{E} and \mathbb{H} -fields can be derived, respectively. Analogously the boundary conditions for the normal components of the \mathbb{E} and \mathbb{H} -fields can be derived by instead applying equation (2.1c) or equation (2.1d) on the pillbox and taking the limit when it lies solely on the interface of the two media. The resulting boundary conditions are^[13]

$$\hat{\mathbf{n}} \times (\mathbb{E}_2 - \mathbb{E}_1) = -\mathbb{M}_i \quad (2.5a)$$

$$\hat{\mathbf{n}} \times (\mathbb{H}_2 - \mathbb{H}_1) = \mathbb{J}_i \quad (2.5b)$$

$$\hat{\mathbf{n}} \cdot (\mathbb{D}_2 - \mathbb{D}_1) = q_e \quad (2.5c)$$

$$\hat{\mathbf{n}} \cdot (\mathbb{B}_2 - \mathbb{B}_1) = q_m \quad (2.5d)$$

2.2 Waves in Rectangular Waveguides

Consider a rectangular PEC waveguide extending along the \hat{z} -axis. Further assume it is either infinitely long or perfectly matched at its ends such that only traveling waves need to be considered. The solution space to the wave equation in such a structure is expanded by its eigenmodes^[14] which come in the two varieties Transverse Electric (TE) and Transverse Magnetic (TM)^[2]. They are named as such due to the electric and magnetic mode fields only containing components transverse to the direction of propagation, respectively. The TE and TM eigenmodes traveling in the positive \hat{z} direction may be written in phasor form as^[13]

$$\mathbf{e}(x,y) = [\hat{x}e_x(x,y) + \hat{y}e_y(x,y) + \hat{z}e_z(x,y)] \quad (2.6a)$$

$$\mathbf{h}(x,y) = [\hat{x}h_x(x,y) + \hat{y}h_y(x,y) + \hat{z}h_z(x,y)] \quad (2.6b)$$

where each component can be written as^[2]

$$\left. \begin{aligned} e_x &= -\frac{\omega\mu n\pi}{k_c^2 b} \cos \frac{m\pi x}{a} \sin \frac{n\pi y}{b} \\ e_y &= \frac{\omega\mu m\pi}{k_c^2 a} \sin \frac{m\pi x}{a} \cos \frac{n\pi y}{b} \\ e_z &= 0 \\ h_x &= -\frac{\beta m\pi}{k_c^2 a} \sin \frac{m\pi x}{a} \cos \frac{n\pi y}{b} \\ h_y &= -\frac{\beta n\pi}{k_c^2 b} \cos \frac{m\pi x}{a} \sin \frac{n\pi y}{b} \\ h_z &= j \cos \frac{m\pi x}{a} \cos \frac{n\pi y}{b} \end{aligned} \right\} \text{TE}_{m,n} \quad (2.7a)$$

for TE waves, and similarly

$$\left. \begin{aligned} e_x &= \frac{\beta m\pi}{k_c^2 a} \cos \frac{m\pi x}{a} \sin \frac{n\pi y}{b} \\ e_y &= \frac{\beta n\pi}{k_c^2 b} \sin \frac{m\pi x}{a} \cos \frac{n\pi y}{b} \\ e_z &= j \sin \frac{m\pi x}{a} \sin \frac{n\pi y}{b} \\ h_x &= -\frac{\omega\epsilon n\pi}{k_c^2 b} \sin \frac{m\pi x}{a} \cos \frac{n\pi y}{b} \\ h_y &= \frac{\omega\epsilon m\pi}{k_c^2 a} \cos \frac{m\pi x}{a} \sin \frac{n\pi y}{b} \\ h_z &= 0 \end{aligned} \right\} \text{TM}_{m,n} \quad (2.7b)$$

for TM waves. Here, m and n are the mode numbers, a and b are the waveguide dimensions along \hat{x} and \hat{y} , $\beta = \sqrt{k^2 - k_c^2}$ is the propagation constant, and $k_c = \sqrt{\left(\frac{m\pi}{a}\right)^2 + \left(\frac{n\pi}{b}\right)^2}$ is the cut-off wave number where $\pm\beta > 0$ for waves traveling along the $\pm\hat{z}$ direction, respectively^[13]. If β is real, the wave propagates along the

2. Background Theory

waveguide and if it is imaginary, it does not and is called an evanescent wave. Although evanescent waves do not propagate, they still retain reactive electromagnetic energy in a localized neighborhood and therefore cannot be ignored when considering the fields in waveguides^[13]. Note that there exists infinitely many eigenmode expansions as any expansion can be recombined or re-scaled to yield another full expansion of the solution space.

Expanding the fields of a general cylindrical waveguide in a set of eigenmodes traveling along the waveguide, the total electric and magnetic fields may be written as

$$\mathbb{E}(x,y,z) = \sum_{i=0}^{\infty} \mathbf{e}_i(x,y)(E_i^+ e^{-j\beta z} + E_i^- e^{j\beta z}) \quad (2.8a)$$

$$\mathbb{H}(x,y,z) = \sum_{i=0}^{\infty} \mathbf{h}_i(x,y)(H_i^+ e^{-j\beta z} + H_i^- e^{j\beta z}) \quad (2.8b)$$

where $\{\mathbf{e}_i, \mathbf{h}_i\}$ are the eigenmodes with index i taken over all m,n for both TE and TM modes. E_i^\pm, H_i^\pm are then the respective amplitudes of the forward and backward traveling waves for each eigenmode.

The transverse components of the electric and magnetic waves are related by the wave impedance Z_{wave} of the waveguide mode as^[13]

$$\mathbb{H}_\perp = \frac{1}{Z_{wave}} \hat{\mathbf{n}} \times \mathbb{E}_\perp \quad (2.9)$$

where $\hat{\mathbf{n}}$ is the direction of travel for the wave. Which for waves E^\pm and H^\pm traveling in the positive and negative directions

$$Z_{wave} = \frac{E^+}{H^+} = -\frac{E^-}{H^-} \quad (2.10)$$

respectively. Note that the change in sign means that reflection coefficients change sign for electric and magnetic waves, or $\Gamma = \frac{E^+}{E^-} = -\frac{H^+}{H^-}$. In a rectangular waveguide the wave impedance is known analytically as

$$Z_{wave} = \begin{cases} \frac{k}{\beta} \eta & \text{if wave is TE}_{m,n} \\ \frac{\beta}{k} \eta & \text{if wave is TM}_{m,n} \end{cases} \quad (2.11)$$

where $\eta = \sqrt{\frac{\mu}{\epsilon}}$ is the intrinsic impedance of the waveguide medium.^[13]

Further, the waves in a waveguide

$$\mathbb{E}_i(x,y,z) = E_i^\pm \mathbf{e}(x,y) e^{\mp j\beta z} = E_i^\pm [\hat{\mathbf{x}}e_x(x,y) + \hat{\mathbf{y}}e_y(x,y) + \hat{\mathbf{z}}e_z(x,y)] e^{\mp j\beta z} \quad (2.12a)$$

$$\mathbb{H}_i(x,y,z) = H_i^\pm \mathbf{h}(x,y) e^{\mp j\beta z} = H_i^\pm [\hat{\mathbf{x}}h_x(x,y) + \hat{\mathbf{y}}h_y(x,y) + \hat{\mathbf{z}}h_z(x,y)] e^{\mp j\beta z} \quad (2.12b)$$

are orthogonal with respect to mode number and type av wave due to the general orthogonality of integrated sinusoids. This may be written as^[2]

$$\iint_S (\mathbb{E}_i \times \mathbb{H}_j) \cdot d\mathbf{s} = \begin{cases} S_i & i = j \\ 0 & \text{Otherwise} \end{cases} \quad (2.13)$$

where S_i is the Poynting vector integrated over the waveguide cross-section S for the mode and i is again taken over all modes of both TE and TM waves. S_i can be interpreted as the rate of energy flow through the cross section of the waveguide.

Furthermore, for a source free region of a general cylindrical waveguide bounded by the closed surface S

$$\iint_S (\mathbb{E}_1 \times \mathbb{H}_2 - \mathbb{E}_2 \times \mathbb{H}_1) \cdot d\mathbf{s} = 0 \quad (2.14)$$

for two electromagnetic fields $(\mathbb{E}_1, \mathbb{H}_1)$ and $(\mathbb{E}_2, \mathbb{H}_2)$ and is a corollary to the reciprocity theorem^[3].

2.3 Mode Matching

Mode matching is a method which allows for adjacent sections of a waveguide to be considered separately with the addition a boundary condition on the shared cross-section. The method builds upon the fact that any field within a waveguide may be described as a linear expansion of its eigenmodes and may be written according to equation (2.8). Moreover, the space of eigenmodes is orthogonal according to equation (2.13), that is^[14]

$$\iint_S \mathbf{e}_i(x,y) \cdot \mathbf{e}_j(x,y) dx dy = \begin{cases} \iint_S \|\mathbf{e}_i\|^2 dr & \text{if } i = j \\ 0 & \text{otherwise} \end{cases} \quad (2.15)$$

where $\{\mathbf{e}_i\}$ is the set of eigenmodes, i, j are the mode numbers taken over all modes of both TE and TM waves, and S is the cross-section of the waveguide.

Consider the two sides of a cross-section, the electric field must remain the same on both sides if the media is homogeneous in the waveguide. Using equation (2.8), this can be written as

$$\sum_{i=0}^{\infty} \mathbf{e}_i(x,y)(E_i^{1+}e^{j\beta z} + E_i^{1-}e^{-j\beta z}) = \sum_{i=0}^{\infty} \mathbf{e}_i(x,y)(E_i^{2+}e^{j\beta z} + E_i^{2-}e^{-j\beta z}) \quad (2.16)$$

where 1 and 2 denotes which side of the cross-section is considered. If the waveguide is uniform and both eigenmode sets are the same, then due to the orthogonality of the eigenmodes each mode can be considered independently^[14] and equation (2.16) becomes

$$E_i^{1+} = E_i^{2+} \quad (2.17a)$$

$$E_i^{1-} = E_i^{2-} \quad (2.17b)$$

or equivalently for the magnetic modes

$$H_i^{1+} = H_i^{2+} \quad (2.18a)$$

$$H_i^{1-} = H_i^{2-} \quad (2.18b)$$

for all i .

Thus any uniform section of a waveguide may be split and each side solved independently while considering the interface a perfectly matched port. As long as the boundary conditions in equation (2.17) or equation (2.18) hold, the wave solution on either side is equivalent to the original wave solution. Note that the use of S-parameters and T-parameters uses mode matching as they consider only a single mode where all ports are perfectly matched.

2.4 Surface Equivalence Theorem

Originally introduced by Schelkunoff^[15], based on Huygens's principle, the Surface Equivalence theorem allows for the replacement of all electromagnetic sources beyond a volume of interest with surface current sources on the volume boundary such that the field inside the volume remains unchanged. The surface equivalence theorem depends on the uniqueness theorem, stated as^[1]

Theorem (Uniqueness Theorem). *A field (\mathbb{E}, \mathbb{H}) in a lossy region V , created by sources \mathbb{J} and \mathbb{M} , is unique within V when one of the following is known*

1. *The tangential component of the electric field \mathbb{E} over the entire boundary δV*
2. *The tangential component of the magnetic field \mathbb{H} over the entire boundary δV*
3. *The tangential component of \mathbb{E} over part of the boundary δV and the tangential component of \mathbb{H} over the rest of δV .*

Further, the fields in a lossless medium may be considered the limit of the fields in a lossy medium as the losses tend to zero.

According to the uniqueness theorem, the solution to Maxwell's equations in a given region V is unique for a given set of sources within the region and knowledge of the tangential components of either \mathbb{E} or \mathbb{H} over all parts of the region boundary δV . Thus it is possible to separate a problem along an imaginary surface and remove all sources from one side without perturbing the solution on the other. The requirement is to ensure that the tangential components of either the electric or magnetic field remains the same on all points of the surface boundary.

A typical utilization of the surface equivalence theorem is to completely fill a region of non-interest with PEC and place an equivalent magnetic current distribution on its boundary. The equivalent magnetic current will ensure that the tangential electric field remains unperturbed by the addition of the PEC according to equation (2.5). The solutions within the PEC will however clearly be invalid. The magnetic current is found from equation (2.5) by selecting \mathbb{E}_1 as the original electric field and noting that $\mathbb{E}_2 = 0$ inside the PEC, leading to

$$\mathbb{M} = -\hat{\mathbf{n}} \times \mathbb{E} \tag{2.19}$$

in order to fulfill the boundary condition. Since the tangential electric field is then unchanged, the uniqueness theorem says that so is the field solution within the

region of interest. Through the use of the surface equivalence theorem, problems can often be simplified immensely by cleverly selecting the boundary of the volume of interest.

Figure 2.1 demonstrates how the surface equivalence theorem may be used to replace an uninteresting region with a PEC and a magnetic current distribution. Since the magnetic current distribution is selected such that the tangential fields at the regions' interface are unaffected, the solution in the region of interest remains unchanged.

2.5 Green's Function

Green's functions are the impulse responses to inhomogeneous ordinary differential equations. Through convolution they allow for quick construction of solutions to their respective differential equation. This section gives a brief explanation of their use in electromagnetics as a full description is beyond the scope of this thesis. Moreover, only the Green's function's use in \mathfrak{R}^3 will be presented, however its use is valid in other spaces as well.

For a linear differential operator $\mathcal{L} = \mathcal{L}(\mathbf{r})$ on a subset of \mathfrak{R}^3 , the Green's function is defined via

$$\mathcal{L} \mathbb{G}(\mathbf{r}, \mathbf{r}_s) = \delta(\mathbf{r} - \mathbf{r}_s) \quad (2.20)$$

for $\mathbf{r}, \mathbf{r}_s \in \mathfrak{R}^3$, where δ is the three dimensional delta function $\delta(\mathbf{r}) = \delta(r_x)\hat{\mathbf{x}} + \delta(r_y)\hat{\mathbf{y}} + \delta(r_z)\hat{\mathbf{z}}$, $\mathbf{r} = r_x\hat{\mathbf{x}} + r_y\hat{\mathbf{y}} + r_z\hat{\mathbf{z}}$, and δ is the Dirac delta function.

Then for the partial differential equation

$$\mathcal{L} \mathbf{u} = \mathbf{f} \quad (2.21)$$

the solution \mathbf{u} may be calculated from the spatial convolution of the Green's function and \mathbf{f}

$$\mathbf{u}(\mathbf{r}) = \iiint \mathbb{G}(\mathbf{r}, \mathbf{r}_s) \mathbf{f}(\mathbf{r}_s) d\mathbf{r}_s \quad (2.22)$$

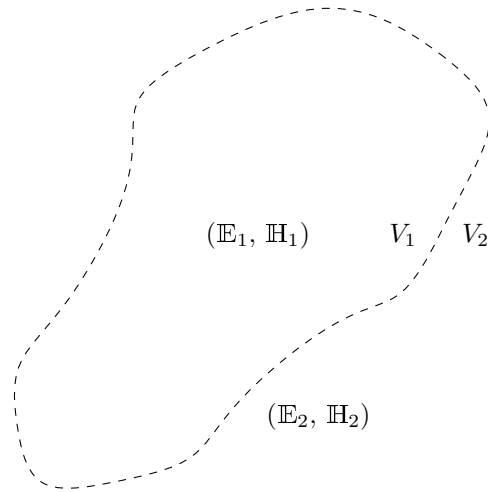
since

$$\mathcal{L} \mathbf{u}(\mathbf{r}) = \iiint \mathcal{L} \mathbb{G}(\mathbf{r}, \mathbf{r}_s) \mathbf{f}(\mathbf{r}_s) d\mathbf{r}_s = \iiint \mathbf{f}(\mathbf{r}_s) \delta(\mathbf{r} - \mathbf{r}_s) d\mathbf{r}_s = \mathbf{f}(\mathbf{r}), \quad (2.23)$$

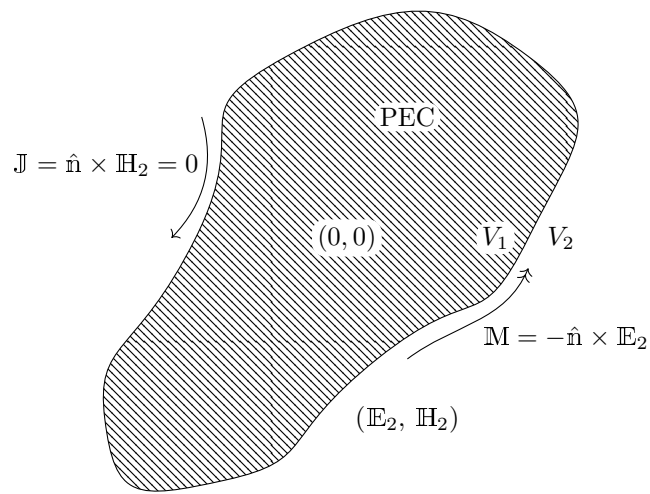
as \mathcal{L} is a linear operator acting on a function of \mathbf{r} , not of \mathbf{r}_s .^{[16][17]}

Green's functions have a lot of uses in conjunction with the differential form of Maxwell's equations (2.1). It is possible to create expressions for Green's functions relating different sources to their respective impressed fields. One Green's function of certain importance for this thesis is that relating the magnetic current distributions in a domain V to its impressed magnetic field, denoted as $\mathbb{G}_V^{[m]}$. The corresponding calculation of the magnetic field is then given by 2.22 as

$$\mathbb{H}_V(\mathbf{r}) = \iiint_V \mathbb{G}_V^{[m]}(\mathbf{r}, \mathbf{r}_s) \mathbb{M}(\mathbf{r}_s) d\mathbf{r}_s \quad (2.24)$$



(a) Actual problem



(b) Equivalent problem

Figure 2.1: Demonstration of how an uninteresting domain (V_1) may be replaced with a PEC and surface magnetic currents without disturbing the solution in the interesting domain (V_2) through use of the surface equivalence theorem.

where \mathbb{H}_V is the magnetic field in V due to the magnetic current distribution \mathbb{M} . Since this integral will be used repeatedly in this thesis, it will be denoted

$$\mathbb{H}_V = \mathbb{G}_V^{[m]}|\mathbb{M}\rangle \quad (2.25)$$

in order to increase readability.

This thesis will not explicitly derive any Green's functions. However they will be used as tools to relate sources and fields in the coming sections. Green's functions will help motivate the decomposition of the complex problems and the subsequent simulations of their parts.

2.6 Reflection From a Single Slot in an Infinite Wave-Guide

Discontinuities in a waveguide, such as slots or irises, induce scattering in incident waves. This section will derive the scattering of a general slot in the wall of a cylindrical waveguide. The result gives an insight into both how a slot is excited and how it interacts with the traveling waves of a waveguide.

Consider a cylindrical waveguide along the \hat{z} -direction. The reflections due to a slot in the waveguide will be shown by considering two waves, one induced by and traveling away from the slot in both directions, and one auxiliary wave traveling in a single direction unaffected by the slot. By considering the interaction of these two waves the scattering will be found.

Therefore, firstly let the waveguide have a slot from z_1 to z_2 , where $z_2 > z_1$. Assuming the electric field in the slot is known, let $(\mathbb{E}_1, \mathbb{H}_1)$ be the field induced into the waveguide by the field in the slot. $(\mathbb{E}_1, \mathbb{H}_1)$ will, according to equation (2.8), consist of a superposition of all eigenmodes traveling in the positive and negative \hat{z} -direction for $z > z_2$ and $z < z_1$, respectively. For $z_1 \leq z \leq z_2$ the eigenmode expansion remains unknown due to the slot. Let the amplitudes for the forward and backward traveling waves be A_i and B_i respectively, where i is again a collection of all mode numbers taken over all m, n for both TE and TM modes.

Then let the auxiliary wave $(\mathbb{E}_2, \mathbb{H}_2)$ be a normalized wave consisting only of the waveguide's eigenmodes traveling in the positive \hat{z} -direction. The eigenmode expansion according to equation (2.8) is valid in the whole waveguide as the auxiliary wave is unaffected by the slot.

Finally let S be the boundary of a generalized cylindrical section V of the waveguide which fully includes the slot. S then consists of three parts: two faces intersecting the waveguide, positioned at $z = z_3 < z_1$ (called S^-) and $z = z_4 > z_2$ (called S^+), and a cylindrical waveguide section which includes the slot (called S_{wg}). Now apply equation (2.14) to the boundary $S = S^- + S^+ + S_{wg}$.

Since \mathbb{E}_2 has no tangential components at the waveguide walls, $(\mathbb{E}_2 \times \mathbb{H}_1) \cdot \hat{n} = \mathbb{H}_1 \cdot (\hat{n} \times \mathbb{E}_2) = 0$ over all of S_{wg} . Similarly \mathbb{E}_1 is also perpendicular to all PEC

2. Background Theory

surfaces and thus $(\mathbb{E}_1 \times \mathbb{H}_2) \cdot \hat{\mathbf{m}} = 0$ over all of S_{wg} , save the portion over the slot, S_{slot} . The integrand over S_{wg} is therefore zero everywhere except over the slot where only the first part of the integrand remains.

At subsurface S^+ all waves are traveling in the same direction. According to the orthogonality property in equation (2.13) the integral (2.14) is zero unless $(\mathbb{E}_1, \mathbb{H}_1) = (\mathbb{E}_2, \mathbb{H}_2)$ in which case the integrand is zero instead. The integral over S^+ is therefore zero.

Over the final cylinder face S^- , equation (2.13) again requires the two waves to be the same mode in order to interact, however due to the waves traveling in opposite directions, the integrand in (2.14) remains non-zero for equal modes and the integral becomes $\sum_i -2B_i S_i$, where S_i is the Poynting energy flux through S^- for mode i . What is then left of the integral (2.14) is

$$\begin{aligned} \int_S (\mathbb{E}_1 \times \mathbb{H}_2 - \mathbb{E}_2 \times \mathbb{H}_1) \cdot d\mathbf{s} &= \int_{S^-} 2(\mathbb{E}_1 \times \mathbb{H}_2) \cdot d\mathbf{s} + \int_{slot} (\mathbb{E}_1 \times \mathbb{H}_2) \cdot d\mathbf{s} = 0 \\ &\Leftrightarrow \int_{slot} (\mathbb{E}_1 \times \mathbb{H}_2) \cdot d\mathbf{s} = -2 \sum_i B_i S_i \end{aligned} \quad (2.26a)$$

which now relates the energy flux through S^- to the electric field distribution in the slot. By instead letting the auxiliary wave $(\mathbb{E}_2, \mathbb{H}_2)$ travel in the opposite direction, the energy flux relation at S^+ is calculated analogously as

$$\int_{slot} (\mathbb{E}_1 \times \mathbb{H}_2) \cdot d\mathbf{s} = -2 \sum_i A_i S_i \quad (2.26b)$$

where A_i is the amplitude of forward traveling mode i of field 1.

In order to get a better understanding of the interaction between the wave in the waveguide and the field in the slot, split the wave components into their $\hat{\mathbf{z}}$ and $\hat{\mathbf{u}} = \hat{\mathbf{z}} \times \hat{\mathbf{m}}$ components. Then evaluate each mode individually and the integrals of each mode in (2.26) become

$$2B_i S_i = - \int_{slot} (e_{1u} h_{iz} - e_{1z} h_{iu}) e^{-j\beta_i z} dS \quad (2.27a)$$

$$2A_i S_i = - \int_{slot} (e_{1u} h_{iz} + e_{1z} h_{iu}) e^{j\beta_i z} dS \quad (2.27b)$$

Since $\mathbb{J} = \hat{\mathbf{m}} \times \mathbb{H}$ on a PEC surface according to equation (2.5) the magnetic fields above may be replaced by equivalent electric surface current densities $\mathbb{J} = \hat{\mathbf{m}} \times \mathbb{H}$; $-J_{iu}$ and J_{iz} for h_{iz} and h_{iu} respectively. The resulting relation between the slot field and the waveguide currents is then

$$2B_i S_i = \int_{slot} (e_{1u} J_{iu} + e_{1z} J_{iz}) e^{-j\beta_i z} dS \quad (2.28a)$$

$$2A_i S_i = \int_{slot} (e_{1u} J_{iu} - e_{1z} J_{iz}) e^{j\beta_i z} dS \quad (2.28b)$$

which may be interpreted such that a mode i will only interact with the slot if its current lines are clipped. Thus the slot will only induce scattered waves in the modes

which surface currents it cuts. Further, the amplitude of the scattered wave will be proportional to the amount of cut current lines and amplitude of the slot field.

If the phase components in equations (2.28) are either canceled due to symmetry in the slot mode or if the slot's dimensions are small enough that phase effects can be neglected two interesting cases can occur^[2]:

1. If e_{1u} or J_{iu} is zero over the slot, then $A_i = -B_i$. This indicates a continuity in \mathbb{H}_\perp and a discontinuity in \mathbb{E}_\perp at the slot, representing a *series* element in the waveguide for the i -th mode.
2. If e_{1z} or J_{iz} is zero over the slot, then $A_i = B_i$. This indicates a continuity in \mathbb{E}_\perp and a discontinuity in \mathbb{H}_\perp at the slot, representing a *shunt* element in the waveguide for the i -th mode.

An especially interesting case of this is for rectangular slots which only accommodate the TE₁₀ mode, oriented parallel or perpendicular to the waveguide axis. The field of such a slot fulfills the required symmetry by being an even function of z . If such a slot is oriented perpendicular to the waveguide, then $e_{1u} = 0$ and case (1) above applies, if however the orientation is parallel, then $e_{1z} = 0$ and case (2) applies.

For the general case $|A_i| \neq |B_i|$ the slot may instead be represented by the more general S-parameter matrix for each frequency point.

2.7 Radiation Pattern From an Arbitrary Slot in an Infinite Ground Plane

Consider an arbitrary slot in an infinite ground plane with the electric field distribution \mathbb{E}_{slot} . Let the ground plane have the normal $\hat{\mathbf{n}} = \hat{\mathbf{z}}$ and be placed at $z = 0$. Using the surface equivalence theorem, the slot may be replaced by a PEC with a magnetic current

$$\mathbb{M}_{source} = -\hat{\mathbf{n}} \times \mathbb{E}_{slot} \quad (2.29)$$

without affecting the radiation pattern of the slot. The infinite ground plane may then be removed using the imaging method. The imaging method is an implementation of the surface equivalence principle which here replaces the infinite ground plane by doubling the amplitude of \mathbb{M}_{source} . Again the radiation pattern of the slot is unaffected, however one must remember that the field solution for $z \leq 0$ is invalid due to the infinite ground plane.

After applying the Fraunhofer approximation² the radiation pattern from the single

²Valid when considering a field in the far-field, that is when the distance to the source is $\leq 2D^2/\lambda$ for D being the largest dimension of the antenna. When calculating amplitudes, the distance from an observation point \mathbf{r} to any point of the antenna \mathbf{r}_s can then be simplified as $\|\mathbf{r} - \mathbf{r}_s\| \approx |r|$. When calculating phase, the assumption $k\|\mathbf{r} - \mathbf{r}_s\| \approx k(\|\mathbf{r}\| - \|\mathbf{r}_s\|)$ is instead made.^[4]

2. Background Theory

free space magnetic current source can be described in the far-field as^[4]

$$\mathbb{E}_{rad}(\mathbf{r}) = \frac{e^{-jkr}}{r} \mathbb{G}(\mathbf{r}) = \frac{e^{-jkr}}{r} \mathbb{I}_M \times \hat{\mathbf{r}} \quad (2.30)$$

$$\mathbb{I}_M = -\frac{jk}{4\pi} \iint_S 2\mathbb{M}_{source}(\mathbf{r}_s) e^{jk(\mathbf{r}_s \cdot \hat{\mathbf{r}})} dS_s \quad (2.31)$$

where S is the slot aperture, \mathbf{r}_s is the reference vector for the integral, \mathbf{r} is the point the radiating field is evaluated at, and $\hat{\mathbf{r}} = \frac{\mathbf{r}}{|\mathbf{r}|}$ is the direction in which the radiating field is being considered. The resulting radiation field from an arbitrary slot in an infinite ground plane is then described as

$$\mathbb{E}_{rad} = \frac{jk e^{-jkr}}{2\pi r} \hat{\mathbf{r}} \times \iint_S (\mathbb{E}_{slot} \times \hat{\mathbf{n}}) e^{jk(\mathbf{r}_s \cdot \hat{\mathbf{r}})} dS_s. \quad (2.32)$$

Additional slots can be considered by simply letting S and \mathbb{E}_{slot} be over several slots. The final radiating field will however only represent the radiating field due to the given electric fields, assuming any interaction and coupling between the slots already has taken place to yield the given field distributions.

For the simple case of a flat rectangular slot with width $w \ll \lambda$ and length $l \approx \lambda/2$, only the dominant TE₁₀ mode will propagate^[4]. If the slot is centered at the origin, aligned along the $\hat{\mathbf{x}}$ -axis, and normal to $\hat{\mathbf{z}}$, its field distribution is described by

$$\mathbb{E}_{slot} = E_0 \cos\left(\frac{\pi x}{l}\right) \hat{\mathbf{y}} \quad (2.33)$$

where E_0 is the amplitude of the slot field. Equation (2.32) then becomes

$$\begin{aligned} \mathbb{E}_{rad} &= \frac{jk e^{-jkr}}{2\pi r} \hat{\mathbf{r}} \times \iint_S \hat{\mathbf{x}} E_0 \cos\left(\frac{\pi x_s}{l}\right) e^{jk(\mathbf{r}_s \cdot \hat{\mathbf{r}})} dS_s = \\ &= \frac{jk w E_0 e^{-jkr}}{2\pi r} (\hat{\mathbf{r}} \times \hat{\mathbf{x}}) \int_{-l/2}^{l/2} \cos\left(\frac{\pi x_s}{l}\right) e^{jk x_s (\hat{\mathbf{x}} \cdot \hat{\mathbf{r}})} dx_s = \\ &= \frac{jk w E_0 e^{-jkr}}{2\pi r} (\hat{\mathbf{r}} \times \hat{\mathbf{x}}) \frac{2\pi l \cos\left(\frac{kl}{2} (\hat{\mathbf{x}} \cdot \hat{\mathbf{r}})\right)}{\pi^2 - (kl (\hat{\mathbf{x}} \cdot \hat{\mathbf{r}}))^2} \end{aligned} \quad (2.34)$$

For the special case when the slot is exactly half a wavelength wide ($l = \lambda/2$), the substitutions $\hat{\mathbf{x}} \cdot \hat{\mathbf{r}} = \sin \theta \cos \phi$ and $\hat{\mathbf{r}} \times \hat{\mathbf{x}} = \sin \phi \hat{\boldsymbol{\theta}} + \cos \theta \cos \phi \hat{\boldsymbol{\phi}}$ can be used to instead yield

$$\mathbb{E}_{rad} = \frac{jw E_0 e^{-jkr}}{\pi r} \frac{\cos\left(\frac{\pi}{2} \sin \theta \cos \phi\right)}{1 - (\sin \theta \cos \phi)^2} (\sin \phi \hat{\boldsymbol{\theta}} + \cos \theta \cos \phi \hat{\boldsymbol{\phi}}) \quad (2.35)$$

Note that the radiating field is still undefined for the space below the ground plane ($z < 0$). Since the radiated power of the slot is given by^[4]

$$P_{rad} = \int_0^{2\pi} \int_0^{\pi/2} |\mathbb{G}(\theta, \phi)|^2 \sin \theta d\theta d\phi \propto V^2 \quad (2.36)$$

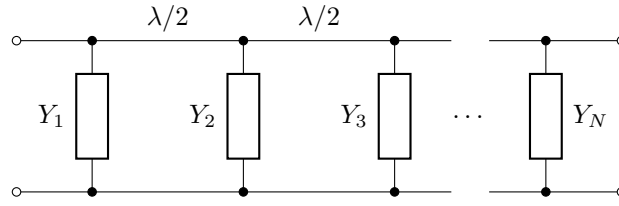


Figure 2.2: Representation of RF circuit consisting of N shunt elements, separated by $\lambda_{wg}/2$.

where V is the voltage gathered by the line integral $\int \mathbb{E} \cdot d\mathbb{l}$ along the centerline of the slot. The radiated power of the slot antenna is therefore quadratically proportional to the voltage over the slot's centerline.

Moreover, changing the excitation and depth of the slot slightly, or truncating the infinite ground plane does not affect the final field much^[4].

2.8 Equivalent RF Circuit of a Slotted Waveguide

Section 2.6 showed that certain waveguide slots may be represented by shunts or series elements, whereas the general slot is represented by its S-parameters. It is instructive to show how the voltage and current varies along a cascade of such elements in order to model a full slotted waveguide. This section first shows how to find equivalent S-parameters for N cascaded shunt elements, spaced $\lambda/2$ apart, and then for a general cascaded network.

2.8.1 Equivalent Circuit of N Cascaded Shunts

Consider N shunt loads on a transmission line equally spaced $\lambda/2$ apart as shown in figure 2.2. In order to find the equivalent load, first consider how loads transform along a lossless transmission line:^[13]

$$Z_{in}(z) = Z_0 \frac{Z_L + jZ_0 \tan(kz)}{Z_0 + jZ_L \tan(kz)} \quad (2.37a)$$

$$Y_{in}(z) = Y_0 \frac{Y_L + jY_0 \tan(kz)}{Y_0 + jY_L \tan(kz)} \quad (2.37b)$$

where Z_0 is the transmission line's intrinsic impedance, Z_L is the loads impedance, $k = \frac{2\pi}{\lambda}$ is the wavenumber, and z is distance along the transmission line to the load. Note that $Y_0 = Z_0^{-1}$ and $Y_L = Z_L^{-1}$ are the admittance counterparts to the impedances. As this example consists of shunts, only the admittance form will be used, however the work flow is valid for series elements and impedances as well.

Since the tangent function is periodic in π , Y_{in} is periodic in $z = \lambda/2$. Therefore for the $\lambda/2$ of transmission lines between each shunt element may be ignored, resulting

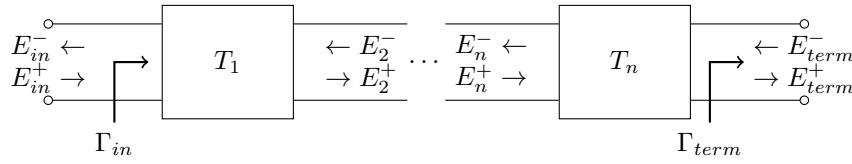


Figure 2.3: Representation of N -component cascaded RF network.

in a simple system of N shunt admittances with no separation. The N shunts may be replaced with a single equivalent shunt component with admittance^[13]

$$Y_{equiv} = \sum_{i=1}^N Y_i \quad (2.38)$$

where Y_i are the admittances of replaced shunts. The S-parameters for the single shunt element is^[13]

$$S_{equiv} = \frac{1}{2 + y_{equiv}} \begin{bmatrix} -y_{equiv} & 2 \\ 2 & -y_{equiv} \end{bmatrix} \quad (2.39)$$

where $y_{equiv} = \frac{Y_{equiv}}{Y_0}$ is the normalized equivalent shunt admittance. Note however that the voltage and current along a transmission line are periodic in λ . The off-diagonal elements of the equivalent S-matrix are therefore negative for odd N . The equivalent S-matrix for the circuit in figure 2.2 is therefore

$$S_{equiv} = \frac{1}{2 + y_{equiv}} \begin{bmatrix} -y_{equiv} & 2(-1)^N \\ 2(-1)^N & -y_{equiv} \end{bmatrix} \quad (2.40)$$

2.8.2 Equivalent Circuit of a General Cascade

For the more general slot the series or shunt representation is insufficient, however two-port S-parameters can be used to describe any slot at a single frequency point. This section considers N such slots in a cascaded network. No restriction is made in regards to the separation of the slots, however the S-parameters reference planes are chosen such that they coincide for adjacent components. Since each set of S-parameters are valid for a single frequency and mode, so are the following calculations.

Assuming N two-ports in cascade, let $[T_i]$ denote the T-parameter³ matrix for the i th component, as seen from the generator. Figure 2.3 shows a diagram of such a circuit. Each two-port component has the possibility to introduce a phase shift or discontinuity in the current and voltage, depending on its scattering parameters.

The termination at the end of the network together with the incident wave are the boundary conditions which decide the waves at each two-port interface along the

³The T-parameters of a component are easily calculated from its S-parameters, described in more detail in appendix A.

transmission line. The termination decides the relative amplitudes of the waves and the incident wave decides the final magnitudes and phases.

Maintaining the $[T]$ -matrix notation, the termination of the network takes the form

$$[T_{term}] = \begin{bmatrix} \Gamma_{term} \\ 1 \end{bmatrix} \quad (2.41)$$

with forward and backward traveling waves

$$\mathbb{E}_{term} = \begin{bmatrix} E_{term}^- \\ E_{term}^+ \end{bmatrix} = E_{term}^+ [T_{term}] \quad (2.42)$$

where Γ_{term} is the electric reflection coefficient of the circuit termination and E_{term}^\pm are the amplitudes of the electric waves traveling forward and backward, as seen from the generator, respectively. Typical terminations are short circuit ($\Gamma_{term} = -1$) and open circuit ($\Gamma_{term} = 1$), however any termination may be used.

The relation between the forward (E_i^+) and backward (E_i^-) traveling waves before each component may then be calculated through the use of the T-parameters as

$$\mathbb{E}_i = \left(\prod_{k=i}^N [T_k] \right) \mathbb{E}_{term} = [T_i][T_{i+1}] \dots [T_N] \mathbb{E}_{term} \quad (2.43)$$

allowing for calculation of the relative wave amplitudes between each component pair.

It now remains to find the absolute magnitude and phase of the wave amplitudes, due to the incident wave. At the start of the cascade, the waves traveling in either direction are

$$\mathbb{E}_{in} = E_{in}^+ \begin{bmatrix} \Gamma_{in} \\ 1 \end{bmatrix} = E_{term}^+ \left(\prod_{k=1}^N [T_k] \right) [T_{term}] = E_{term}^+ [T_{total}] \quad (2.44)$$

where $[T_{total}]$ contains the boundary condition at the termination, transformed to the input of the transmission line. If $[T_{total}] = \begin{bmatrix} T_{total}^{[1]} \\ T_{total}^{[2]} \end{bmatrix}$, it is clear that

$$E_{term}^+ = \frac{E_{in}^+}{T_{total}^{[2]}} \quad (2.45a)$$

$$\Gamma_{in} = \frac{T_{total}^{[1]}}{T_{total}^{[2]}} \quad (2.45b)$$

Thus the wave amplitudes for the electric waves traveling in each direction are known at all points from equation (2.43) and equation (2.45a), as well as the input reflection coefficient Γ_{in} from equation (2.45b).

3

Method Derivation

This chapter derives the methodology which allows for relating an RF network to a slotted waveguide antenna. The resulting equations take on a form similar to that of scattering parameters. If all the constituents of the equations are known, it becomes possible to quickly find both the wave amplitudes in the waveguide and the excitations of the slots. The derivation is performed while considering a general single mode waveguide slot antenna with constant outer geometry.

3.1 Domain Decomposition

Through the use of the surface equivalence theorem and the uniqueness theorem it is possible to take a large electromagnetic problem and split it into smaller, more manageable sub-problems through a so called domain decomposition.

First the full domain is split into canonical regions, replacing the boundaries of which with PEC and magnetic current distributions in accordance with equation (2.19). Since the domains are then separated by PEC and effectively isolated from each other, they can be considered and solved independently.

Moreover, in order to equate the independent field solutions and that of the original problem, the boundary conditions in equation (2.5) must be adapted for the magnetic current distributions in each domain. The full solution to the original problem can then be achieved by solving each domain separately and combining the results.

As an instructive example, the following section will apply domain decomposition to a simplified waveguide antenna. Figure 3.1 shows the cross section of a single waveguide antenna with three slots spaced $\lambda_{wg}/2$ apart and fed from both ends. This section will consider such a design with N slots.

First the problem is split into two canonical domains consisting of the inner and outer regions of the antenna. Secondly the inner domain is identified as a series of similar unit cells of $\lambda_{wg}/2$ length, bounded by the ports of the waveguide. Therefore three types of domain can be identified in the design as

- I The free space beyond the antenna exterior. This domain is bounded to regions Π_i by the slots in the antenna.

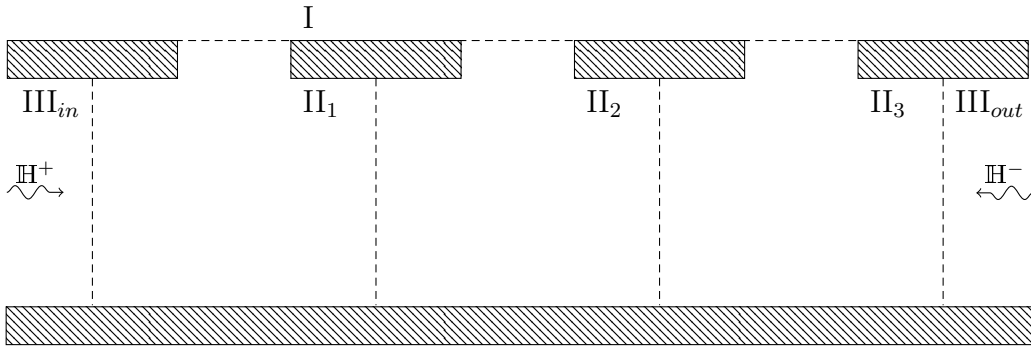


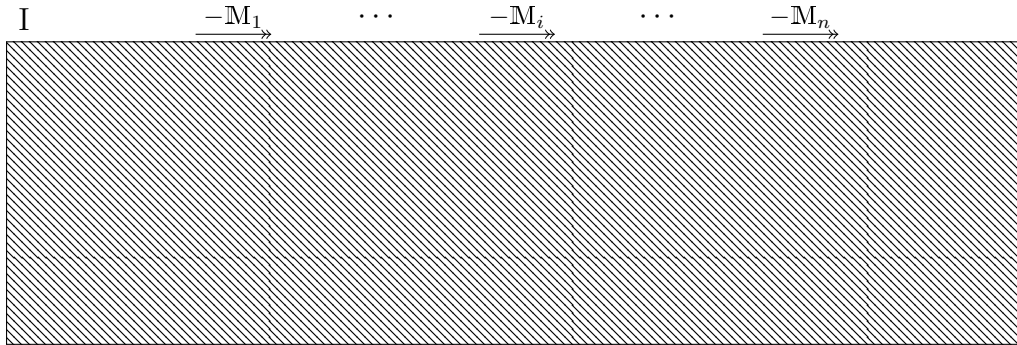
Figure 3.1: Cross section of a single waveguide antenna with three slots. Three classes of domains have been identified for decomposition.

- II_{*i*}** Each $\lambda_{wg}/2$ section of the waveguide interior, centered at each slot. These domains are cavities with the same cross-section as the original waveguide and length $\lambda_{wg}/2$. The domains are bounded to the previous and next sections II_{*i*} (or the ports III) as well as the exterior I.
- III_{*+*}(-)** The beginning (end) port of the waveguide. These domains can be seen as semi-infinite waveguides with the same cross-section as the original waveguide, bounded by the first (last) domain II_{*i*}. These domains also contain the only sources in the problem; incoming TE₁₀ waves (\mathbb{E} , \mathbb{H}), which can be considered to originate from sources infinitely far away.

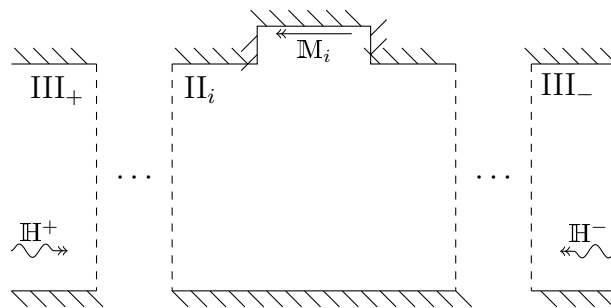
Using domain decomposition to separate the outer and inner domains, each slot is covered by a PEC with a magnetic current distribution \mathbb{M} in accordance with equation (2.19). The domains are then split apart and solved individually. Figures 3.2a and 3.2b show the two separated problems. Note that the signs of the magnetic currents change due to the normal of the respective planes pointing in opposite directions. Since the PEC perfectly shields each canonical domain, it may be assumed to fill all but the interesting region without affecting the individual solutions.

Furthermore, by implementing mode matching along the waveguide at the interface of each $\lambda_{wg}/2$ section, where the waveguide is simply a uniform rectangular waveguide, the problem may be split up further. Figure 3.2c shows one such interior section where either side is considered a perfectly matched port with incoming and outgoing waves. The ports must fulfill the boundary conditions in equation (2.18) in order to not perturb the field solution. This separation effectively isolates each domain II_{*i*}, allowing for individual solving of the field solution within.

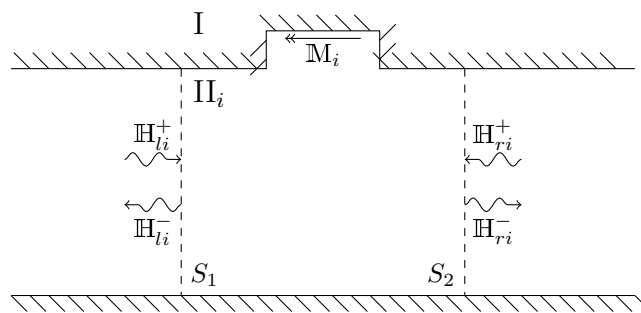
The resulting magnetic fields in domains I and II_{*i*} due to all sources may then be



(a) Domain I; the exterior of the antenna.



(b) Domains II and III; the interior of the antenna.



(c) Domain II_{*i*}; each isolated interior waveguide section.

Figure 3.2: The different domains in figure 3.1 after domain decomposition. Note that the selection of magnetic current distributions are selected to ensure that the boundary conditions between each domain is fulfilled.

calculated using Green's functions and superposition as

$$\text{I :} \quad \mathbb{H}_I = - \sum_{i=1}^N \mathbb{G}_I^{[m]} |\mathbb{M}_i\rangle \quad (3.1a)$$

$$\text{II}_i : \quad \mathbb{H}_{\text{II}_i} = \mathbb{H}_{li} + \mathbb{H}_{ri} + \mathbb{G}_{\text{II}_i}^{[m]} |\mathbb{M}_i\rangle \quad (3.1b)$$

$$\text{III}_+ : \quad \mathbb{H}_{\text{III}_+} = \mathbb{H}_{l1} \quad (3.1c)$$

$$\text{III}_- : \quad \mathbb{H}_{\text{III}_-} = \mathbb{H}_{rN} \quad (3.1d)$$

for $i = 1, \dots, N$. Here $\mathbb{G}_V^{[m]}$ is again the Green's function from magnetic current to magnetic field for domain V , and \mathbb{M}_i is the magnetic current distribution over the new PEC surface covering the slot in section i . Note that the Green's function not only depends on the shape but also the position of \mathbb{M}_i in each domain. $\mathbb{H}_{li} = \mathbb{H}_{li}^+ + \mathbb{H}_{li}^-$ and $\mathbb{H}_{ri} = \mathbb{H}_{ri}^+ + \mathbb{H}_{ri}^-$ are the resulting waves in the waveguide due to the waves incoming from the left and right port respectively.

3.1.1 Single Mode Analysis

Since the full solution space to the wave equation may be expanded by any of the infinitely many eigenmode expansions for a given geometry, then equivalently so can the corresponding magnetic current distributions, written as

$$\mathbb{M} = \sum_{k=0}^{\infty} V_k^{[m]} \mathbb{m}_k \quad (3.2)$$

where $\{\mathbb{m}_k\}$ are the unit eigenmode distributions, $V_k^{[m]}$ are their corresponding amplitudes and k is taken over all modes.

Depending on the choice of eigenmode set $\{\mathbb{m}_k\}$, equation (3.2) may be approximated by only considering the first few terms. Further, if the shape of \mathbb{M}_i in equation (3.1) only experiences minor changes for different i , the same sub-set of eigenmodes may be used to expand all the magnetic currents. Moreover, if the sub-set of eigenmodes can be reduced to a single eigenmode, many calculations can be simplified. The magnetic currents in equation (3.1) and figure 3.2 then become

$$\mathbb{M}_i = V_i^{[m]} \mathbb{m}_i \quad (3.3)$$

where \mathbb{m}_i all have the same distribution save a translation in the geometry.

Under these assumptions equation (2.25) may be rewritten according to

$$\mathbb{G}_V^{[m]} |\mathbb{M}\rangle = V^{[m]} \mathbb{G}_V^{[m]} |\mathbb{m}\rangle \quad (3.4)$$

where $\mathbb{G}_V^{[m]} |\mathbb{m}\rangle$ is a magnetic field distribution in domain V , due to the magnetic current at \mathbb{m} . Such a field does not change its distribution but only its magnitude and phase, controlled by the current amplitude $V^{[m]}$. In turn, equation (3.1) may

be rewritten as

$$\text{I :} \quad \mathbb{H}_I = - \sum_{i=0}^N V_i^{[m]} \mathbb{G}_I^{[m]} |m_i\rangle \quad (3.5a)$$

$$\text{II}_i : \quad \mathbb{H}_{\text{II}_i} = \mathbb{H}_{l_i} + \mathbb{H}_{r_i} + V_i^{[m]} \mathbb{G}_{\text{II}_i}^{[m]} |m\rangle \quad (3.5b)$$

$$\text{III}_+ : \quad \mathbb{H}_{\text{III}_+} = \mathbb{H}_{l1} \quad (3.5c)$$

$$\text{III}_- : \quad \mathbb{H}_{\text{III}_-} = \mathbb{H}_{r1} \quad (3.5d)$$

reducing the complexity of the problem immensely.

Furthermore, the incident waves ($\mathbb{H}_{l_i}^+, \mathbb{H}_{r_i}^+$) can be written in accordance with equation (2.8) at the edges of the waveguide section, S_1, S_2 . If the same single mode assumption may be made for these waves at S_1 and S_2 , the calculations can be simplified further. Assuming only the principal TE₁₀ mode exists, the waves there may be written as

$$\mathbb{H}(x, y, z) = \mathbb{h}_{10}(x, y) (H^+ e^{-j\beta z} + H^- e^{j\beta z}) \quad (3.6)$$

where H^\pm is the wave's amplitude in each traveling direction and $\mathbb{h}_{10}(x, y)$ is the TE₁₀ field distribution.

3.1.2 Boundary Conditions

In order to fulfill the boundary conditions of the electromagnetic fields, the magnetic currents must ensure that the \mathbb{H} field's tangential components are continuous between each domain in absence of surface currents. This must still be true when the interfaces between each domain are covered by PEC, which is

$$\hat{\mathbf{n}} \times \mathbb{H}_j(\mathbf{r}) = -\hat{\mathbf{n}} \times \mathbb{H}_k(\mathbf{r}) \quad (3.7a)$$

for all \mathbf{r} on the newly created PEC surface between domain j and k . The sign change is due to the normal vector $\hat{\mathbf{n}}$ changing sign on either side of the surface. If this boundary condition can be enforced, in accordance with the uniqueness theorem the solution of each isolated domain will then be equivalent to the original field solution.

To more simply represent this point-wise boundary condition, the field at each slot may be integrated over. Then by comparing the integrals, the point-wise equivalence becomes a scalar equivalence. Moreover, by using Galerkin's method, symmetries arise which can be used to simplify calculations further. Galerkin's method is performed by weighting the integral with the unit mode of the slot itself^[18]. It may be expressed as

$$\langle m_i | \mathbb{G}_V^{[m]} | m_j \rangle = \iiint_{S_i} m_i(\mathbf{r}) \cdot \iiint_{S_j} \mathbb{G}_V^{[m]}(\mathbf{r}, \mathbf{r}_s) m_j(\mathbf{r}_s) d\mathbf{r}_s d\mathbf{r} \quad (3.8)$$

where m_i is the unit field over slot i and S_i is the PEC surface replacing slot i . For linear, isotropic media, the dyadic is symmetric with reference to \mathbf{r} and \mathbf{r}_s as^[19]

$$\mathbb{G}^{[m]}(\mathbf{r}, \mathbf{r}_s) = \mathbb{G}^{[m]}(|\mathbf{r}_s - \mathbf{r}|) = \mathbb{G}^{[m]}(\mathbf{r}_s, \mathbf{r}) \quad (3.9)$$

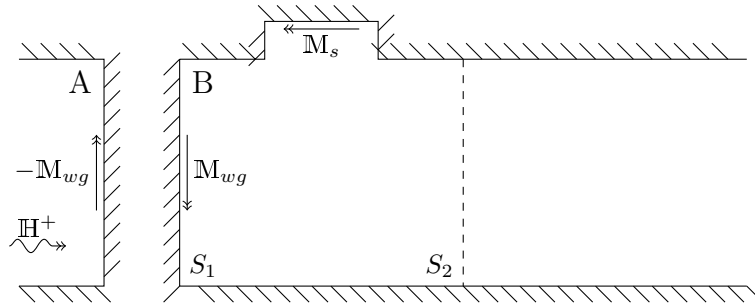


Figure 3.3: A second domain decomposition of domain II_i in figure 3.2c

and therefore so are the weighted integrals in equation (3.8), leading to the equivalence

$$\langle \mathbf{m}_i | \mathbf{G}_V^{[m]} | \mathbf{m}_j \rangle = \langle \mathbf{m}_j | \mathbf{G}_V^{[m]} | \mathbf{m}_i \rangle \quad (3.10)$$

This is often referred to as the reciprocity of electromagnetic fields.

When evaluating a field over a surface, Galerkin's method may again be used, in this thesis it will be written according to

$$\langle \mathbf{m} | \mathbb{H} \rangle = \iint_S \mathbf{m} \cdot \mathbb{H} \, d\mathbf{r} \quad (3.11)$$

where S is again the surface upon which \mathbf{m} is defined.

The requirement of having a continuous tangential field along at the new PEC surfaces after the domain decomposition yields the following boundary condition between the outer domain I and the inner waveguide sections II_i :

$$-\sum_{j=0}^N V_j^{[m]} \langle \mathbf{m}_i | \mathbf{G}_I^{[m]} | \mathbf{m}_j \rangle = V_i^{[m]} \langle \mathbf{m}_i | \mathbf{G}_{\text{II}_i}^{[m]} | \mathbf{m}_i \rangle + \langle \mathbf{m}_i | \mathbb{H}_{li} \rangle + \langle \mathbf{m}_i | \mathbb{H}_{ri} \rangle \quad (3.12)$$

which can be simplified by identifying the admittance of port i in domain V as $Y_i^V = -\langle \mathbf{m}_i | \mathbf{G}_V^{[m]} | \mathbf{m}_i \rangle$, yielding

$$V_i^{[m]} Y_i^I - \sum_{j \neq i} V_j^{[m]} \langle \mathbf{m}_i | \mathbf{G}_I^{[m]} | \mathbf{m}_j \rangle = \langle \mathbf{m}_i | \mathbb{H}_{li} \rangle + \langle \mathbf{m}_i | \mathbb{H}_{ri} \rangle - V_i^{[m]} Y_i^{\text{II}_i} \quad (3.13)$$

3.2 Coupling Between Ports and Slots

In order to find the relation between the waves in the waveguide and the excitation of the slot, a second domain decomposition is performed at S_1 in figure 3.2c. The resulting domains are (A) a semi-infinite waveguide and (B) the waveguide section II_i attached to another semi-infinite waveguide, see figure 3.3. For this section the index i is dropped temporarily to increase readability.

The magnetic field in each domain is then

$$\text{A :} \quad \mathbb{H}_A = \mathbb{H}^+ - \Gamma \mathbb{H}^+ - V_{wg}^{[m]} \mathbb{G}_A^{[m]} | \mathbb{m}_{wg} \rangle \quad (3.14a)$$

$$\text{B :} \quad \mathbb{H}_B = V_{wg}^{[m]} \mathbb{G}_B^{[m]} | \mathbb{m}_{wg} \rangle + V_s^{[m]} \mathbb{G}_B^{[m]} | \mathbb{m}_s \rangle \quad (3.14b)$$

where $\Gamma = \Gamma(l) = \frac{\mathbb{E}^-(l)}{\mathbb{E}^+(l)} = -e^{-2j\beta l}$ is the electric reflection coefficient of the new PEC in domain A at distance l along the waveguide^[13], and \mathbb{m}_{wg} and \mathbb{m}_s are the equivalent magnetic currents in the waveguide and over the slot, respectively. Furthermore the single mode assumption has again been made such that $\mathbb{G}^{[m]} | \mathbb{M}_j \rangle = V_j^{[m]} \mathbb{G}^{[m]} | \mathbb{m}_j \rangle$.

The boundary condition, $-\hat{\mathbf{n}} \times \mathbb{H}_A = \hat{\mathbf{n}} \times \mathbb{H}_B \quad \forall \mathbf{r} \in S_1$, of the domain decomposition may be written as

$$\begin{aligned} \langle \mathbb{m}_{wg} | \mathbb{H}^+ \rangle (1 - \Gamma(0)) - V_{wg}^{[m]} \langle \mathbb{m}_{wg} | \mathbb{G}_A^{[m]} | \mathbb{m}_{wg} \rangle = \\ V_{wg}^{[m]} \langle \mathbb{m}_{wg} | \mathbb{G}_B^{[m]} | \mathbb{m}_{wg} \rangle + V_s^{[m]} \langle \mathbb{m}_{wg} | \mathbb{G}_B^{[m]} | \mathbb{m}_s \rangle \end{aligned} \quad (3.15)$$

where again Galerkin's method has been used. $V_{wg}^{[m]}$ may then be found through reordering as

$$V_{wg}^{[m]} = \frac{V_s^{[m]} \langle \mathbb{m}_{wg} | \mathbb{G}_B^{[m]} | \mathbb{m}_s \rangle - 2 \langle \mathbb{m}_{wg} | \mathbb{H}^+ \rangle}{Y_{wg}^A + Y_{wg}^B} \quad (3.16)$$

where $\Gamma(0) = -1$ has been used and the admittances in the different domains have again been identified.

The field over the new PEC at S_1 is then calculated by inserting equation (3.16) into equation (3.14) and applying Galerkin's method, yielding

$$\begin{aligned} \langle \mathbb{m}_{wg} | \mathbb{H}_A \rangle = 2 \langle \mathbb{m}_{wg} | \mathbb{H}^+ \rangle + V_{wg}^{[m]} Y_{wg}^A = \\ \langle \mathbb{m}_{wg} | \mathbb{H}^+ \rangle \frac{2Y_{wg}^B}{Y_{wg}^A + Y_{wg}^B} + V_s^{[m]} \frac{\langle \mathbb{m}_{wg} | \mathbb{G}_B^{[m]} | \mathbb{m}_s \rangle Y_{wg}^A}{Y_{wg}^A + Y_{wg}^B} \end{aligned} \quad (3.17)$$

which can easily be shown equals $\langle \mathbb{m}_{wg} | \mathbb{H}_B \rangle$. The outgoing wave in domain A, that is everything save the incoming wave \mathbb{H}^+ , evaluated at S_1 and weighted by \mathbb{m}_{wg} is then

$$\begin{aligned} \langle \mathbb{m}_{wg} | \mathbb{H}^- \rangle = \langle \mathbb{m}_{wg} | \mathbb{H}_A \rangle - \langle \mathbb{m}_{wg} | \mathbb{H}^+ \rangle = \\ - \langle \mathbb{m}_{wg} | \mathbb{H}^+ \rangle \frac{Y_{wg}^A + \Gamma Y_{wg}^B}{Y_{wg}^A + Y_{wg}^B} + V_s^{[m]} \frac{\langle \mathbb{m}_{wg} | \mathbb{G}_B^{[m]} | \mathbb{m}_s \rangle Y_{wg}^A}{Y_{wg}^A + Y_{wg}^B} \end{aligned} \quad (3.18)$$

Analogously the field over the PEC covering the slot can be calculated as

$$\begin{aligned} \langle \mathbb{m}_s | \mathbb{H}_B \rangle = V_{wg}^{[m]} \langle \mathbb{m}_s | \mathbb{G}_B^{[m]} | \mathbb{m}_{wg} \rangle - V_s^{[m]} Y_s^B = \\ - \langle \mathbb{m}_{wg} | \mathbb{H}^+ \rangle \frac{2 \langle \mathbb{m}_s | \mathbb{G}_B^{[m]} | \mathbb{m}_{wg} \rangle}{Y_{wg}^A + Y_{wg}^B} + V_s^{[m]} \left[\frac{\langle \mathbb{m}_s | \mathbb{G}_B^{[m]} | \mathbb{m}_{wg} \rangle^2}{Y_{wg}^A + Y_{wg}^B} - Y_s^B \right] \end{aligned} \quad (3.19)$$

where the reciprocity in equation (3.10) has been used to equate $\langle \mathfrak{m}_s | \mathbb{G}_B^{[m]} | \mathfrak{m}_{wg} \rangle = \langle \mathfrak{m}_{wg} | \mathbb{G}_B^{[m]} | \mathfrak{m}_s \rangle$.

After describing the magnetic fields at both the covered slot and the covered waveguide (S_1), finding their respective coupling is only a matter of identification. Here the notation of S_{1m} and S_{m1} is introduced analogously to the scattering parameters. Defining S_{1m} , the contribution to the field at S_1 from \mathbb{M}_s , as

$$S_{1m} = -Z_{wave} \frac{\langle \mathfrak{m}_{wg} | \mathbb{H}^- \rangle}{V_s^{[m]}} \Big|_{\mathbb{H}^+=0} = -Z_{wave} Y_{wg}^A \frac{\langle \mathfrak{m}_{wg} | \mathbb{G}_B^{[m]} | \mathfrak{m}_s \rangle}{Y_{wg}^A + Y_{wg}^B} \quad (3.20a)$$

and likewise S_{m1} , the contribution to the field at the slot from the incoming wave, as measured at S_1 , as

$$S_{m1} = \frac{\langle \mathfrak{m}_s | \mathbb{H}_B \rangle}{\langle \mathfrak{m}_{wg} | \mathbb{H}^+ \rangle} \Big|_{V_s^{[m]}=0} = -2 \frac{\langle \mathfrak{m}_s | \mathbb{G}_B^{[m]} | \mathfrak{m}_{wg} \rangle}{Y_{wg}^A + Y_{wg}^B} \quad (3.20b)$$

where the multiplication of $-Z_{wave}$ is added such that $\mathbb{E}_{S_1}^- = V_s^{[m]} S_{1m} = -Z_{wave} \mathbb{H}_{S_1}^-$. Using this notation, note that the field over the slot due to the incoming field \mathbb{H}^+ in the original problem (before domain decomposition) is then

$$\langle \mathfrak{m}_s | \mathbb{H}^+ \rangle = S_{m1} \langle \mathfrak{m}_{wg} | \mathbb{H}^+ \rangle \quad (3.21)$$

Analogously, by performing the domain decomposition at S_2 instead, leads to the coupling coefficients S_{2m} and S_{m2} . However the signs of the terms in equation (3.20) change as the magnetic waves change direction.

3.2.1 Proof of Reciprocity

Due to the reciprocity of electromagnetic fields in linear isotropic media^[1] it is expected that $S_{1m} = S_{m1}$. This equality will be shown under the assumption that the fields at S_1 exist solely in the TE₁₀ mode. Since $\langle \mathfrak{m}_{wg} | \mathbb{G}_B^{[m]} | \mathfrak{m}_s \rangle = \langle \mathfrak{m}_s | \mathbb{G}_B^{[m]} | \mathfrak{m}_{wg} \rangle$ due to equation (3.10), it remains to show that $Z_{wave} Y_{wg}^A = 2$.

From equation (2.7) the electric and magnetic modes of the TE₁₀ mode are

$$\mathfrak{e}_{10}(x,y) = C_{10} \frac{\omega \mu a}{\pi} \sin \frac{\pi x}{a} \hat{y} \quad (3.22a)$$

$$\mathfrak{h}_{10}(x,y) = C_{10} \left(-\frac{\beta a}{\pi} \sin \frac{\pi x}{a} \hat{x} + j \cos \frac{\pi x}{a} \hat{z} \right) \quad (3.22b)$$

where C_{10} is a proportionality constant here chosen such that the power propagated through the waveguide by the wave is normalized. For the TE₁₀ mode it is

$$C_{10} = \frac{2\pi}{\sqrt{a^3 b \beta \mu \omega}} \quad (3.23)$$

which gives the time average power propagating through the waveguide

$$\frac{1}{2} \int_0^a \int_0^b \mathbf{e}_{10} \times \mathbf{h}_{10}^* dy dx = \text{sgn } \beta \quad (3.24)$$

as expected. Note that the tangential components of \mathbf{h}_{10} change sign when traveling backwards while \mathbf{e}_{10} maintains its sign for backward propagating waves.

The magnetic current distribution \mathbf{m}_{wg} in domain A then has the distribution

$$\frac{\mathbf{m}_{wg}}{C_s} = -\hat{\mathbf{n}} \times \mathbf{e}_{10} = \hat{\mathbf{z}} \times \mathbf{e}_{10} = Z_{wave} (\mathbf{h}_{10} - (\mathbf{h}_{10} \cdot \hat{\mathbf{z}})\hat{\mathbf{z}}) \quad (3.25)$$

where equation (2.10) has been used. C_s is another proportionality constant, here chosen such that the $\langle \mathbf{m}_{wg} | \mathbf{m}_{wg} \rangle = 1$. This can be written out as

$$\langle \mathbf{m}_{wg} | \mathbf{m}_{wg} \rangle = \left(C_s C_{10} Z_{wave} \frac{\beta a}{\pi} \right)^2 \int_0^a \int_0^b \sin^2 \frac{\pi x}{a} dy dx = 1 \quad (3.26)$$

yielding

$$C_s = \sqrt{\frac{2}{ab} \frac{\pi}{a\beta Z_{wave} C_{10}}} = \frac{1}{\sqrt{2Z_{wave}}} \quad (3.27)$$

The dyadic Green's function in a semi-infinite waveguide stretching from $z = -\infty$ to $z = 0$ with a magnetic current distribution at $z = 0$ is^[20]

$$\mathbf{G}_A^{[m]}(\mathbf{r}, \mathbf{r}_s) = \frac{1}{2} \sum_i \mathbf{h}_i^-(\mathbf{r}) \left[\mathbf{h}_i^+(\mathbf{r}_s) - \mathbf{h}_i^-(\mathbf{r}_s) \right] \quad (3.28)$$

for $z < 0$ where the sum is over all modes in the waveguide, \mathbf{h}_i^\pm are the modes traveling in each respective direction. These become for the TE_{10} mode: $\mathbf{h}_{i=\text{TE}_{10}}^\pm = \pm \mathbf{h}_{10} e^{\mp j\beta z}$ in either direction. A dyadic Green's function on the form $\mathbf{A}\mathbf{B}$ acts on a vector \mathbf{C} as

$$(\mathbf{A}\mathbf{B})\mathbf{C} = \mathbf{A}(\mathbf{B} \cdot \mathbf{C}) \quad (3.29)$$

Furthermore, due to the orthogonality of the modes and the fact that \mathbf{m}_{wg} and \mathbf{h}_{10} have the same shape in the transverse plane, leads to the only non-zero component of the sum being $i = \text{TE}_{10}$.

The magnetic field in domain A when $\mathbb{H}^+ = 0$ is then

$$\begin{aligned} \mathbb{H}_A(\mathbf{r}) &= \mathbf{G}_A^{[m]} | \mathbf{m}_{wg} \rangle = \iiint_{S_1} \mathbf{G}_A^{[m]}(\mathbf{r}, \mathbf{r}_s) \mathbf{m}(\mathbf{r}_s) d\mathbf{r}_s = \\ &= -C_s Z_{wave} \mathbf{h}_{10}(x, y) e^{j\beta z} \int_0^a \int_0^b \mathbf{h}_{10}(x_s, y_s) \cdot (\mathbf{h}_{10}(x_s, y_s) - (\mathbf{h}_{10}(x_s, y_s) \cdot \hat{\mathbf{z}})\hat{\mathbf{z}}) dy_s dx_s = \\ &= -C_s Z_{wave} \left(C_{10} \frac{\beta a}{\pi} \right)^2 \mathbf{h}_{10}(x, y) e^{j\beta z} \int_0^a \int_0^b \sin^2 \frac{\pi x_s}{a} dy_s dx_s = \\ &= -C_s Z_{wave} \left(C_{10} \frac{\beta a}{\pi} \right)^2 \frac{ab}{2} \mathbf{h}_{10}(x, y) e^{j\beta z} = -2C_s \mathbf{h}_{10}(x, y) e^{j\beta z} \quad (3.30) \end{aligned}$$

which when evaluated on the short end of the semi-infinite waveguide, weighted by \mathbb{m}_{wg} becomes

$$\begin{aligned}
 \langle \mathbb{m}_{wg} | \mathbb{H}_A \rangle &= \langle \mathbb{m}_{wg} | \mathbb{G}_A^{[m]} | \mathbb{m}_{wg} \rangle = -Y_{wg}^A = \iiint_{S_1} \mathbb{m}_{wg}(\mathbf{r}) \cdot \mathbb{H}_A(\mathbf{r}) \, d\mathbf{r} = \\
 &- 2C_s^2 Z_{wave} \int_0^a \int_0^b (\mathbb{h}_{10}(x,y) - (\mathbb{h}_{10}(x,y) \cdot \hat{\mathbf{z}})\hat{\mathbf{z}}) \cdot \mathbb{h}_{10}(x,y) \, dy \, dx = \\
 &- 2C_s^2 Z_{wave} \left(C_{10} \frac{\beta a}{\pi} \right)^2 \int_0^a \int_0^b \sin^2 \frac{\pi x}{a} \, dy \, dx = \\
 &- 2C_s^2 Z_{wave} \left(C_{10} \frac{\beta a}{\pi} \right)^2 \frac{ab}{2} = \frac{-2}{Z_{wave}} \quad (3.31)
 \end{aligned}$$

and thus it is shown that $Z_{wave} Y_{wg}^A = 2$ or $S_{1m} = S_{m1}$.

Analogously the coupling coefficients S_{2m} and S_{m2} are also reciprocal. Moreover this can be shown more generally using the reaction theorem^[1]

Theorem (Reaction Theorem). *For fields $(\mathbb{E}_1, \mathbb{H}_1)$ produced by current sources $(\mathbb{J}_1, \mathbb{M}_1)$, and fields $(\mathbb{E}_2, \mathbb{H}_2)$ produced by current sources $(\mathbb{J}_2, \mathbb{M}_2)$ in a linear, isotropic medium, however not necessarily homogeneous, the reaction of the fields on the currents is reciprocal according to*

$$\iiint_V (\mathbb{E}_1 \cdot \mathbb{J}_2 - \mathbb{H}_1 \cdot \mathbb{M}_2) \, dV = \iiint_V (\mathbb{E}_2 \cdot \mathbb{J}_1 - \mathbb{H}_2 \cdot \mathbb{M}_1) \, dV \quad (3.32)$$

That is, the magnetic field in the waveguide (due to some source) couples with the magnetic current in the slot in the same manner as the magnetic wave due to the current in the slot would couple to the source of the mode in the waveguide.

Finally, if the cross-section of S_1 and S_2 are the same and domain B is symmetric in regards to the ports, $S_{1m} = S_{2m} = S_{m2} = S_{m1}$, the proof of which is left as an exercise for the reader.

3.3 Scattering Parameters of a Single Waveguide Section

With the knowledge of the coupling between all ports and sources of a closed waveguide section, parameters relating wave amplitudes can be derived. Further it will be seen that these parameters may be constructed and used similar to S-parameters.

Consider a single section Π_i from figure 3.2c, yielded through both domain decomposition and mode matching. The sources of the problem are partly the magnetic current \mathbb{M}_i , and partly the waves \mathbb{H}_{li} , \mathbb{H}_{ri} which exist in the whole waveguide and can be considered originating from sources infinitely far to the left and right, respectively. Select two waveguide cross-sections, here called ports S_1 and S_2 , on either side of the slot, far enough away from the slot that the fields may be considered to

consist of only the TE₁₀ mode. At these interfaces the total field may be written according to equation (3.6) as

$$\begin{aligned} \mathbb{H}_{S_1} &= \mathbb{H}_{\mathbf{II}_i}(\mathbf{r}), & \mathbf{r} \in S_1 \\ \mathbb{H}_{S_2} &= \mathbb{H}_{\mathbf{II}_i}(\mathbf{r}), & \mathbf{r} \in S_2 \\ \mathbb{H}_{S_1} &= H_1^+ \mathfrak{h}_{10} e^{-j\beta z} + H_1^- \mathfrak{h}_{10} e^{j\beta z} \\ \mathbb{H}_{S_2} &= H_2^- \mathfrak{h}_{10} e^{-j\beta z} + H_2^+ \mathfrak{h}_{10} e^{j\beta z} \end{aligned} \quad (3.33)$$

$$\mathbb{H}_{S_2} = H_2^- \mathfrak{h}_{10} e^{-j\beta z} + H_2^+ \mathfrak{h}_{10} e^{j\beta z} \quad (3.34)$$

where H_k^\pm is the amplitude of the TE₁₀ waves traveling in to and out of the waveguide section at port S_k , respectively. Through the superposition of electromagnetic fields, the amplitudes of the waves may be seen as combinations of contributions from the three sources. The wave amplitudes at each port then become

$$\mathbb{H}_{S_1} = (H_{1l}^+ + H_{1r}^+ + H_{1m}^+) \mathfrak{h}_{10} e^{-j\beta z} + (H_{1l}^- + H_{1r}^- + H_{1m}^-) \mathfrak{h}_{10} e^{j\beta z} \quad (3.35a)$$

$$\mathbb{H}_{S_2} = (H_{2l}^- + H_{2r}^- + H_{2m}^-) \mathfrak{h}_{10} e^{-j\beta z} + (H_{2l}^+ + H_{2r}^+ + H_{2m}^+) \mathfrak{h}_{10} e^{j\beta z} \quad (3.35b)$$

where $H_{il}^\pm, H_{ir}^\pm, H_{im}^\pm$ are the contributions to the amplitude of the incoming and outgoing waves originating from the left source, right source, and magnetic current source respectively. Since a source can only give rise to outgoing waves, not incoming waves, it is clear that

$$H_{1r}^+ = H_{1m}^+ = H_{2l}^+ = H_{2m}^+ = 0 \quad (3.36)$$

leading to

$$\mathbb{H}_{S_1} = H_{1l}^+ \mathfrak{h}_{10} e^{-j\beta z} + (H_{1l}^- + H_{1r}^- + H_{1m}^-) \mathfrak{h}_{10} e^{j\beta z} \quad (3.37a)$$

$$\mathbb{H}_{S_2} = (H_{2l}^- + H_{2r}^- + H_{2m}^-) \mathfrak{h}_{10} e^{-j\beta z} + H_{2r}^+ \mathfrak{h}_{10} e^{j\beta z} \quad (3.37b)$$

Then by using their definition, the scattering parameters in the waveguide when $V_u^{[m]} = 0$ can be identified as

$$\begin{aligned} H_{1l}^- &= -S_{11}^{\text{closed}} H_{1l}^+, & H_{1r}^- &= S_{12}^{\text{closed}} H_{2r}^+ \\ H_{2l}^- &= S_{21}^{\text{closed}} H_{1l}^+, & H_{2r}^- &= -S_{22}^{\text{closed}} H_{2r}^+ \end{aligned} \quad (3.38)$$

which is simply the S-parameters that would be measured when simulating a waveguide section with its slot covered (with null amplitude magnetic current) and reference planes at S_1 and S_2 .

It then remains to calculate the contributions H_{1m}^-, H_{2m}^- , which are known from section 3.2 and equation (3.20) as

$$H_{1m}^- = -V_i^{[m]} \frac{S_{1m}}{Z_{\text{wave}}} \quad (3.39a)$$

$$H_{2m}^- = V_i^{[m]} \frac{S_{2m}}{Z_{\text{wave}}} \quad (3.39b)$$

Then by combining equations (3.38) and (3.39) the outgoing magnetic wave amplitudes $H_{S_1}^- = H_{1l}^- + H_{1r}^- + H_{1m}^-$ and $H_{S_2}^- = H_{2l}^- + H_{2r}^- + H_{2m}^-$ can be written as

$$H_{S_1}^- = -S_{11}^{\text{closed}} H_{S_1}^+ + S_{12}^{\text{closed}} H_{S_2}^+ - V_i^{[m]} \frac{S_{1m}}{Z_{\text{wave}}} \quad (3.40a)$$

$$H_{S_2}^- = S_{21}^{\text{closed}} H_{S_1}^+ - S_{22}^{\text{closed}} H_{S_2}^+ + V_i^{[m]} \frac{S_{2m}}{Z_{\text{wave}}} \quad (3.40b)$$

or by using equation (2.10) to instead find the electric wave relations as

$$E_{S_1}^- = S_{11}^{\text{closed}} E_{S_1}^+ + S_{12}^{\text{closed}} E_{S_2}^+ + V_i^{[m]} S_{1m} \quad (3.41a)$$

$$E_{S_2}^- = S_{21}^{\text{closed}} E_{S_1}^+ + S_{22}^{\text{closed}} E_{S_2}^+ + V_i^{[m]} S_{2m} \quad (3.41b)$$

or simply

$$\begin{bmatrix} E_{S_1}^- \\ E_{S_2}^- \end{bmatrix} = [S^{\text{closed}}] \begin{bmatrix} E_{S_1}^+ \\ E_{S_2}^+ \end{bmatrix} + V_i^{[m]} \begin{bmatrix} S_{1m} \\ S_{2m} \end{bmatrix} \quad (3.42)$$

which is similar to the traditional S-parameter form with an additional contribution from the magnetic current.

The value of $V_i^{[m]}$ due to the sources in domains I and II_i can be solved from the boundary condition in equation (3.13) yielding

$$V_i^{[m]} = \frac{\langle \mathbb{m}_i | \mathbb{H}_{li} \rangle + \langle \mathbb{m}_i | \mathbb{H}_{ri} \rangle + \sum_{j \neq i} V_j^{[m]} \langle \mathbb{m}_i | \mathbb{G}_I^{[m]} | \mathbb{m}_j \rangle}{Y_i^{\text{I}} + Y_i^{\text{II}_i}} \quad (3.43)$$

. Further, from the definition of S_{m1} and S_{m2} in section 3.2 the substitutions

$$\langle \mathbb{m}_i | \mathbb{H}_{li} \rangle = S_{m1} H_{S_1}^+ = \frac{S_{m1}}{Z_{\text{wave}}} E_{S_1}^+ \quad (3.44a)$$

$$\langle \mathbb{m}_i | \mathbb{H}_{ri} \rangle = -S_{m2} H_{S_2}^+ = \frac{S_{m2}}{Z_{\text{wave}}} E_{S_2}^+ \quad (3.44b)$$

can be made, yielding

$$V_i^{[m]} = \frac{\frac{E_{S_1}^+}{Z_{\text{wave}}} + \frac{E_{S_2}^+}{Z_{\text{wave}}} + \sum_{j \neq i} V_j^{[m]} \langle \mathbb{m}_i | \mathbb{G}_I^{[m]} | \mathbb{m}_j \rangle}{Y_i^{\text{I}} + Y_i^{\text{II}_i}} \quad (3.45)$$

which relates the incoming waves of the waveguide to the excitation of the slot. Then by inserting the solved $V^{[m]}$ from equation (3.45) into equation (3.41) and collecting all sources, yet another form similar to the traditional scattering parameters is found as

$$E_{S_1}^- = \left[S_{11}^{\text{closed}} + \frac{S_{1m} S_{m1}}{Z_{\text{wave}} (Y_i^{\text{I}} + Y_i^{\text{II}_i})} \right] E_{S_1}^+ + \left[S_{12}^{\text{closed}} + \frac{S_{1m} S_{m2}}{Z_{\text{wave}} (Y_i^{\text{I}} + Y_i^{\text{II}_i})} \right] E_{S_2}^+ + \frac{S_{1m}}{Y_i^{\text{I}} + Y_i^{\text{II}_i}} \sum_{j \neq i} V_j^{[m]} \langle \mathbb{m}_i | \mathbb{G}_I^{[m]} | \mathbb{m}_j \rangle \quad (3.46a)$$

$$E_{S_2}^- = \left[S_{21}^{\text{closed}} + \frac{S_{2m} S_{m1}}{Z_{\text{wave}} (Y_i^{\text{I}} + Y_i^{\text{II}_i})} \right] E_{S_1}^+ + \left[S_{22}^{\text{closed}} + \frac{S_{2m} S_{m2}}{Z_{\text{wave}} (Y_i^{\text{I}} + Y_i^{\text{II}_i})} \right] E_{S_2}^+ + \frac{S_{2m}}{Y_i^{\text{I}} + Y_i^{\text{II}_i}} \sum_{j \neq i} V_j^{[m]} \langle \mathbb{m}_i | \mathbb{G}_I^{[m]} | \mathbb{m}_j \rangle \quad (3.46b)$$

or

$$\begin{aligned} \begin{bmatrix} E_{S_1}^- \\ E_{S_2}^- \end{bmatrix} &= \left([S^{closed}] + \frac{1}{Z_{wave} (Y_i^I + Y_i^{II})} \begin{bmatrix} S_{1m} S_{m1} & S_{1m} S_{m2} \\ S_{2m} S_{m1} & S_{2m} S_{m2} \end{bmatrix} \right) \begin{bmatrix} E_{S_1}^+ \\ E_{S_2}^+ \end{bmatrix} \\ &+ \frac{\sum_{j \neq i} V_j^{[m]} \langle \mathbb{m}_i | \mathbb{G}_I^{[m]} | \mathbb{m}_j \rangle}{Y_i^I + Y_i^{II}} \begin{bmatrix} S_{1m} \\ S_{2m} \end{bmatrix} \end{aligned} \quad (3.46c)$$

Thus if it is possible to calculate

- the S-parameters of the closed waveguide section without the magnetic current, $[S^{closed}]$,
- the coupling between the slot and the ports, $S_{1m} = S_{m1}$ and $S_{2m} = S_{m2}$,
- the total slot admittance, $Y_i^I + Y_i^{II}$,
- the outer coupling of the slots, $\langle \mathbb{m}_i | \mathbb{G}_I^{[m]} | \mathbb{m}_j \rangle$

the original EM-problem of finding the slot excitations and waves within the waveguide may be constructed as an RF circuit problem. Using equations (3.45) and (3.46) it is possible to describe such an RF problem in a similar manner to working with S-parameters. Note that the only approximation made when replacing the full wave solution with the RF solution is the single mode assumption.

3.3.1 Transmission Parameters from Scattering Parameters

The generalized S-parameters in equation (3.46) give a good description of the wave relations within the waveguide section. However when trying to find the wave relations in a cascade of waveguide sections, T-parameters would be more useful. In accordance with appendix A.3 the generalized scattering parameters in equation (3.46) can be re-written as

$$\begin{bmatrix} E_{S_1}^- \\ E_{S_1}^+ \end{bmatrix} = [\mathbb{T}] \begin{bmatrix} E_{S_2}^+ \\ E_{S_2}^- \end{bmatrix} + \mathbb{A} = \begin{bmatrix} T_{11} & T_{12} \\ T_{21} & T_{22} \end{bmatrix} \begin{bmatrix} E_{S_2}^+ \\ E_{S_2}^- \end{bmatrix} + \begin{bmatrix} A_1 \\ A_2 \end{bmatrix} \quad (3.47)$$

where

$$T_{11} = \frac{2S_{12}^{closed} S_{m1} S_{m2} - S_{11}^{closed} S_{m2}^2 - S_{22}^{closed} S_{m1}^2 - Y Z_{wave} \det([S^{closed}])}{S_{m1} S_{m2} + Y Z_{wave} S_{12}^{closed}} \quad (3.48a)$$

$$T_{12} = \frac{S_{m1}^2 + Y Z_{wave} S_{11}^{closed}}{S_{m1} S_{m2} + Y Z_{wave} S_{12}^{closed}} \quad (3.48b)$$

$$T_{21} = -\frac{S_{m2}^2 + Y Z_{wave} S_{22}^{closed}}{S_{m1} S_{m2} + Y Z_{wave} S_{12}^{closed}} \quad (3.48c)$$

$$T_{22} = \frac{Y Z_{wave}}{S_{m1} S_{m2} + Y Z_{wave} S_{12}^{closed}} \quad (3.48d)$$

$$\mathbb{A} = -\frac{Z_{wave} \sum_{j \neq i} V_j^{[m]} \langle \mathbb{m}_i | \mathbb{G}_I^{[m]} | \mathbb{m}_j \rangle}{S_{m1} S_{m2} + Y Z_{wave} S_{12}^{closed}} \begin{bmatrix} S_{11}^{closed} S_{m2} - S_{12}^{closed} S_{m1} \\ S_{m2} \end{bmatrix} \quad (3.48e)$$

3. Method Derivation

using $Y = Y_i^I + Y_i^{II}$ as well as the reciprocities $S_{12} = S_{21}$ and $S_{im} = S_{mi}$. Further, if domain Π_i is symmetric with regards to its two ports, then $S_{11} = S_{22}$ and $S_{1m} = S_{2m}$, reducing the number of unknowns and simplifying the equations.

Therefore if all the constituents of $[T]$ and \mathbb{A} are known, it is possible to find all the wave amplitudes and slot excitations quickly in a waveguide with constant exterior geometry using a work-flow similar to that in described in section 2.8.2.

4

Practical work

The previous chapters of this master's thesis have focused on the theoretical derivation of a methodology for finding the waves within, and excitations of, a slotted waveguide antenna through RF circuit theory. The resulting equations are based on a few, simple, assumptions which need to be verified for a certain geometry before the methodology may be implemented using said design.

This section therefore explores how the excitation of slotted rectangular waveguides are controlled and presents the design used for the practical work of this master's thesis. Once a design is selected, the assumptions made, namely the single mode assumption, are verified in order to show the validity of the theory for the design in question.

4.1 Slot Excitation

There are many ways of exciting a slot in a waveguide. In section 2.6 it is shown that the level of excitation of a slot in a waveguide wall is dependent on to which degree the slot cuts a mode's surface currents. Thus by controlling the amount of surface current clipped one can control the level of excitation within a slot. This is typically done by either changing the slot's rotation, offset or by perturbing the fields within the waveguide along with its surface currents. This thesis focuses on narrow wall slots, however first we will explore the general slot in a rectangular TE_{10} waveguide.

Assume one wishes to excite a slot in a rectangular waveguide which only allows for propagation of the fundamental TE_{10} mode, oriented along the \hat{z} -axis with broad wall $0 \leq x \leq a$ and narrow wall $0 \leq y \leq b$. The slot may be placed either on the broad wall, the narrow wall or a combination of both, figure 4.1 shows a few such slots. The surface currents of the PEC waveguide are

$$\mathbb{J} = \hat{n} \times \mathbb{H} \tag{4.1}$$

which can be derived from equation (2.5). For the principal TE_{10} mode the surface

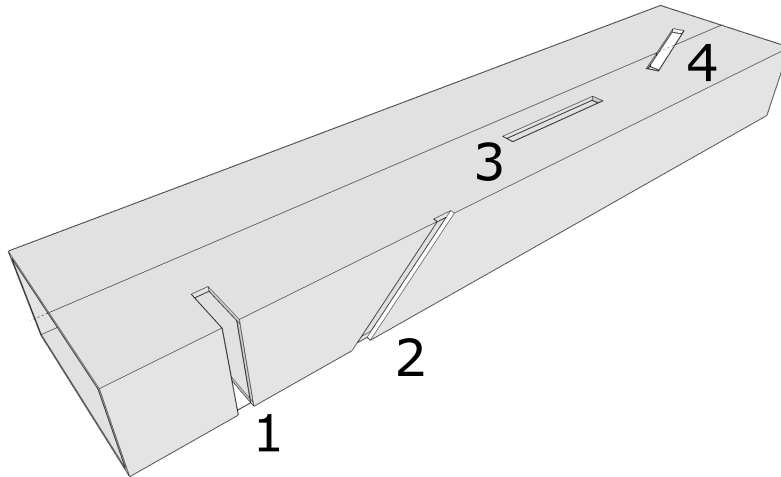


Figure 4.1: Different ways of exciting a slot in a rectangular waveguide. Note that the vertical narrow wall slot (1) requires inner perturbations to the wave environment in order to steer the TE_{10} modes electric surface currents over the slot.

currents are therefore

$$\mathbb{J} \propto \begin{cases} \pm \left(j \cos \left(\frac{x\pi}{a} \right) \hat{x} + \frac{\beta a}{\pi} \sin \left(\frac{x\pi}{a} \right) \hat{z} \right) e^{-j\beta z} & \text{on broad walls} \\ -j e^{-j\beta z} \hat{y} & \text{on narrow walls} \end{cases} \quad (4.2a)$$

where the \pm is positive on the lower wall ($y = 0$) and negative on the upper ($y = b$). Note that all currents are proportional to $e^{-j\beta z}$, meaning that to have slots radiating in phase, their required spacing needs to be λ_{wg} . However if it is possible to flip the phase of every second slot by 180° , the spacing only needs to be $\lambda_{wg}/2$.

The surface currents of the broad wall allow a slot to have its excitation level controlled by either varying its offset from the center-line (along \hat{x}) or by changing its rotation. The surface currents of the narrow wall are however all constant along \hat{y} , making it impossible to control the excitation by offsetting the slot, it can however still be controlled by changing the slot's rotation.

Another approach to controlling the slot excitation is to perturb the interior of the waveguide, changing the surface currents such that they cross the slot in an increased or decreased fashion. Such a perturbation can take many forms, for this master's thesis however it will consist of rectangular irises set on either side of the slot, see figure 4.2. The excitation may then be controlled by varying the iris design. Deriving a full model of the effect of the iris on the slot excitation is beyond the scope of this thesis. However, an examination of which design parameters are most significant for excitation control is performed. This allows for a simple parameterization of the slot excitation as a function of those parameters.

From this point in this master's thesis and onward, the waveguides considered will be rectangular with cross-section dimensions 40 mm by 20 mm. The frequency which will be examined is 5 GHz, meaning that the waveguide will only allow the TE_{10}

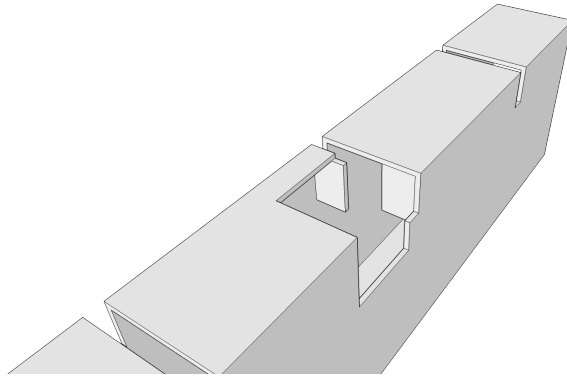


Figure 4.2: Single waveguide slot with pair of rectangular irises with see-through window cut out.

mode to propagate with all higher order modes below their respective cut-off frequencies.

4.1.1 Slot Geometry

A slot may take many forms, however often the slot has a rectangular shape with length $l \approx \lambda/2$ and width $w \ll \lambda$ such that only the TE_{10} mode may propagate^[4]. If the narrow wall is too small to accommodate a slot of length $\lambda/2$, the slot may be extended to also cover a bit of the broad side walls, see slot (1) in figure 4.1.

Since the focus of this master's thesis is on slotted waveguide antennas with constant outer geometries, the design of all slots will be fixed as rectangular TE_{10} slots. Such slots have the added benefit of experiencing high levels of linear polarization with low cross-polarization. From this point and onward of the master's thesis, the slots considered will be along the narrow wall extending into the broadwall. The slots have a width of 3 mm and a length of 30 mm when measured along the inside of the waveguide. Furthermore the slot spacing will be $\lambda_{wg}/2 \approx 45.28$ mm.

4.1.2 Selecting Iris Parameters

For this master's thesis two design-parameters will be used to control the excitation of the narrow wall slot. The available design parameters for the rectangular irises are width, height, thickness, and offset from the slot. The choice of control parameters is done by firstly examining the change in S-parameters whilst varying the design parameters of the iris. The two parameters which then cover the largest swath of S-parameters in the Smith-chart are chosen as they will yield the most control over the inner electromagnetic environment of the waveguide.

Figure 4.3 shows the S-parameters when varying the height and widths for fixed offsets and thicknesses of the irises. The magnitude of the S-parameters scales well with the height of the irises while the phase scales with the width. Figure 4.4 shows the S-parameters when varying the offset and thickness for fixed heights and widths

Table 4.1: Fixed dimensions of the rectangular waveguides under consideration in this master's thesis.

Waveguide width (a)	40 mm
Waveguide height (b)	20 mm
Waveguide wall thickness	1 mm
Frequency (f)	5 GHz
Slot spacing	$\lambda_{wg}/2$
Slot length (inner)	30 mm
Slot width	3 mm
Iris design parameters	h_{iris}, w_{iris}
Iris offset (edge-to-edge)	2.5 mm
Iris thickness	1 mm

of irises. The offset seems to control both magnitude and phase, while the thickness allows for less control.

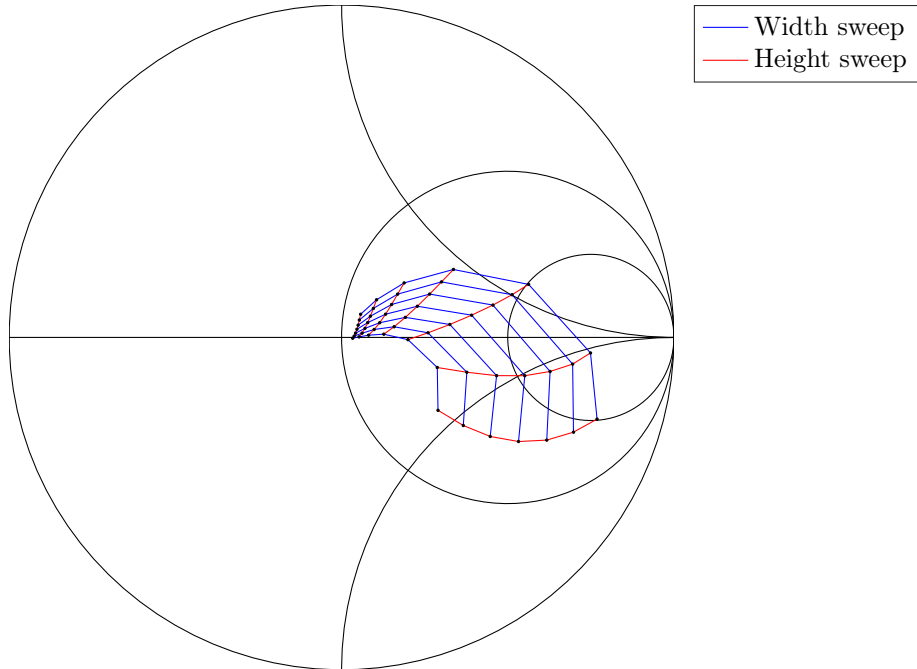
The width and height give the best control as they control the phase and magnitude mostly independently. Further, they cover a large section of the smithchart and are therefore selected as iris parameters for controlling the slots' excitations. From this point and forward, the term iris parameters will therefore be in reference to the variable height and width of each iris pair. The thickness and offset of the irises will be held fixed at 1 mm and 2.5 mm respectively. All fixed dimensions of the rectangular slotted waveguides under consideration are summarized in table 4.1.

4.2 Verifying Assumptions

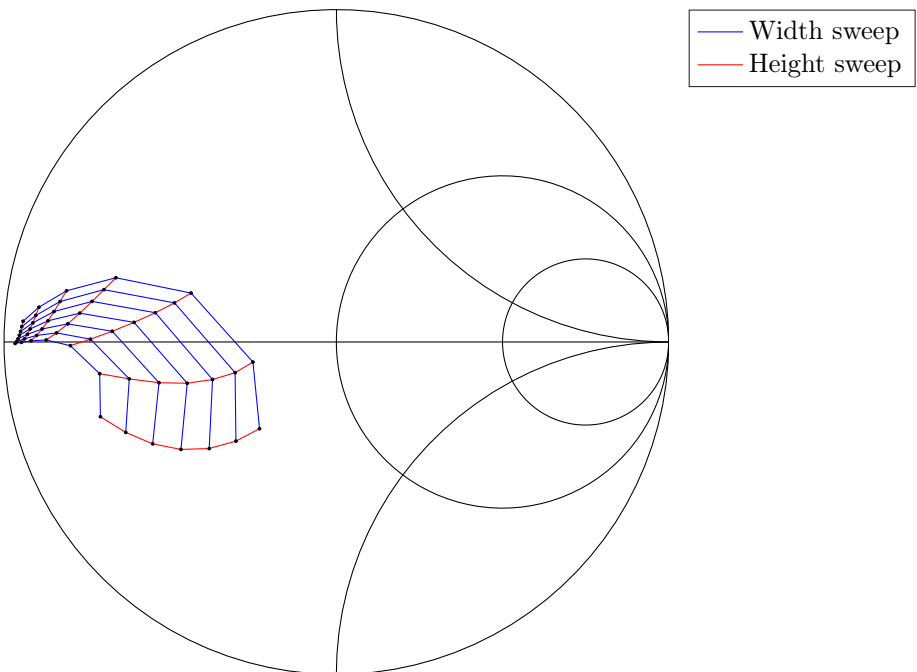
In order to use the methodology in chapter 3, the assumptions made must be verified for the chosen waveguide and slot designs. All assumptions made are in regards to the modal expansion of the fields. The first requires that all slot elements have similar electromagnetic field distributions such that they may be expanded in a single mode without large loss of information. The second requires that a similar single mode assumption can be made for the electromagnetic fields within the waveguide at the interface between each $\lambda_{wg}/2$ section. This section proves these assumptions for the antenna described in table 4.1.

4.2.1 Single Mode at Slot Interface

The most significant assumption made in the methodology in chapter 3 is that the fields in the slot may be described by a single mode. Typically any field (and therefore also its equivalent current distribution) within a geometry can be described as an infinite weighted sum of eigenmodes. This assumption reduces the linear combination to only a single term, making all subsequent calculations easier in the

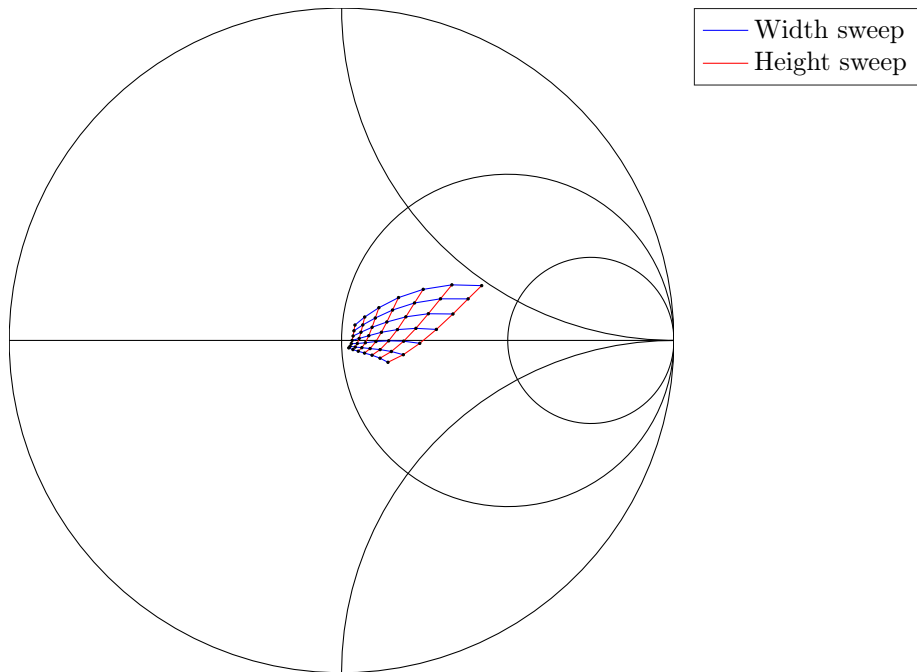


(a) S_{11} when the iris offset is 1 mm and the iris thickness is 1 mm.

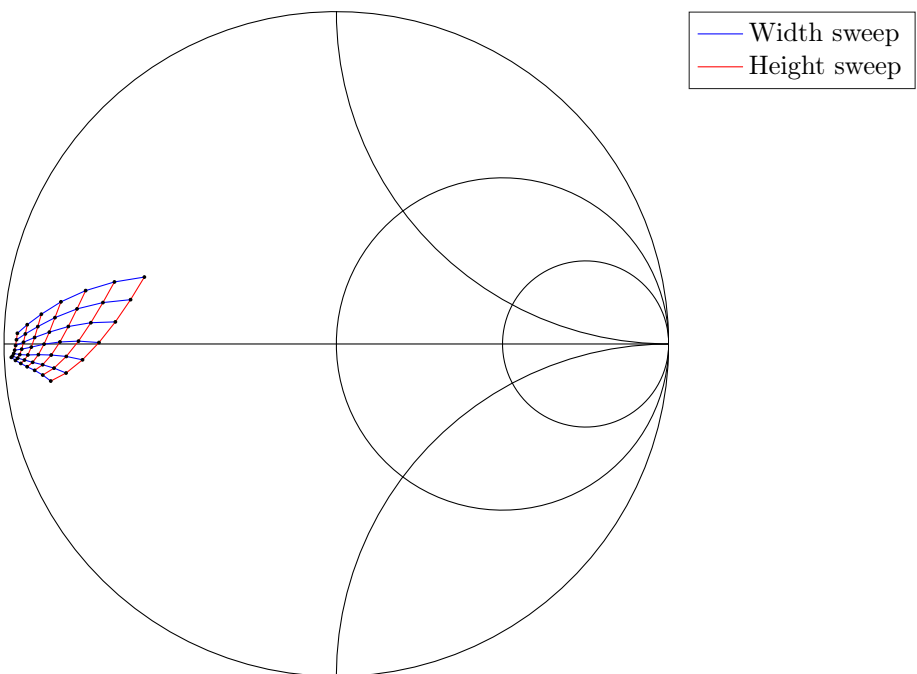


(b) S_{12} when the iris offset is 1 mm and the iris thickness is 1 mm.

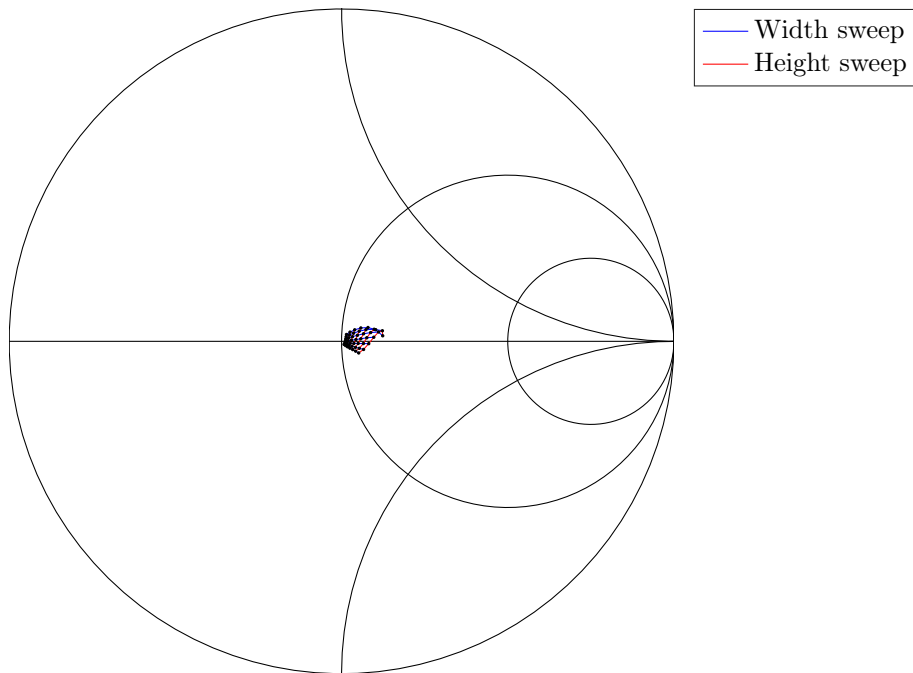
4. Practical work



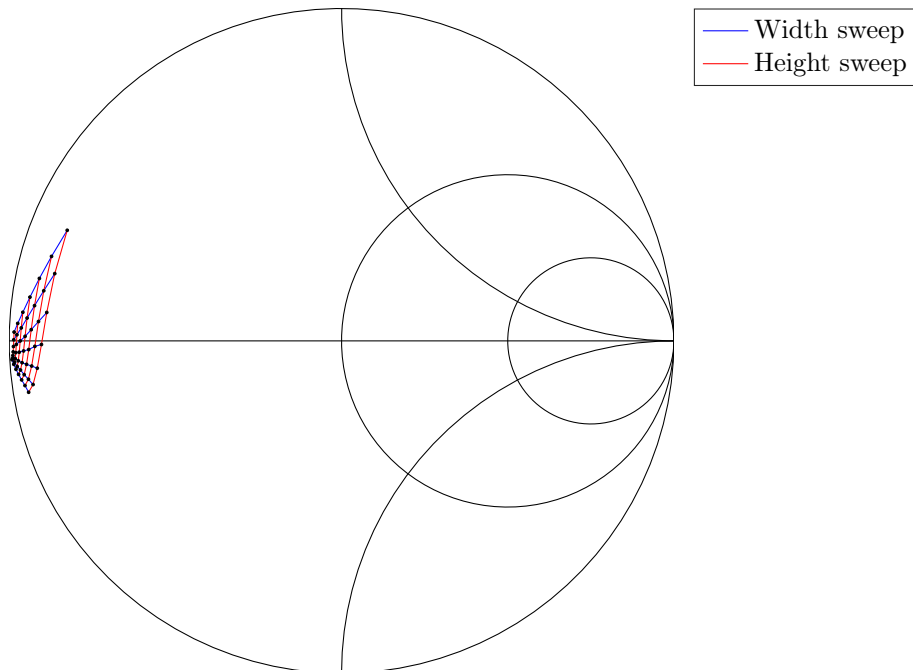
(c) S_{11} when the iris offset is 4 mm and the iris thickness is 3 mm.



(d) S_{12} when the iris offset is 4 mm and the iris thickness is 3 mm.



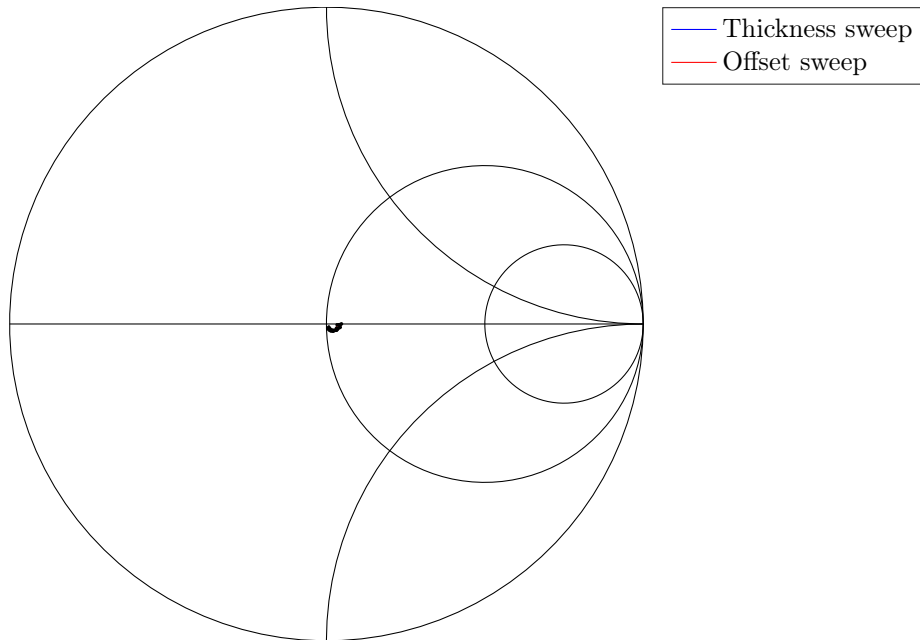
(e) S_{11} when the iris offset is 7 mm and the iris thickness is 5 mm.



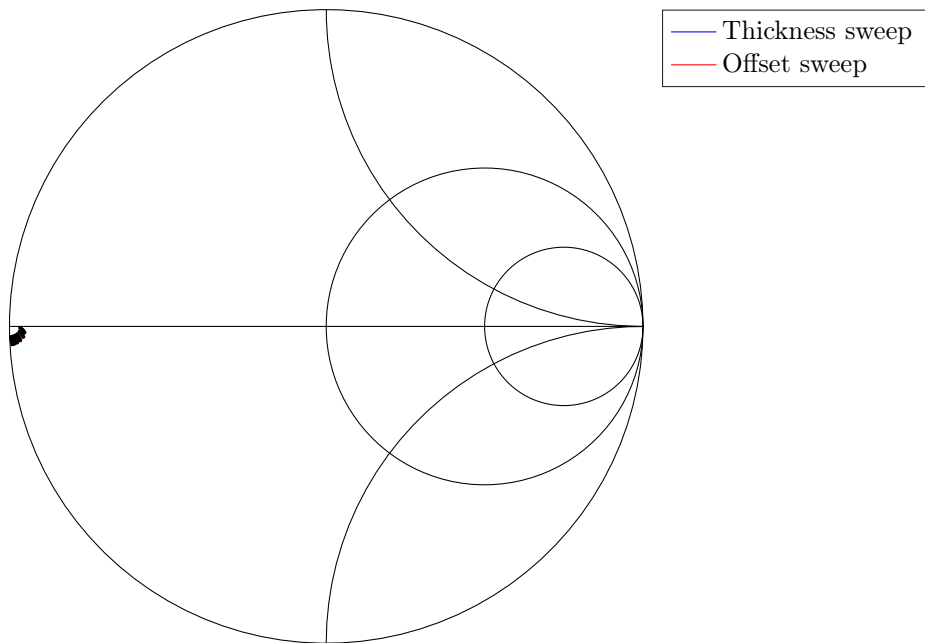
(f) S_{12} when the iris offset is 7 mm and the iris thickness is 5 mm.

Figure 4.3: S_{11} and S_{12} when sweeping the height and width of the irises for several variations of iris offset and thickness. Note that neither S_{22} nor S_{21} are presented due to the symmetries of the irises; $S_{11} = S_{22}$ and $S_{12} = S_{21}$.

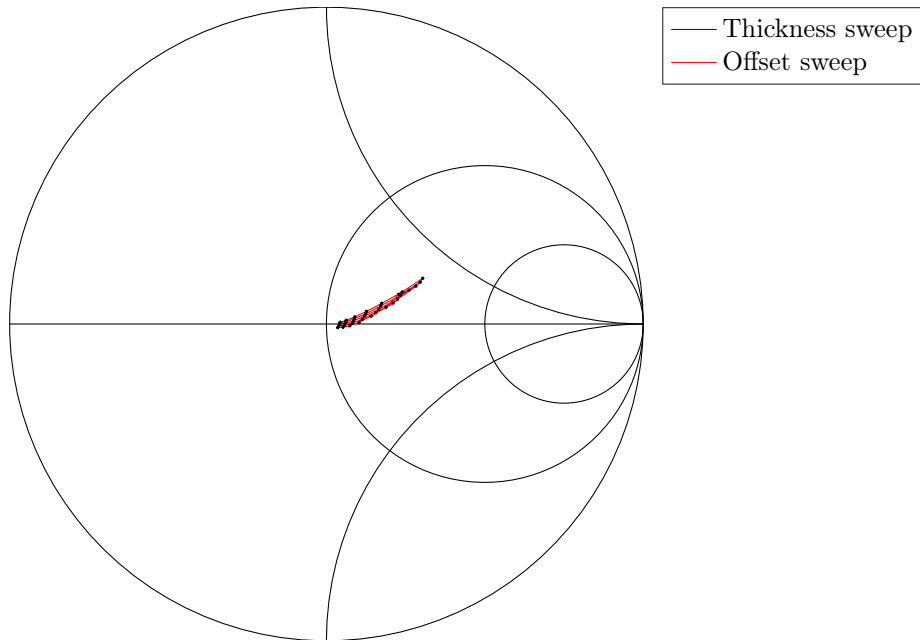
4. Practical work



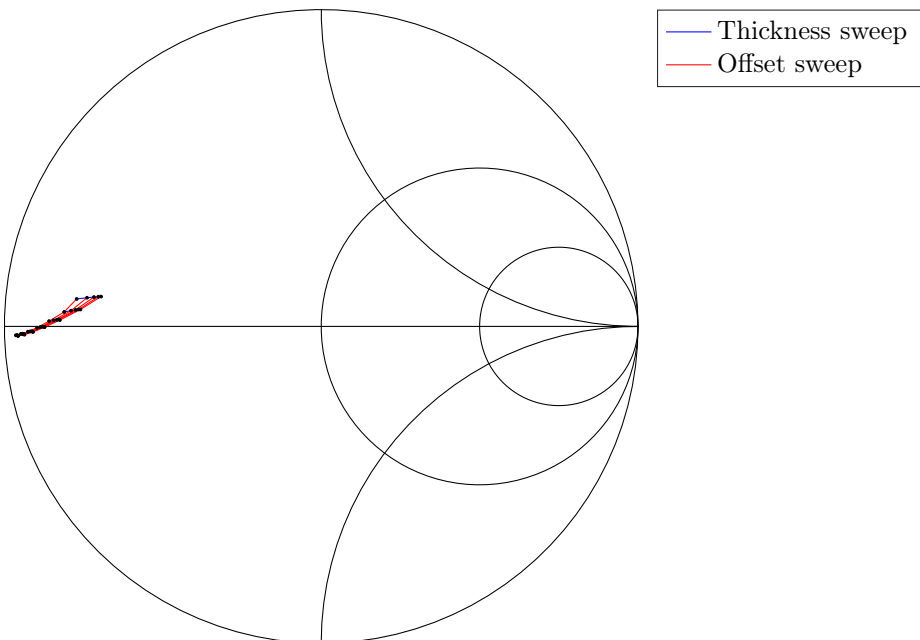
(a) S_{11} when the iris width is 5 mm and the iris height is 8 mm.



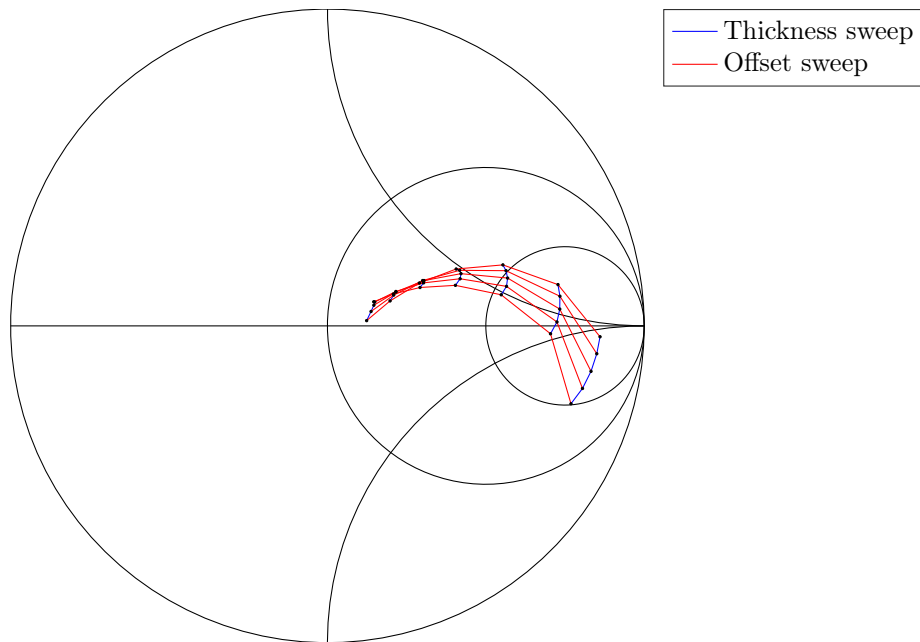
(b) S_{12} when the iris width is 5 mm and the iris height is 8 mm.



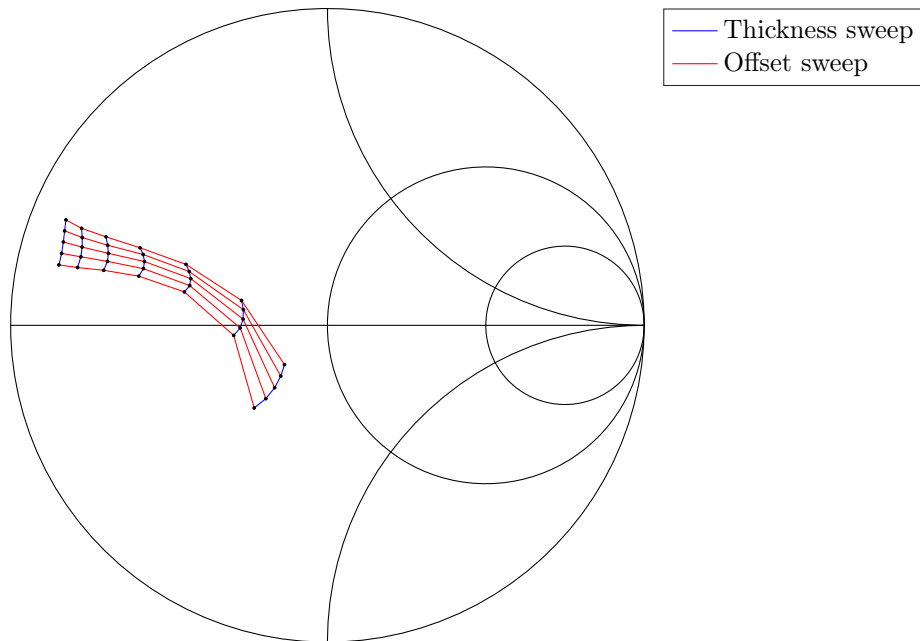
(c) S_{11} when the iris width is 8 mm and the iris height is 11 mm.



(d) S_{12} when the iris width is 8 mm and the iris height is 11 mm.



(e) S_{11} when the iris width is 11 mm and the iris height is 14 mm.



(f) S_{12} when the iris width is 11 mm and the iris height is 14 mm.

Figure 4.4: S_{11} and S_{12} when sweeping the offset and thickness of the irises for several variations of iris height and width. Note that neither S_{22} nor S_{21} are presented due to the symmetries of the irises; $S_{11} = S_{22}$ and $S_{12} = S_{21}$.

process. Thus it is important to compare the field within the slot in a large variety of settings to see if it is sufficient to only use a single eigenmode to describe it and what error such an assumption would entail. The waveguides in this section are placed along the \hat{x} -axis, with the normal of the slotted narrow wall being along the \hat{z} -axis.

In order to best visualize the 3-dimensional shape of the slot cover, its geometry slot will be mapped to a 2-dimensional shape. This is simply done by folding up the sides of the slots such that the cover is a rectangle. Further, if all or most of the field lies along a single direction, the field distribution can instead be represented by integration lines along that direction. Since it is expected that a distribution similar to the TE_{10} mode to exist in the slot, the field is expected to lie mostly along the \hat{x} -axis.

There are several factors which may affect how the slot is excited. Obviously incident waves from both the outer and inner regions will excite the slot, perhaps with different eigenmode expansions making the single mode assumption invalid. Other factors exist as well; by changing the inner or outer electric environment, the active impedance of the slot changes and so does also the way incoming waves interact with it, perhaps changing the modal distribution again. By simulating a single slot in an isolated environment, an infinite array environment, and a truncated array environment whilst also varying the iris design-parameters all the mentioned interactions with the slot can be explored. The single mode assumption will be evaluated by both evaluating in which direction the electric field is oriented, as well as the voltage achieved when integrating the electric slot field along the dominant axis.

4.2.1.1 Inner Excitation

Often the largest contributor to the field in the slot will be from within the waveguide itself. This section explores the cases of a single slot, excited from within, when

1. it is the only slot in a finite antenna and the iris parameters are varied,
2. it is a slot in an infinite array structure and the inner iris parameters are varied,
3. it is a slot in an infinite array structure and the relative phase of adjacent cells are varied,
4. it is the center slot in a truncated 3x3 array and it is the only radiating element,
5. it is the center slot in a truncated 3x3 array where only one other slot is open and only the center element radiates,
6. it is the only element in a truncated 3x3 array where its position in the array is varied.

Together, these cases represent a radiating slot when its interior geometry is changed, when its exterior geometry is changed, and when the surrounding electromagnetic

Table 4.2: Proportion of the field of the center slot which does not lie along the \hat{x} -axis for the cases listed in section 4.2.1.1 according to equation (4.3).

Case	γ [dB]
1	-17.75
2	-16.93
3	-15.49
4	-16.87
5	-17.76
6	-14.74

environment is changed, therefore covering most possible scenarios for a radiating slot in an array antenna. Table 4.2 shows the proportion of the field of the center slot which does not lie along the \hat{x} -axis as

$$\gamma = 10 \log_{10} \left(\frac{\iiint |\mathbb{E}_y|^2 \, d\mathbf{r} + \iiint |\mathbb{E}_z|^2 \, d\mathbf{r}}{\iiint |\mathbb{E}_x|^2 \, d\mathbf{r}} \right) = 10 \log_{10} \left(\frac{P_y + P_z}{P_x} \right) \quad (4.3)$$

for each case above. Note that most of the energy in the slot lies along the \hat{x} -axis and thus the electric field distribution may instead be represented by the voltage across the the slot width. Figure 4.5 shows the voltage achieved by the line integral

$$V = \int_0^w \mathbb{E}(x,y,z) \cdot \hat{x} \, dx \quad (4.4)$$

taken on a straight line across the slot width for points along the length of the slot for case (1). Similarly, figures 4.6 to 4.10 show the integrated voltages for cases (2)-(6). Note how, when normalized¹, the voltage distribution along the slot is fairly constant.

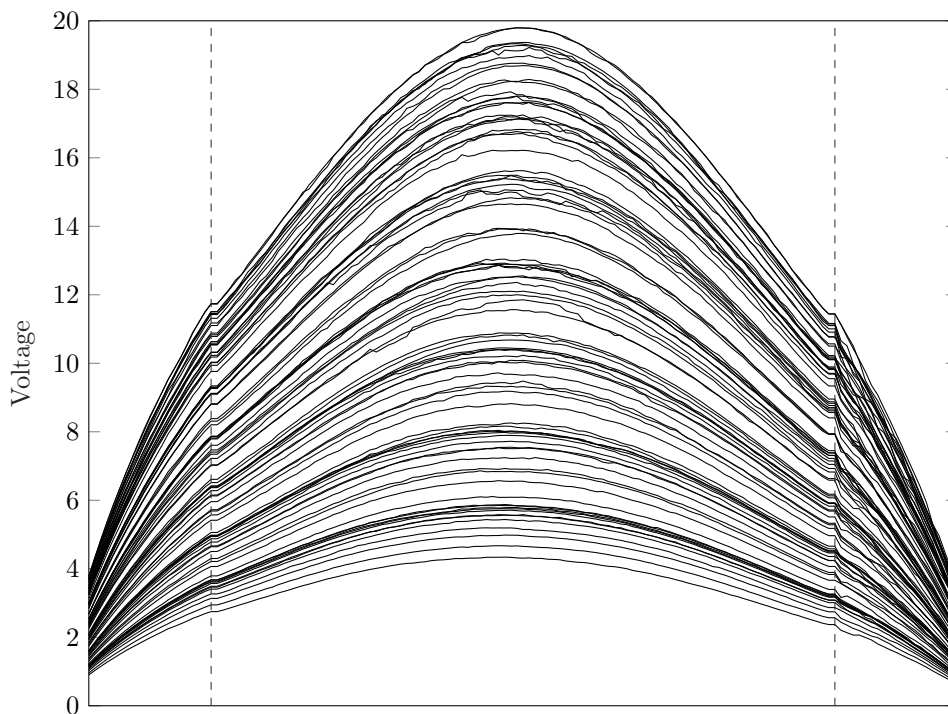
4.2.1.2 Exterior Excitation

It is sometimes possible that the excitation due to coupling from exterior sources is larger than that from the interior. This section explores the cases when a slot is only excited from neighboring slots in two cases

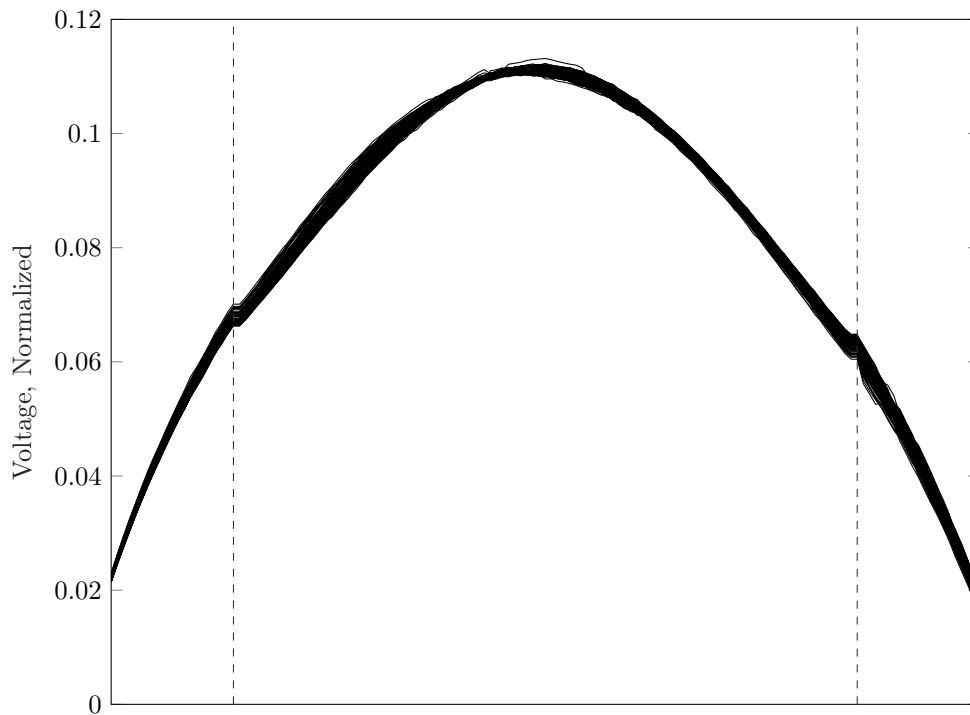
1. when the slot is in a truncated 3x3 array where only a single radiating slot is present,
2. when the slot is in a truncated 3x3 array where all 9 slots are present but only the center slot is radiating.

These cases represent both a single and a more complex coupling case for slots at different positions. Similarly to section 4.2.1.1, most of the power lies along

¹The voltages are normalized such that the integral of the squared voltage along the slot $\int |V(l)|^2 \, dl = 1$.

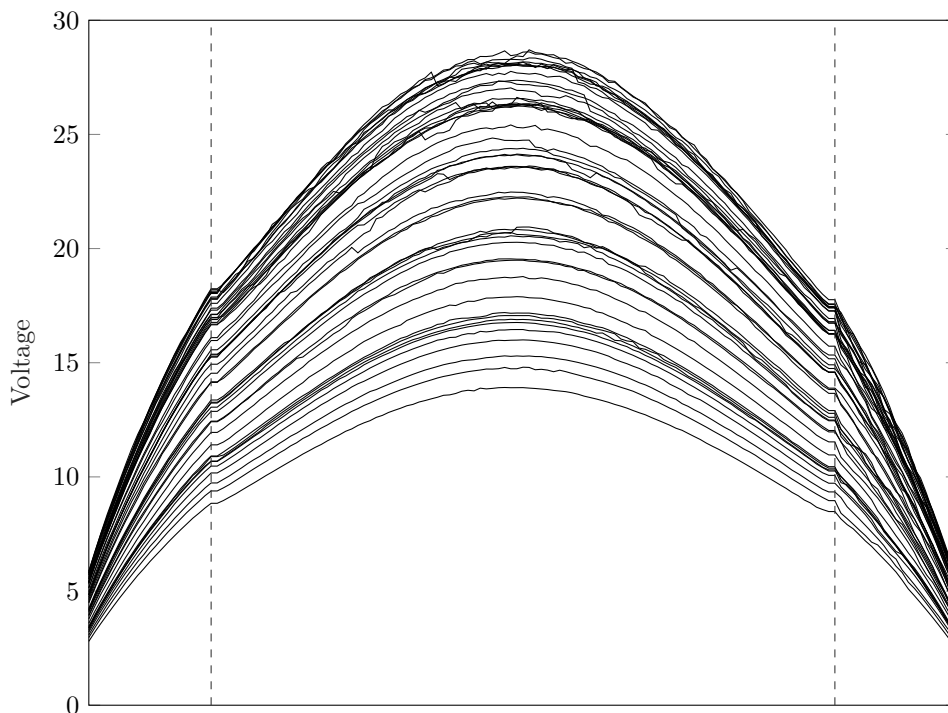


(a) Voltage across the slot width.

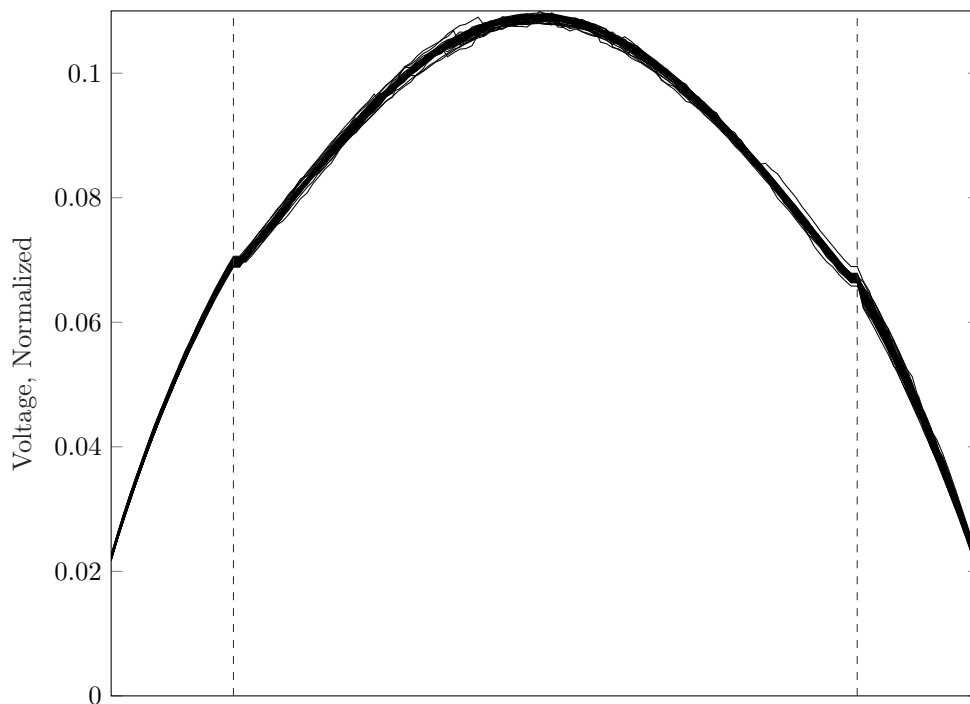


(b) Voltage across the slot width, normalized.

Figure 4.5: The voltage from equation (4.4) for the case of a single slot in a finite waveguide, whilst sweeping the iris parameters (1). The orientation of the slot is un-folded such that it lies in a single plane where the dashed lines denote to folding creases. Both an absolute voltage plot and a normalized voltage plot are presented. The slot is excited by a single 1 W wave from its interior waveguide.

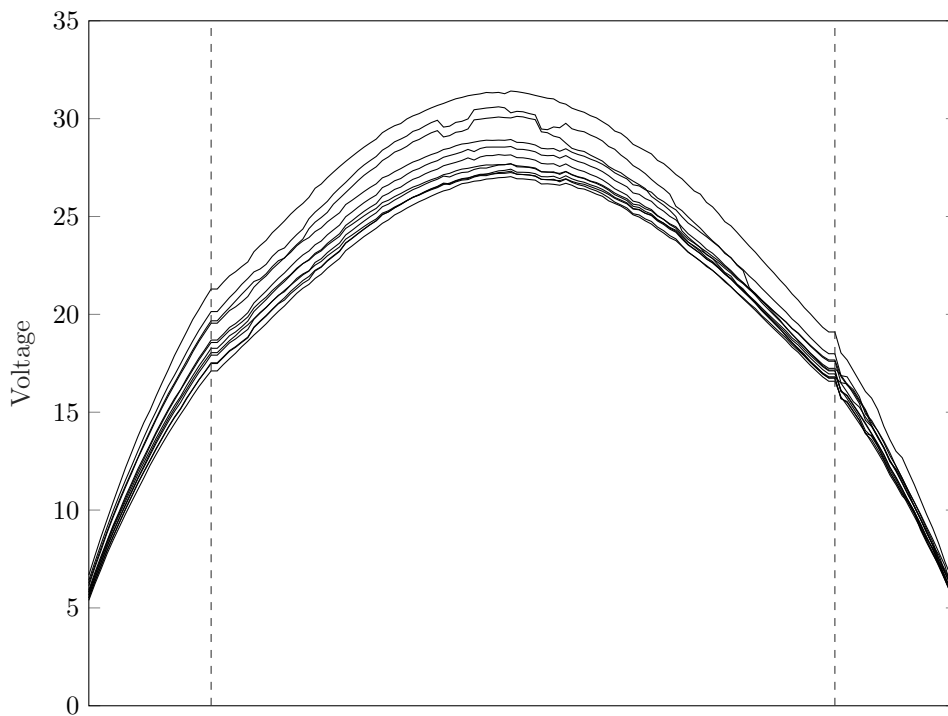


(a) Voltage across the slot width.

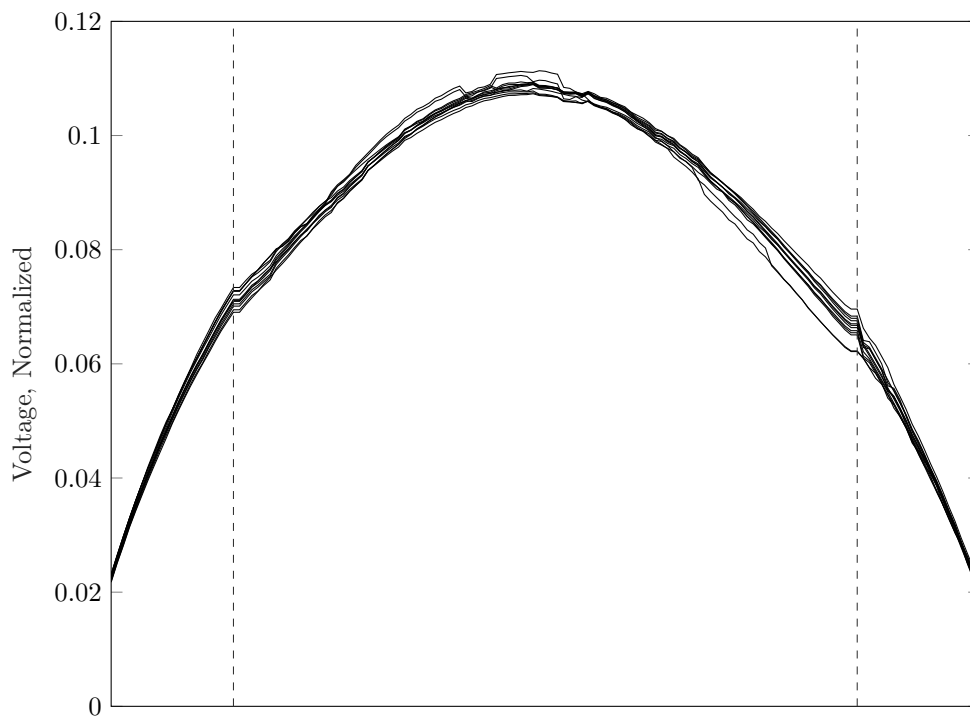


(b) Voltage across the slot width, normalized.

Figure 4.6: The voltage from equation (4.4) for the case of a slot in an infinite waveguide, whilst sweeping the iris parameters (2). The orientation of the slot is un-folded such that it lies in a single plane where the dashed lines denote to folding creases. Both an absolute voltage plot and a normalized voltage plot are presented. The slot is excited by a single 1 W wave from its interior waveguide.

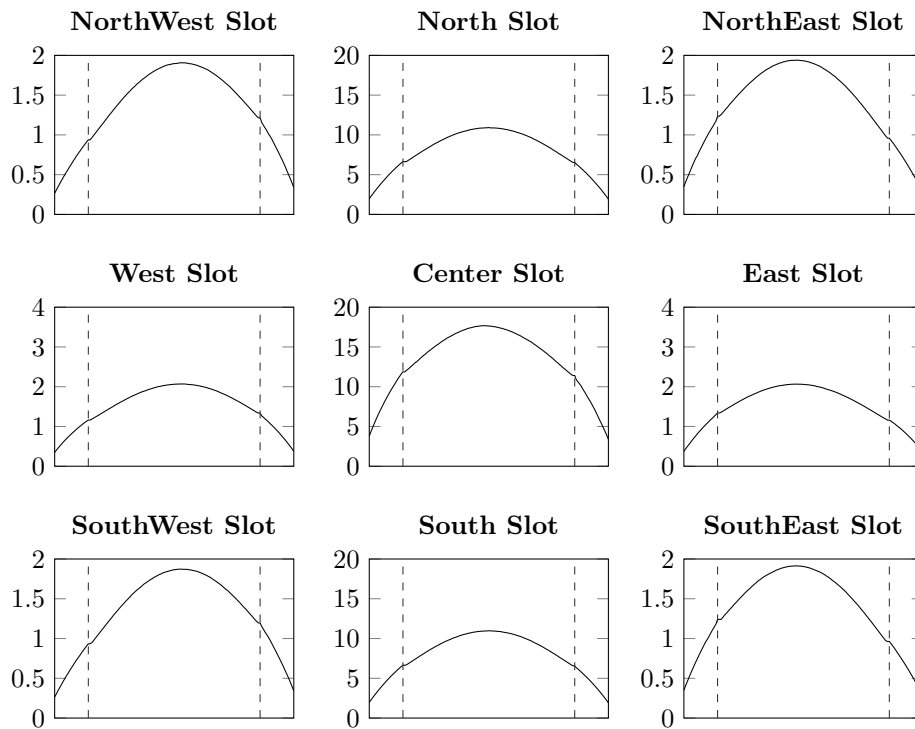


(a) Voltage across the slot width.

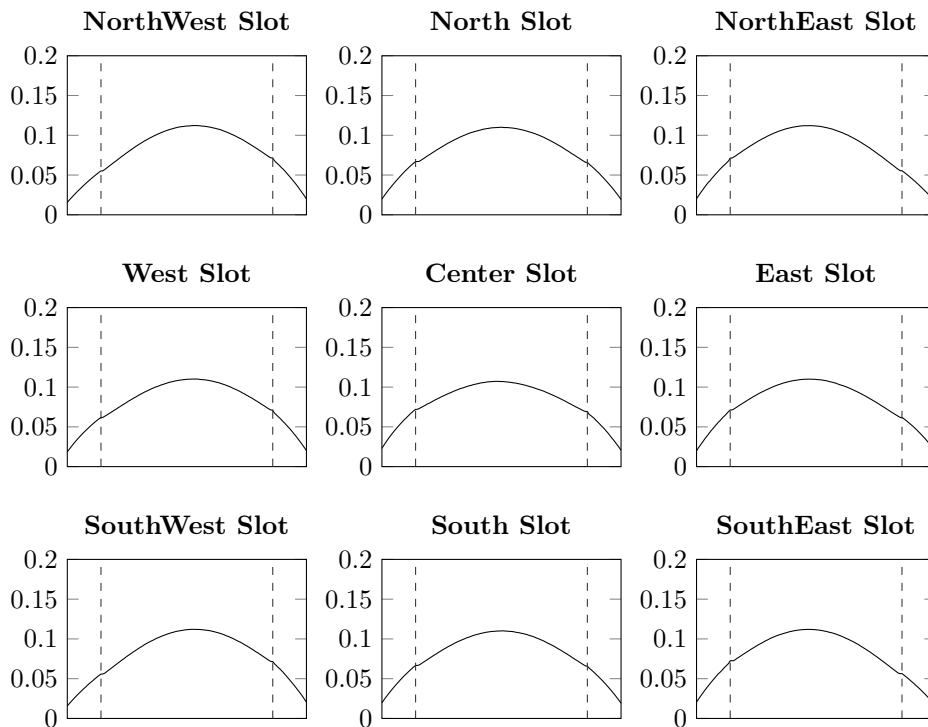


(b) Voltage across the slot width, normalized.

Figure 4.7: The voltage from equation (4.4) for the case of a slot in an infinite waveguide, whilst sweeping the phase of the array cells (3). The orientation of the slot is un-folded such that it lies in a single plane where the dashed lines denote to folding creases. Both an absolute voltage plot and a normalized voltage plot are presented. The slot is excited by a single 1 W wave from its interior waveguide.

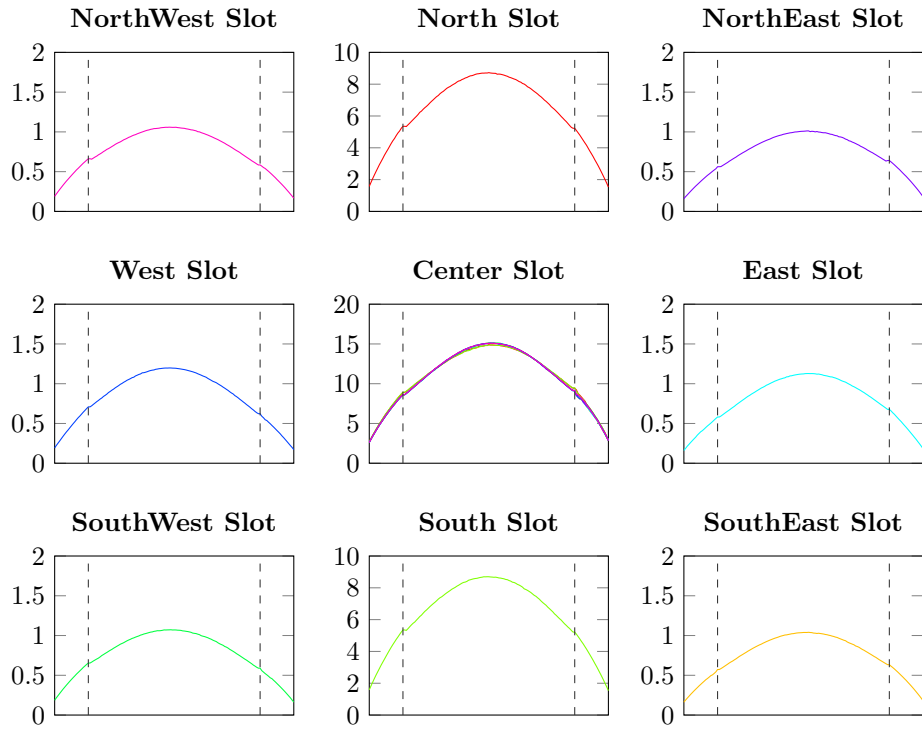


(a) Voltage across the slot width.

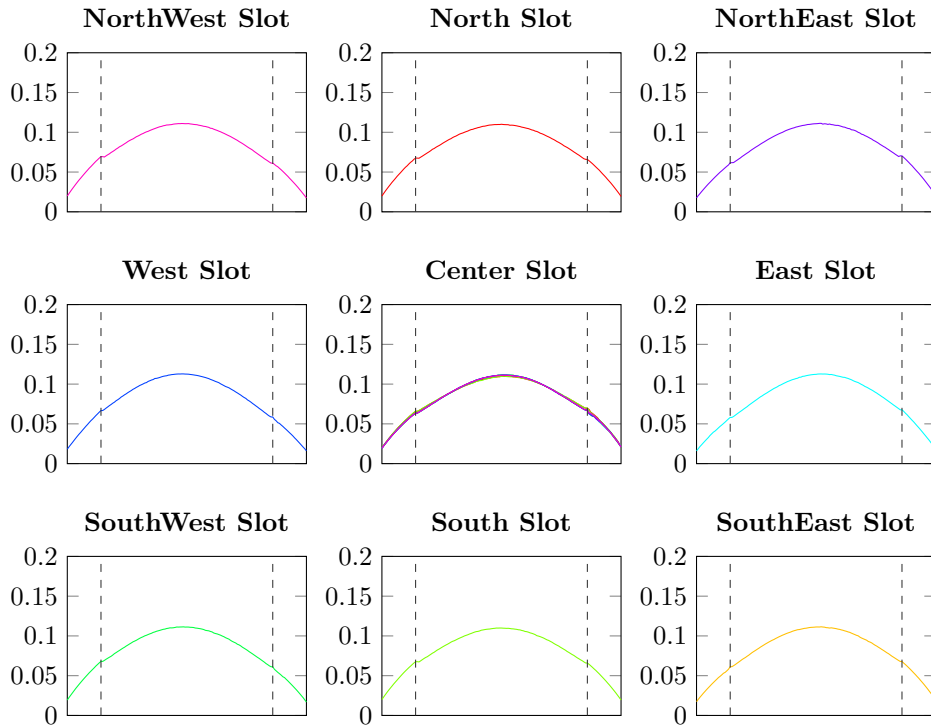


(b) Voltage across the slot width, normalized.

Figure 4.8: The voltage from equation (4.4) for the case of a truncated 3×3 array where only the center slot is excited (4). The orientation of the slot is un-folded such that it lies in a single plane where the dashed lines denote to folding creases. Both an absolute voltage plot and a normalized voltage plot are presented. The slot is excited by a single 1 W wave from its interior waveguide.

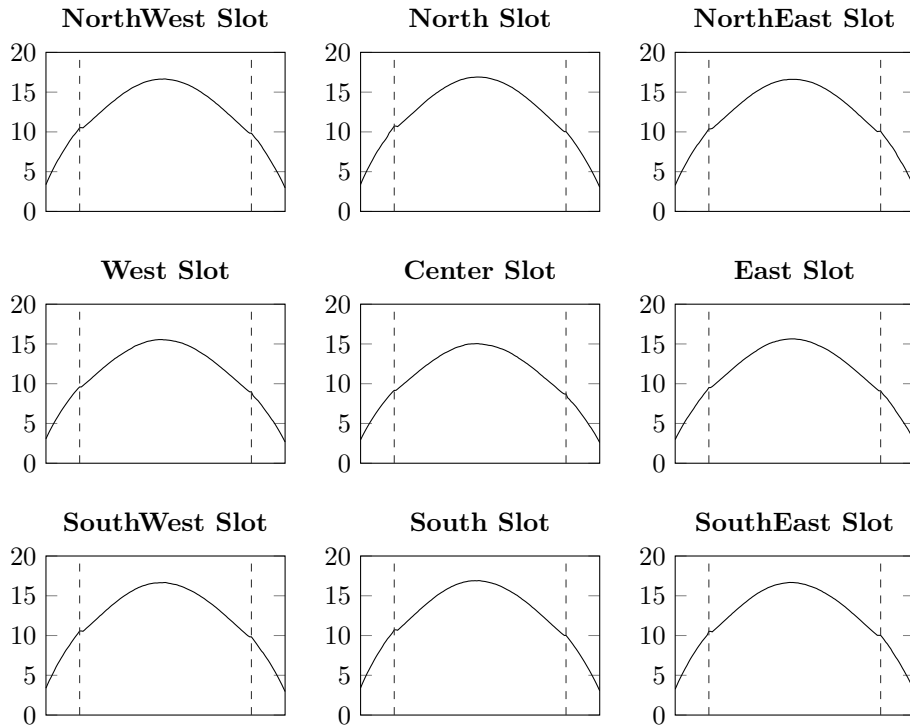


(a) Voltage across the slot width.

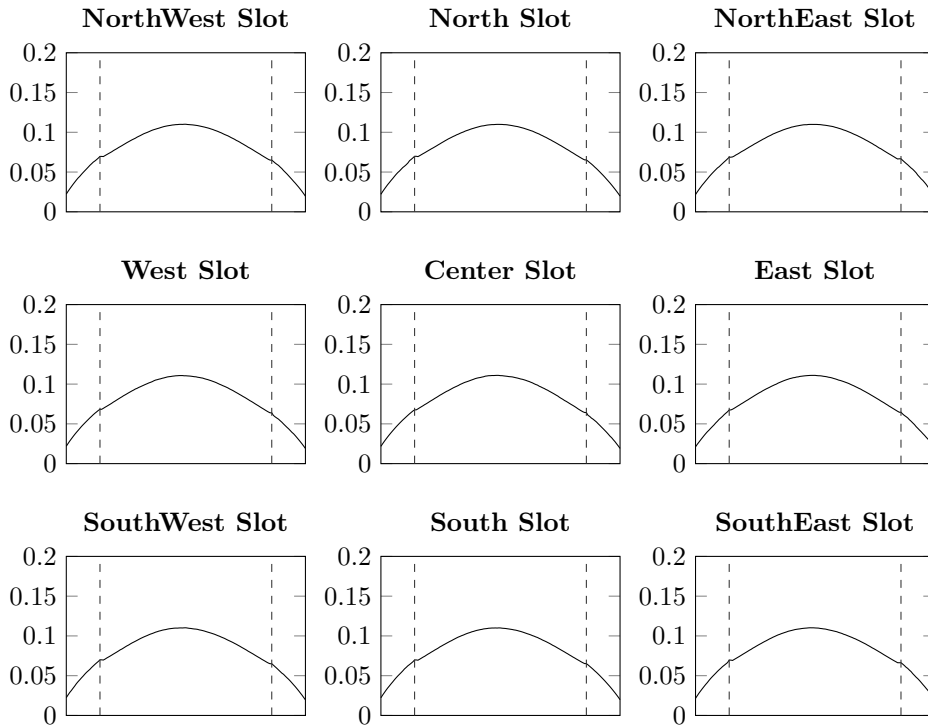


(b) Voltage across the slot width, normalized.

Figure 4.9: The voltage from equation (4.4) for the case of a truncated 3×3 array with only two slots open where only the center slot is excited (5). Each simulated pair shares the same color. The orientation of the slot is un-folded such that it lies in a single plane where the dashed lines denote to folding creases. Both an absolute voltage plot and a normalized voltage plot are presented. The slot is excited by a single 1 W wave from its interior waveguide.



(a) Voltage across the slot width.



(b) Voltage across the slot width, normalized.

Figure 4.10: The voltage from equation (4.4) for the case of a truncated 3x3 array with only a single element, for each possible position (6). The orientation of the slot is un-folded such that it lies in a single plane where the dashed lines denote to folding creases. Both an absolute voltage plot and a normalized voltage plot are presented. The slot is excited by a single 1 W wave from its interior waveguide.

the \hat{x} -axis, applying equation (4.3) on all slots in both cases yields $\gamma = 14.15$ dB. Figures 4.8 and 4.9 show the integrated voltages along the slot for the two cases, respectively.

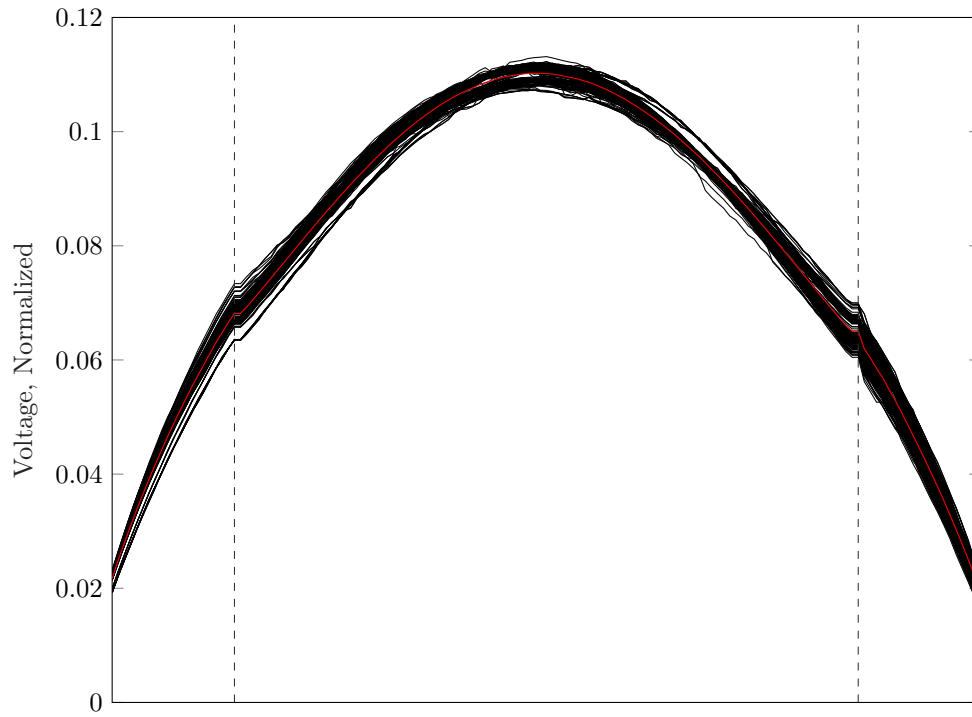
Finally, after showing that the field distribution varies little in each case, a comparison of all cases remains to validate the single mode assumption. Figure 4.11a shows the normalized integrated voltage along the slot from figures 4.6 to 4.10. Figure 4.11b shows the maximum error of the voltages in figure 4.11a when compared to the average for each point along the slot. This shows not only that each slot field can be expanded in a single mode, but also that it is the same mode for all simulations. Note that the error at most passes slightly above 5% error when compared to the average of all lines. It is therefore clear that the single mode assumption can be made without too much error.

4.2.2 Single mode in WG between each III domain

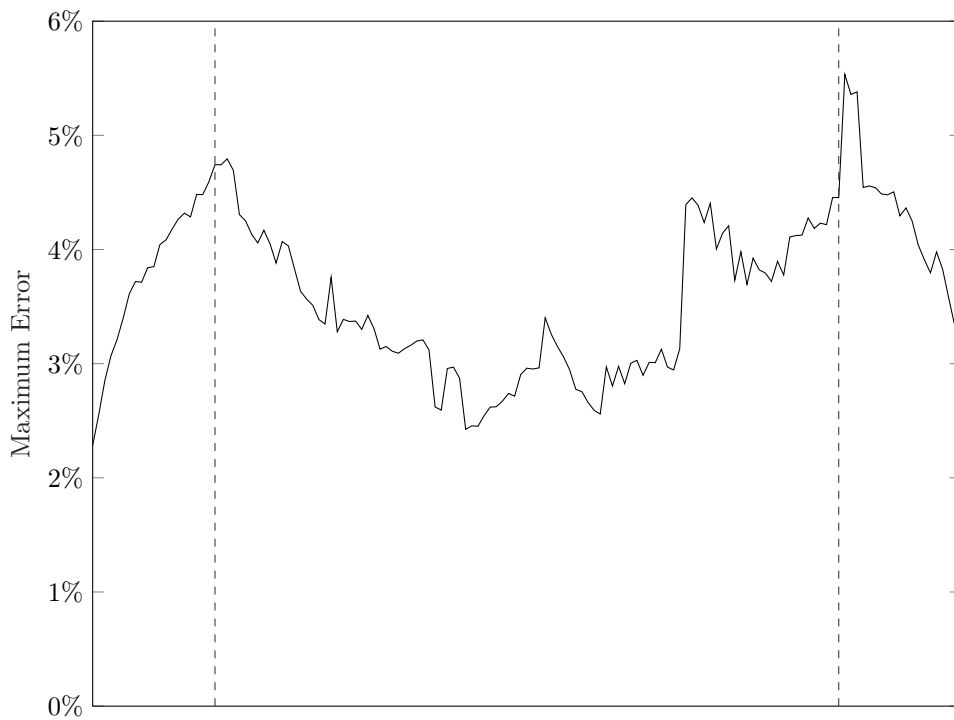
The single mode assumption is also made for the waves propagating in the waveguide. Although the waveguide is constructed such that it only allows for propagation of the TE₁₀ mode, much of the energy near the irises and slot is stored in higher order, evanescent modes. The propagation constant γ_{mn} for a rectangular waveguide may be calculated as^[13]

$$\gamma_{mn} = \alpha + j\beta = \sqrt{k_c - k} = \pi \sqrt{\left(\frac{m}{a}\right)^2 + \left(\frac{n}{b}\right)^2 - \left(\frac{2f}{c_0}\right)^2} \quad (4.5)$$

where α (Np/m) is the attenuation factor, β (rad/m) is the phase factor. Table 4.3 shows the attenuation of the first ten modes within the waveguide and the amount of attenuation expected after 19.14 mm of propagation, the distance from the iris to the unit cell edge. The first higher order mode experiences 19.5 dB of attenuation, which can be considered sufficient to verify the single mode assumption. Furthermore, since the slots and irises are placed at the center of the unit cell, any higher order mode will actually be attenuated at least 38.9 dB before interacting with the next slot and irises.



(a) Normalized Voltage



(b) Maximum Error Compared to Mean

Figure 4.11: The normalized voltages from all simulations presented in figures 4.6 to 4.10 as well as the maximum error from the average at each point along the slot.

Table 4.3: Attenuation factor and attenuation after traveling half a unit cell for the first ten modes in the waveguide used in this master thesis.

(m,n)	α [dB/mm]	$\alpha \cdot 19.14$ mm [dB]
(1, 0)	—	—
(0, 1)	1.02	19.46
(2, 0)	1.02	19.46
(1, 1)	1.22	23.43
(2, 1)	1.70	32.57
(3, 0)	1.83	35.09
(3, 1)	2.29	43.74
(0, 2)	2.57	49.24
(4, 0)	2.57	49.24
(1, 2)	2.66	50.94

5

Implementation

After selecting an antenna design and verifying the assumptions of the theory, it is possible to implement the methodology described in chapter 3. This chapter therefore first suggests an implementation such that any antenna may be quickly modeled and simulated from a library of previously collected unit cells. This may in turn be used with existing optimization schemes to quickly optimize the iris designs of an antenna to yield a certain voltage mask. Then a suggested method for building such a library by calculating all the required components of equation (3.48) through the use of ANSYS HFSS is presented. Finally a simple modification is suggested reducing the number of necessary simulations.

5.1 Suggested Implementation of Theory

The main advantage of splitting a problem into several smaller, independent, problems is that all parts are not forced to be evaluated simultaneously. For the case of an antenna with constant outer geometry, where only small parts of each $\lambda_{wg}/2$ interior section is changed, all outer effects may be solved once and for all. Then, by building a library of solutions for different variations of the interior $\lambda_{wg}/2$ building blocks, it is possible to construct the full solution for any combination of such building blocks and the exterior quickly by combining their solutions.

Consider equations (3.45) and (3.46) which relate the excitation of the slot and waves of the ports of an interior subsection Π_i . If a library of the equation components may be collected a priori for any viable iris design, it is possible to create the corresponding T-matrix in equation (3.47). Then by the work flow presented in section 2.8.2 it is easy to find the wave relations and excitations for each slotted waveguide of the antenna.

Section 3.3 considers a certain waveguide section at a certain position i . However, due to the domain decomposition each section's position in the outer geometry and its interior design may be considered independently. Therefore instead consider a waveguide section Π_k with interior design setup k at outer position i . The slot admittance, consisting of an outer and an inner contribution, may then be re-written as $Y_i^I + Y^{\Pi k}$ by dropping the dependence of position i from the interior term.

The components of the T-matrix can then be divided into two sets; those which

relate to the section's interior ($[S^{closed}]$, S_{1m} , S_{2m} , and Y^{Π_k}), and those which relate to the antenna's exterior (Y_i^I and $\langle m_i | G_I^{[m]} | m_j \rangle$).

Then by first building a library of the interior components and finding the exterior components for each position i it is possible to create the T-matrix in equation (3.47) for any iris design k at any position i . This initial calculation of components are related to costly calculations in terms of both time and resources, however it is only required once. In an optimization method which requires the solution to many design variations, this cost may be spread over all evaluations whereas a full wave electromagnetic simulator would be required to perform the full simulation for each variation. Further, any subsequent optimization of an antenna with the same elements may re-use the library of interior components.

5.1.1 Calculating Equation Components in HFSS

In order to find all the required constituents of equation (3.48) such that the aforementioned implementation can be performed, a method for calculating the components for each iris setup k and position i , preferably independently, must be used. Many commercial EM simulators do not offer the explicit solving of slot self-coupling (called admittance above), mutual coupling, or the use of custom magnetic current sources. However, as the full field solution is typically available and thus intrinsically contains these values, they may be extracted through clever calculations and comparisons of different simulations.

Herein I present a suggested method to calculate all the necessary components through the use of ANSYS HFSS. The interior components are extracted by simulating and comparing each Π_k section with the slot both open and covered. The exterior components are extracted by simulating the slots both separately and in pairs at each position i of the exterior antenna.

5.1.1.1 Interior Components

$[S^{closed}]$ are easily simulated by performing a modal HFSS simulation for each domain Π_k with its slot covered. Since no magnetic current is present, the measured S-parameters are simply $[S^{closed}]$, as mentioned in section 3.3.

Consider now another simulation of domain Π_k , at position i of the antenna, with its slot uncovered when all other slots remain covered. The electric field in the slot will have a distribution corresponding to the theoretical $V_i^{[m]}$ as

$$-\hat{\mathbf{n}} \times \mathbb{E}_{slot} = \mathbb{M}_i = V_i^{[m]} \mathbf{m} \quad (5.1)$$

meaning that $V_i^{[m]}$ may be measured from HFSS's field solution. S_{1m} and S_{2m} may then be found by considering the $V_i^{[m]}$ of the field solution when $E_1^+ \neq E_2^+ = 0$.

Noting from equation (3.42) that

$$E_{S_1}^- = S_{11}^{\text{closed}} E_{S_1}^+ + S_{12}^{\text{closed}} E_{S_2}^+ + V_i^{[m]} S_{1m} \quad (5.2a)$$

$$E_{S_2}^- = S_{21}^{\text{closed}} E_{S_1}^+ + S_{22}^{\text{closed}} E_{S_2}^+ + V_i^{[m]} S_{2m} \quad (5.2b)$$

and using the S-parameter definition, the measured S_{11} and S_{21} of the aforementioned case can be written as

$$S_{11}^{\text{open}} = \frac{S_{11}^{\text{closed}} E_{S_1}^+}{E_{S_1}^+} + V_i^{[m]} \frac{S_{1m}}{E_{S_1}^+} \Big|_{E_1^+ \neq E_2^+ = 0} \quad (5.3a)$$

$$S_{21}^{\text{open}} = \frac{S_{21}^{\text{closed}} E_{S_1}^+}{E_{S_1}^+} + V_i^{[m]} \frac{S_{2m}}{E_{S_1}^+} \Big|_{E_1^+ \neq E_2^+ = 0} \quad (5.3b)$$

where S_{ij}^{open} are the measured S-parameters from a modal HFSS analysis. Since $[S^{\text{closed}}]$ are known, it is possible to calculate the S_{1m} and S_{2m} by re-arranging equation (5.3) as

$$S_{1m} = E_{S_1}^+ \frac{S_{11}^{\text{open}} - S_{11}^{\text{closed}}}{V_i^{[m]}} \Big|_{E_1^+ \neq E_2^+ = 0} \quad (5.4a)$$

$$S_{2m} = E_{S_1}^+ \frac{S_{21}^{\text{open}} - S_{21}^{\text{closed}}}{V_i^{[m]}} \Big|_{E_1^+ \neq E_2^+ = 0} \quad (5.4b)$$

where $V_i^{[m]}$ is extracted from the field solution when $E_1^+ \neq E_2^+ = 0$. S_{m1} and S_{m2} are then also known due to the reciprocity of the coupling between the waves in the waveguide and the field in the slot.

5.1.1.2 Exterior Components

The total slot admittance $Y_i^I + Y^{\text{II}k}$ can also be extracted from the field solution for the single open slot case used to extract S_{1m} and S_{2m} . Consider equation (3.45) which for such a case ($E_{S_2} = V_{j \neq i} = 0$) simplifies as

$$V_i^{[m]} = \frac{E_{S_1}^+ S_{1m}}{Z_{\text{wave}} (Y_i^I + Y^{\text{II}k})} \Big|_{E_1^+ \neq E_2^+ = V_{j \neq i} = 0} \quad (5.5)$$

where Z_{wave} is known analytically from equation (2.11). The admittance $Y_i^I + Y^{\text{II}k}$ is then easily calculated as all other factors are known.

It then remains to find the mutual coupling $\langle \mathbf{m}_i | \mathbb{G}_I^{[m]} | \mathbf{m}_j \rangle$ in order to construct both the T-matrix and A-vector in equation (3.48). Consider therefore an HFSS simulation where two slots, i and j , are open and all other are closed. By measuring $V_i^{[m]}$ and $V_j^{[m]}$ from the field solution when only exciting slot j from within its interior, the mutual coupling may be calculated by re-writing equation (3.45) as

$$\langle \mathbf{m}_i | \mathbb{G}_I^{[m]} | \mathbf{m}_j \rangle = (Y_i^I + Y^{\text{II}k}) \frac{V_i^{[m]}}{V_j^{[m]}} \Big|_{V_{n \notin \{i,j\}}^{[m]} = 0} \quad (5.6)$$

since at port i $E_{S_1}^+ = E_{S_2}^+ = 0$. Further, due to the reciprocity in equation (3.10) only the coupling in one direction needs to be calculated, resulting in $(N^2 - N)/2$ simulations for N slot positions.

5.1.2 Reducing Simulation Requirements

In order to find all the necessary equation components for each section Π_k and position i using the method described, there need to be two simulations for each pair (i, k) . One of only the inner domain Π_k and one of the full antenna when section Π_k is at position i of the antenna. For N slot positions and K domains Π_k in the library, K simulations of only the interior of a single waveguide section and $KN + (N^2 - N)/2$ simulations of the full antenna environment are therefore required.

The full antenna simulations are much larger and therefore more resource expensive than the interior single Π_k simulations. Any possibility of reducing the number of simulations needed of the full antenna model is therefore very valuable in terms of both time and computational costs.

Consider therefore the admittance of slot k at position i

$$Y(i, k) = Y_i^I + Y^{\Pi_k} \quad (5.7)$$

and note that it is separable with regard to i and k . If it is possible to find the parts individually, the number of full antenna simulations may be reduced.

Further, consider the admittance \tilde{Y} of interior domain Π_k positioned in a much smaller, single slot, antenna. Such an admittance is much cheaper to calculate. Since it has no dependence of i , denote it as

$$\tilde{Y}(k) = Y^{simple} + Y^{\Pi_k} \quad (5.8)$$

where Y^{simple} is the outer admittance of the slot in the simple antenna environment and Y^{Π_k} is still the interior admittance of the slot.

Moreover, if each array position i of the full antenna was simulated only once for a given iris design (say $k = 1$) then the admittance of any slot and iris combination $Y(i, k)$ could be calculated as

$$\begin{aligned} Y(i, 1) + \tilde{Y}(k) - \tilde{Y}(1) &= \\ Y_i^I + Y^{\Pi_1} + Y^{simple} + Y^{\Pi_k} - (Y^{simple} + Y^{\Pi_1}) &= \\ Y_i^I + Y^{\Pi_k} &= Y(i, k) \end{aligned} \quad (5.9)$$

Therefore if $Y(i, 1)$ is calculated for each i and $\tilde{Y}(k)$ is calculated for each k , any $Y(i, k)$ can be calculated with a reduced number of full antenna simulations. This separation has the added benefit of enabling the $\tilde{Y}(k)$ to be re-used when simulating an antenna with a new exterior.

Then, for an antenna with N slot positions and K possible inner domains Π_k there needs to be a total of $(N^2 + N)/2$ simulations of the full antenna, K simulations of the simplified domain, and the same K simulations of the closed domains Π_k to find all the necessary components. This method therefore reduces the number of full antenna simulations from KN to N with the additional K simulations in the simpler domain. Note that the simpler domain can be made very small, reducing the simulation cost drastically when compared to the full antenna simulation.

6

Proof-of-Concept

In order to show the viability of the methodology presented in chapter 3, two separate proofs-of-concept will be presented using the suggested implementation in chapter 5 and the design selected in section 4.1. Section 4.2 verifies the necessary assumptions for the design. The library of interior components built for the proof-of-concept contains 48 pairs of iris heights and widths between 8 mm and 15 mm, and 5 mm and 10 mm, respectively. The 48 pairs are then used to create splines in order to accurately interpolate any value within the range. The implementation is performed in MATLAB.

The first proof-of-concept shows the methodology's ability to predict the waves within, and excitations of a slotted waveguide antenna. To show this, a 1x6 slotted waveguide antenna with randomly selected irises is evaluated using the theory presented herein and compared to a corresponding simulation in ANSYS HFSS. Table 6.1 shows the heights and widths of the randomized antenna. Figure 6.1 shows the ANSYS HFSS model of the 1x6 antenna. The implementation follows a workflow similar to that in section 2.8.2 using a convergent algorithm for finding the slot excitations.

Figure 6.2 shows the slot excitation amplitudes and phases as predicted by the theory in this thesis as well as their corresponding results from ANSYS HFSS. Figure 6.3 shows the error between the full wave simulation in ANSYS HFSS and the theory implemented in MATLAB as

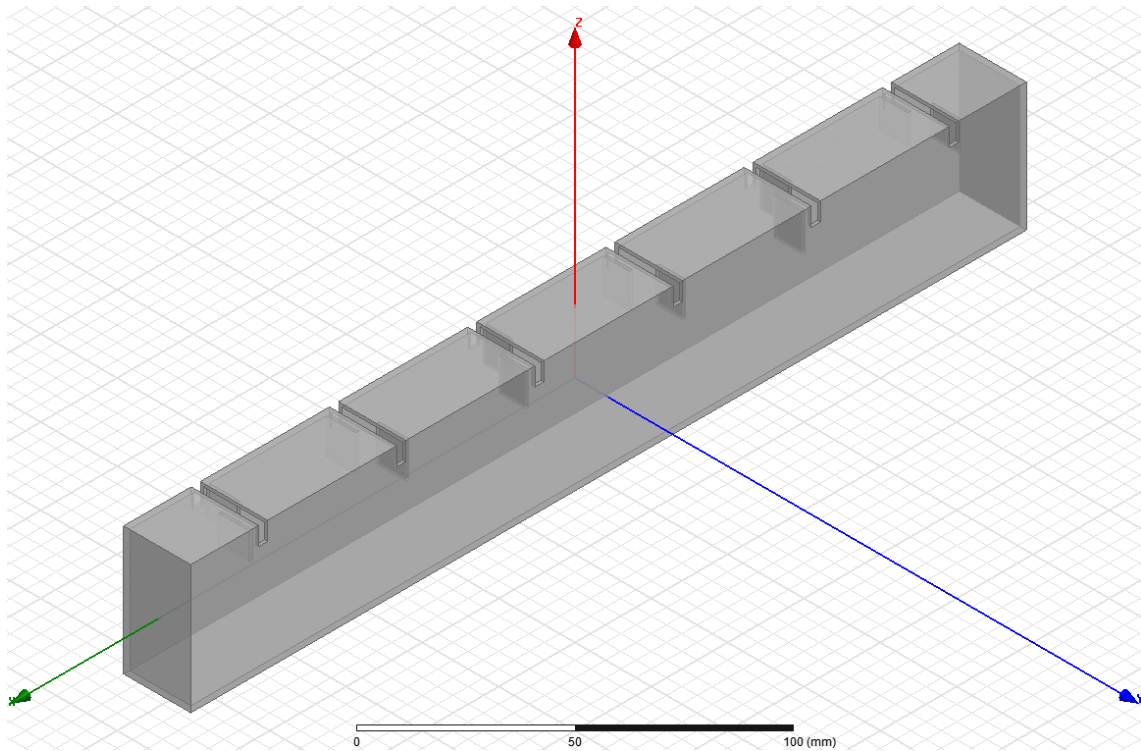
$$\text{Error} = \frac{|V_i^{MATLAB} - V_i^{HFSS}|}{\max_i |V_i^{HFSS}|} \quad (6.1)$$

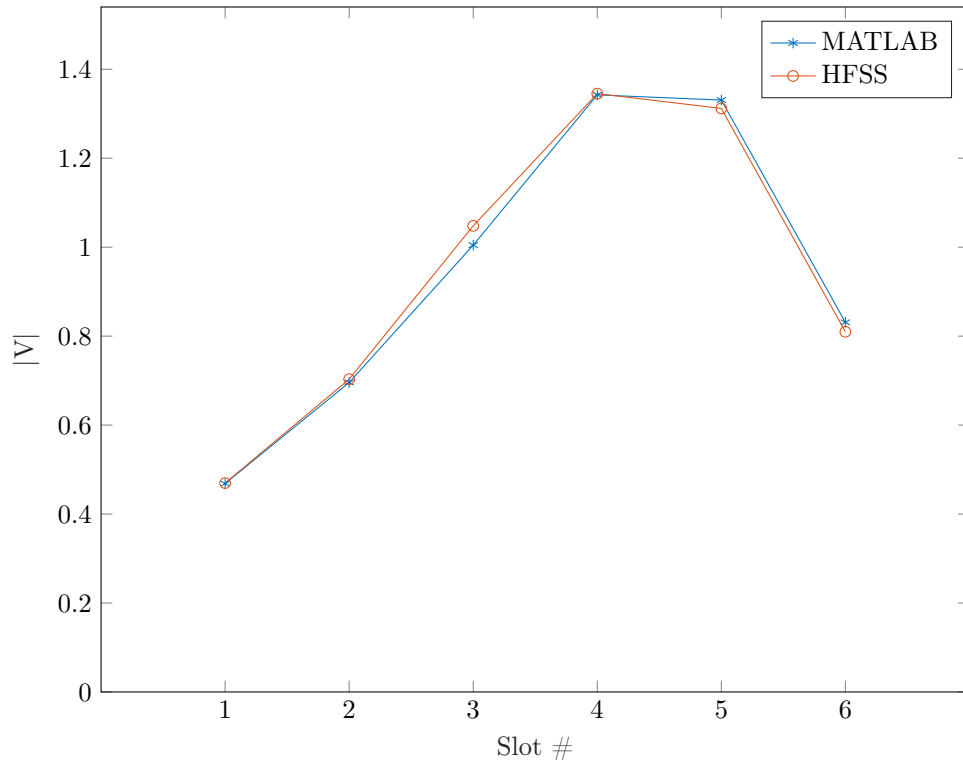
for each slot number i . Note that the maximum error is less than 9%. Further, from equation (2.45b), the reflection coefficient into the antenna is $\Gamma_{in} = 0.57/4.18^\circ$ and $\Gamma_{in} = 0.59/6.66^\circ$ as predicted by MATLAB and HFSS, respectively. The execution time for the HFSS simulation to reach an accuracy of $|\Delta|S| \leq 0.0005$ took approximately 3 hours and 36 minutes whereas MATLAB implementation was executed in approximately 0.1 seconds on the same machine.

The second proof-of-concept shows how the quick evaluation of the method can be utilized to efficiently optimize antenna design for a certain voltage mask. To show this, the design of a 1x6 slotted waveguide antenna is optimized for a Taylor distribution mask^[21], presented in table 6.2. The optimization was performed by

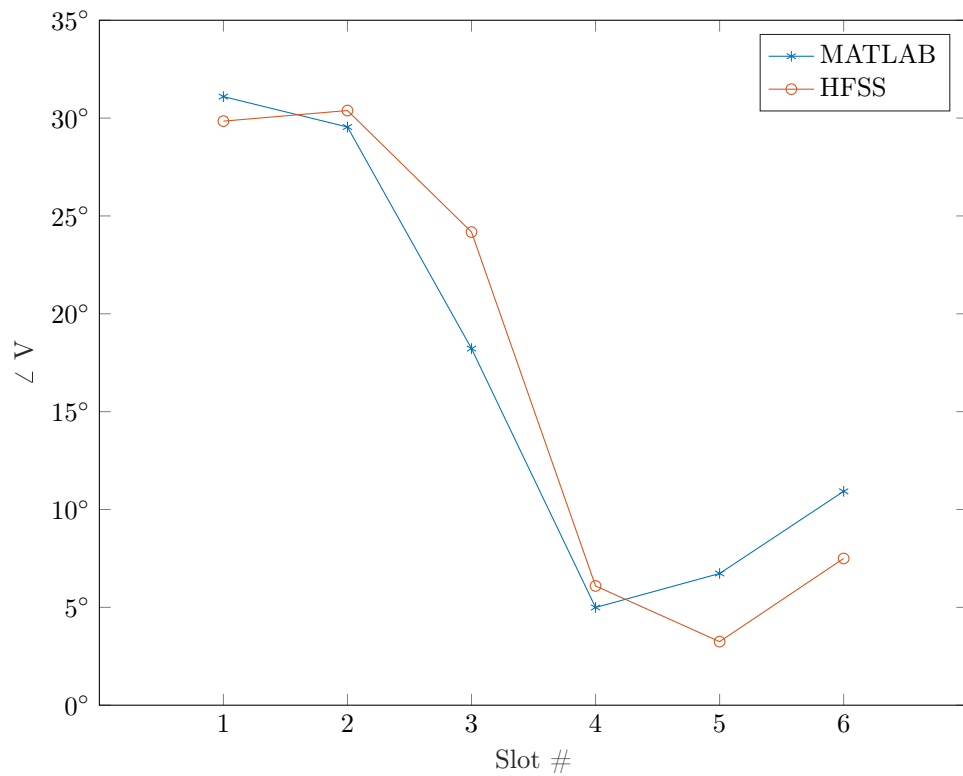
Table 6.1: The randomized iris dimensions for the first proof-of-concept.

Slot #	h_{iris} [mm]	w_{iris} [mm]
1	11.4	6.6
2	10.6	5.6
3	9.3	5.1
4	8.7	8.5
5	13.3	8.8
6	8.5	7.9

**Figure 6.1:** The ANSYS HFSS design of the 1x6 slotted waveguide antenna used in the proofs-of-concept.



(a) Excitation amplitude, normalized.



(b) Excitation phase.

Figure 6.2: The slot excitation amplitudes and phases as predicted by this thesis and their corresponding results from ANSYS HFSS.

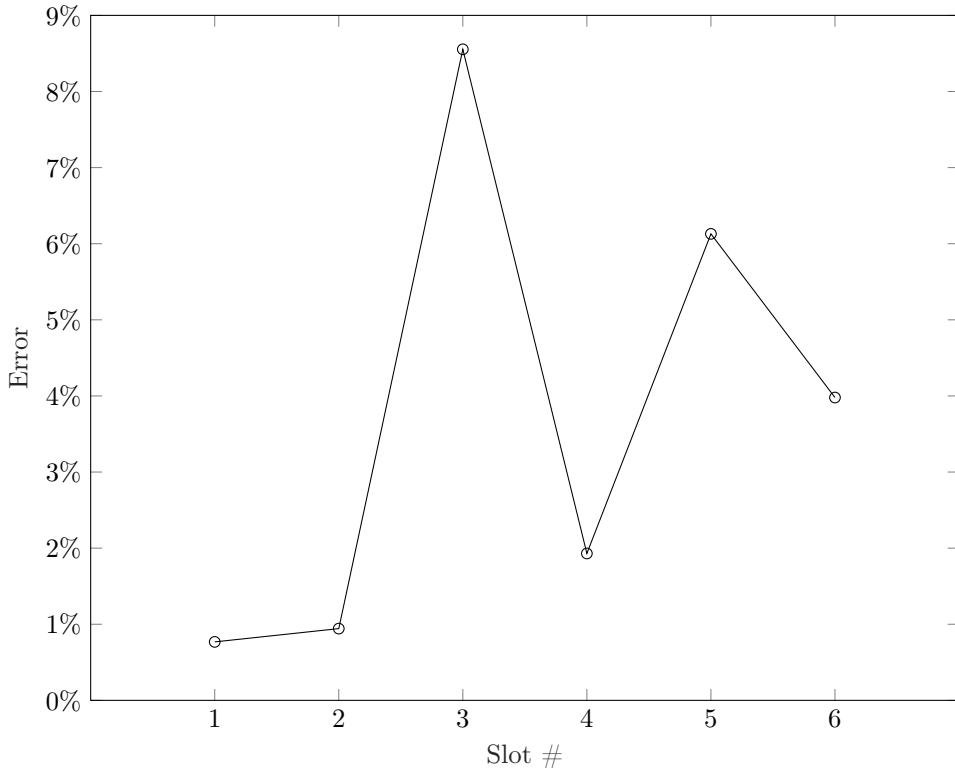


Figure 6.3: The error in slot excitation when comparing those predicted by this thesis and their corresponding results from ANSYS HFSS.

implementing the method from the first proof-of-concept in a particle swarm optimization (PSO) algorithm^[22]. The execution time for the PSO using 20 particles and 500 iterations, with a total of 10^4 antenna evaluations, was approximately 2.5 minutes. Table 6.3 shows the heights and widths of the resulting antenna design. Figure 6.4 shows the Taylor excitations, the predicted excitations and the simulated excitations of the resulting antenna design. Figure 6.5 shows the error of the theory prediction implemented in MATLAB and the corresponding full wave simulation in ANSYS HFSS as compared to the voltage mask as

$$\text{Error} = \frac{|V_i^{HFSS|MATLAB} - V_i^{TAYLOR}|}{\max_i |V_i^{TAYLOR}|} \quad (6.2)$$

for each slot number i . Note that the maximum error is less than 4%.

These two proofs-of-concept show both the validity of the methodology presented in this master's thesis and its possible use in design optimizations. Its main advantage over full wave solvers is the immense reduction in execution time and required resources without large loss of accuracy.

Further, the savings in time and resources increase with the size of the antenna. Figure 6.6 shows that the code execution time for array antennas with less than 10^4 elements scales linearly¹. An implementation with more waveguides would not

¹However, as the number of coupling slots increase as N^2 the code is expected to scale quadrat-

Table 6.2: The relative voltage distribution for a Taylor excitation mask.

Slot #	V^{TAYLOR}
1	0.1025
2	0.1777
3	0.2198
4	0.2198
5	0.1777
6	0.1025

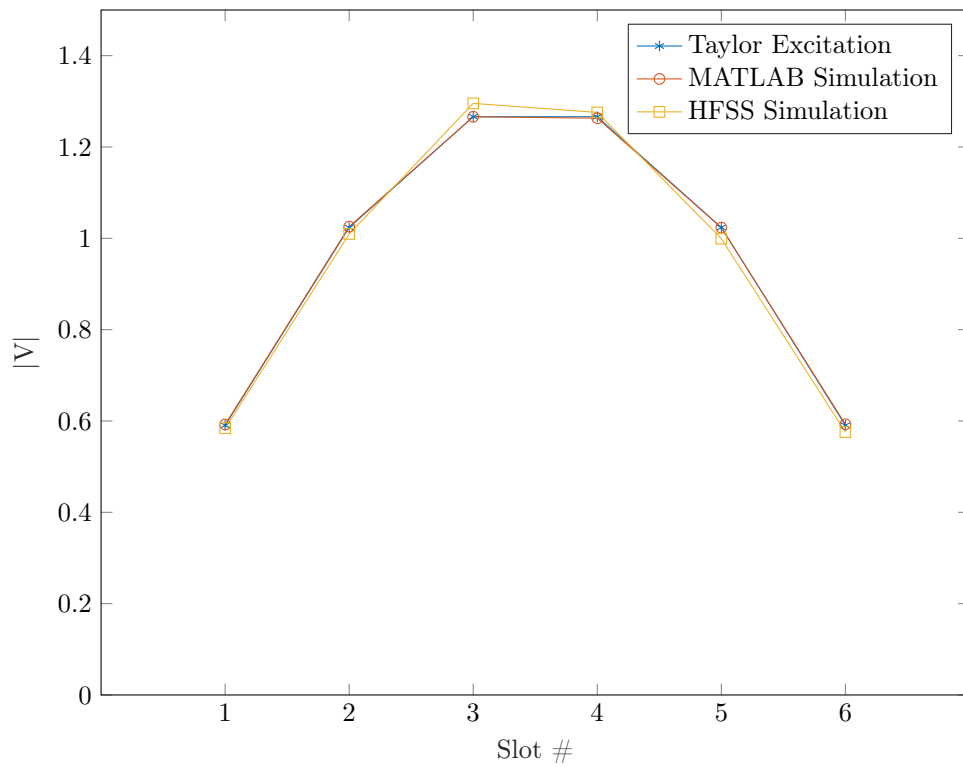
Table 6.3: The resulting iris dimensions for the second proof-of-concept.

Slot #	h_{iris} [mm]	w_{iris} [mm]
1	9.2521	9.3198
2	12.1612	9.3337
3	11.0295	8.6770
4	10.7682	8.6853
5	11.5901	9.5986
6	8.6272	9.9775

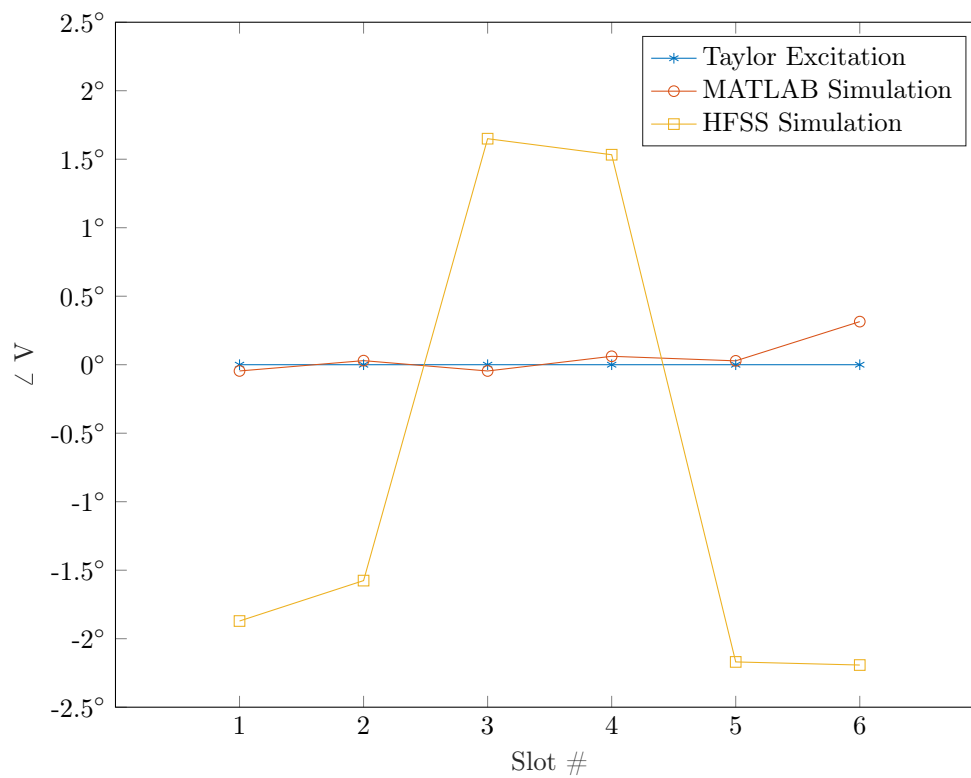
increase scaling of the code as each additional waveguide would be calculated separately, increasing execution time linearly. In comparison, FEM methods without adaptive meshing scale as $\frac{1}{f^4}$, where the frequency f is inversely proportional to the dimensions of the simulated domain²[18].

ically for very large number of elements N .

²Note however that most commercial FEM solvers use adaptive meshing techniques and that the problem does not scale equally in all three dimensions when increasing the number of elements.



(a) Excitation amplitude, normalized.



(b) Excitation phase.

Figure 6.4: The slot excitation amplitudes and phases for the Taylor mask, predicted in MATLAB and simulated in HFSS, respectively.

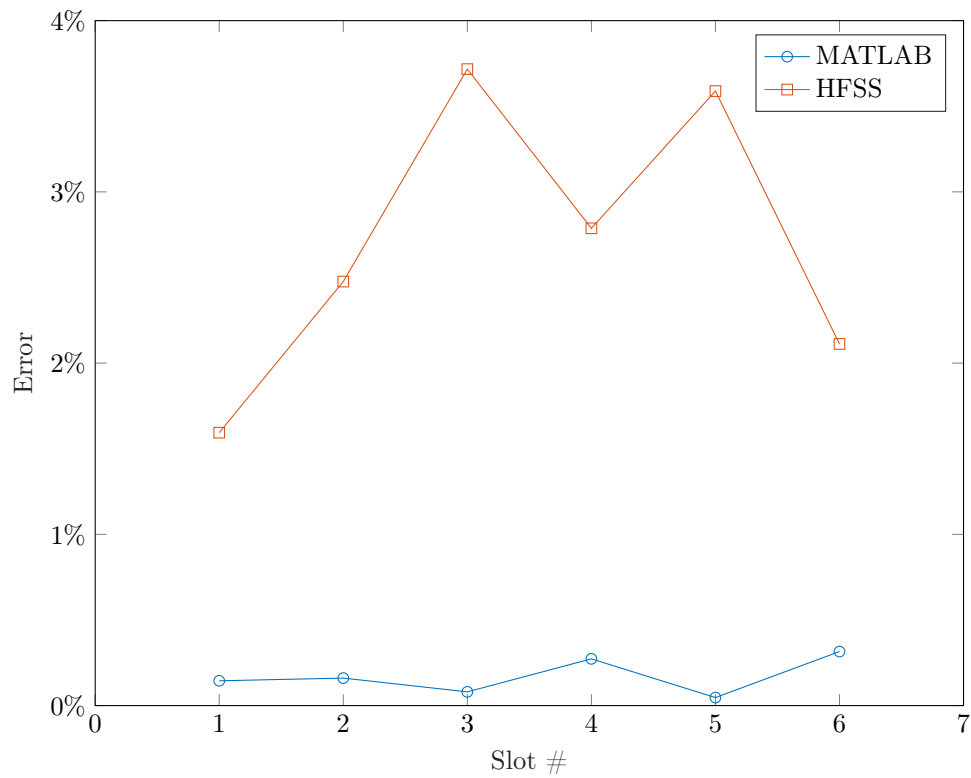


Figure 6.5: The error in slot excitation when comparing those predicted by this thesis in MATLAB and their corresponding results from ANSYS HFSS with the actual Taylor voltage mask.

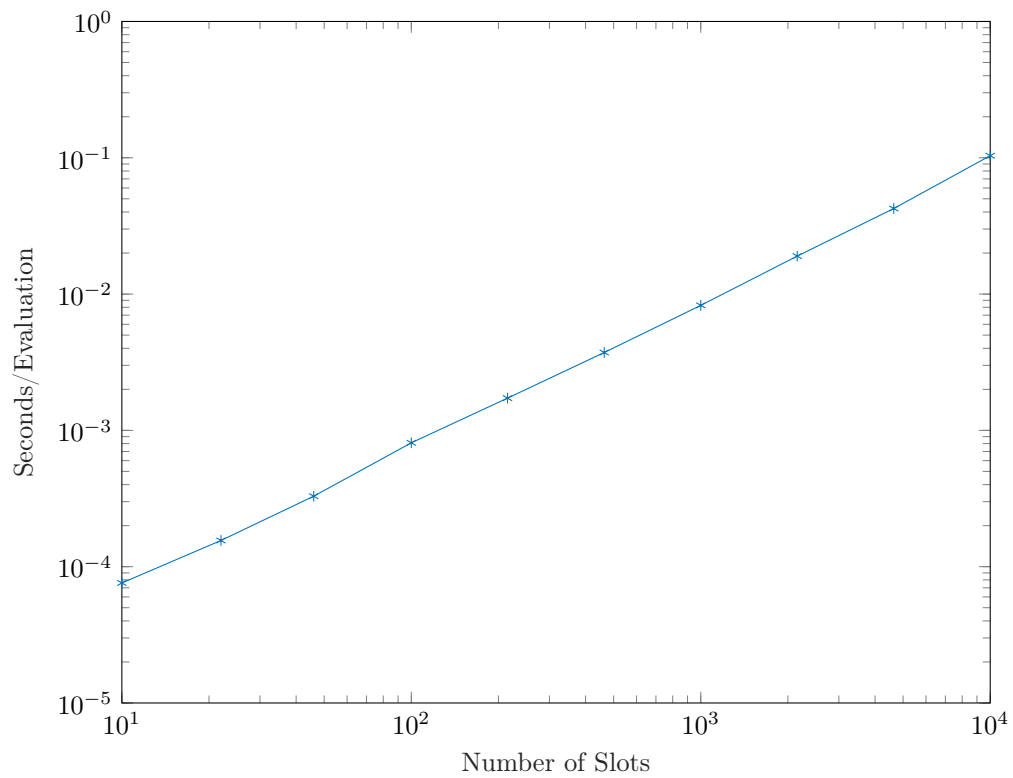


Figure 6.6: Analysis of how the code used in the proof-of-concept scales with the number of slots. Each data point is averaged over 2×10^4 evaluations of random antennas. The angle of the curve, and therefore the scaling of the code, is approximately 1.05.

7

Conclusion

This master's thesis has derived and presented a new methodology for calculating the waves within, and the excitations of, a slotted waveguide array antenna using simple RF circuit methods. The methodology requires an initial set of costly full wave simulations to build a library of unit cells after which it is possible to efficiently and accurately evaluate any array design without the need for further full wave simulations. The possibility of quickly and accurately evaluating many designs makes the methodology especially attractive for implementation in antenna optimization.

The two proofs-of-concept in chapter 6 show both the methodology's validity and power when used in optimization schemes, reducing evaluation times by six orders of magnitude for a simple 1x6 array. Further, it is shown that the implementation scales linearly with the number of elements and thus the time gained will be larger for larger antennas. One of the most probable sources of inaccuracy is the calculation of the components in equations (3.45) and (3.46) as HFSS does not enable finding these properties easily. If the components may be calculated more accurately using other full electromagnetic domain solvers, the accuracy of the methodology may be further increased. Furthermore, if the single mode assumptions made can be adapted to include more modes, the accuracy would increase further.

It is important to note that although the methodology and implementations presented in this thesis have focused on narrow wall slotted rectangular arrays, it is not limited to only this design. The only assumptions made regarding the slotted waveguide array's design are those relating to the single mode expansions in the slots and between each unit cell as well as the assumption that the outer geometry remains constant. Therefore there are no further restrictions of the interior or exterior design. However to most efficiently use the methodology, all unit cells should share the same slot and port dimensions and positions.

Future work for this master's thesis should include analyzing the theory presented herein in order to find which equation components have the largest effect on the method accuracy. Such work could be used to find possible approximations, i.e. using the same outer admittance for similar array elements or ignoring coupling effects from faraway elements, reducing the costs of the initial simulations. Furthermore, implementing this thesis's methodology in an optimization toolbox, including procedural simulation of additional unit cells as needed, optimization implementation, and evaluation of final result in a full wave simulator, would increase its usability. Finally, an expansion of the theory to include more modes in both the slots and

7. Conclusion

within the waveguide would allow the accuracy of the method to be increased for designs where the single mode assumption is not valid.

Bibliography

- [1] Constantine A. Balanis. *Advanced engineering electromagnetics*. Wiley, New York, 1989. ISBN 0471-5031.
- [2] Samuel Silver and IET Digital Library (e-book collection). *Microwave Antenna Theory and Design*, volume 19. P. Peregrinus on behalf of the Institution of Electrical Engineers, London, UK, 1984;1983;. ISBN 0863410170;9780863410178;.
- [3] Robert S. Elliott and IEEE Xplore (e-book collection). *Antenna theory and design*. John Wiley & Sons, Hoboken, N.J, revis edition, 2003. ISBN 9780471449966;0471449962;.
- [4] Per-Simon Kildal. *Foundations of Antennas: a Unified Approach*. Studentlitteratur, Lund, 2000. ISBN 9144013221;9789144013220;.
- [5] Rob Maaskant. *Analysis of large antenna systems*. Technical University of Eindhoven, 2010.
- [6] William Coburn, Marc Litz, Joseph Miletta, Neal Tesny, Lillian Dilks, and Benson King. A slotted-waveguide array for high-power microwave transmission. Technical report, Army Research Lab Adelphi MD, 2001.
- [7] Guo-Xin Fan and Jian-Ming Jin. Scattering from a large planar slotted waveguide array antenna. *Electromagnetics*, 19(1):109–130, 1999.
- [8] MW ElSallal, BJ Herting, and JB West. Planar edge slot waveguide antenna array design using cots em tools. In *Antenna Applications Symposium, Monticello, IL*, pages 76–89, 2007.
- [9] Rodrigo Kenji Enjiu, Marcelo Bender Perotoni, and Santo André UFABC. Slotted waveguide antenna design using 3d em simulation. *Microwave Journal*, 2013.
- [10] Yanyan Li, Zhongchao Lin, Yu Zhang, Sheng Zuo, and Xunwang Zhao. Analysis of large airborne waveguide slotted array using ddm. In *Antennas and Propagation (APCAP), 2015 IEEE 4th Asia-Pacific Conference on*, pages 597–598. IEEE, 2015.
- [11] Ozlem Ozgun and Mustafa Kuzuoglu. A non-iterative domain decomposition method for finite element analysis of 3d electromagnetic scattering problems. In *Antennas and Propagation Society International Symposium, 2008. AP-S 2008. IEEE*, pages 1–4. IEEE, 2008.

- [12] Yang H Kim and Hyo J Eom. Mode-matching model for a longitudinally slotted waveguide array. *IEEE Antennas and Wireless Propagation Letters*, 6:328–331, 2007.
- [13] David M. Pozar and Ebook Central (e-book collection). *Microwave Engineering*. Wiley, Chichester, 4th edition, 2012. ISBN 9780470631553;9781118213636;1118213637;0470631554;.
- [14] Roger F Harrington. *Fields, Time-Harmonic Electromagnetic*. McGraw-Hill, New York, 1961. ISBN 07-026745-6.
- [15] Sergei A Schelkunoff. *Electromagnetic waves*. van Nostrand, 1951.
- [16] George B. Arfken and Hans J. Weber. *Differential Equations*. Academic Press, Boston, fourth edition, 1995. ISBN 978-0-12-059815-1. doi: <http://dx.doi.org/10.1016/B978-0-12-059815-1.50013-X>. URL <http://www.sciencedirect.com/science/article/pii/B978012059815150013X>.
- [17] Christopher Stover. Green’s function. <http://mathworld.wolfram.com/GreensFunction.html>, Accessed: 2017-03-24. From MathWorld—A Wolfram Web Resource, created by Eric W. Weisstein.
- [18] Thomas Rylander, Pär Ingelström, and SpringerLink (e-book collection). *Computational electromagnetics*, volume 51. Springer, New York, N.Y, second;2nd 2013; edition, 2013. ISBN 146145350X;9781461453505;.
- [19] Chen-to Tai. *Dyadic green functions in electromagnetic theory*. Institute of Electrical & Electronics Engineers (IEEE), United States, 1994. ISBN 0780304497;9780780304499;.
- [20] Carl Toft. Moment method analysis of slot coupled waveguides, 2014.
- [21] Constantine A. Balanis. *Antenna theory: analysis and design*. John Wiley, Hoboken, NJ, 3rd;fourth;4;4th; edition, 2005;2016;2015;. ISBN 9780471714613;0471714615;9781118642061;1118642066;.
- [22] Mattias Wahde. *Biologically inspired optimization methods: an introduction*. WIT Press, Southampton, 2008. ISBN 1845641485;9781845641481;.

A

Scattering Parameters

Scattering parameters (S-parameters) are a very powerful tool to find the "black box" model of a device by relating the waves into and out of its ports. Moreover, S-parameters are fairly straight-forward to measure of a device, making it very easy to relate theory with practice. This section first presents the typical S-parameters and their cascade counter-part, the T-parameters, followed by their generalized counter-parts used in this master's thesis.

A.1 S-Parameters

The ordinary S-parameters relate the waves entering the device to the waves leaving. The S-parameters are presented in an S-matrix where the elements are defined as

$$S_{ij} = \left. \frac{E_i^-}{E_j^+} \right|_{E_k^+ = 0 \text{ for } k \neq j} \in \mathfrak{C}. \quad (\text{A.1})$$

Here $E_i^{+(-)}$ is the amplitude of the electric wave traveling into (out of) port i . Figure A.1a shows the signal flow graph for two-port S-parameters. The amplitudes of the waves leaving the device's ports are calculated as

$$\mathbb{E}^- = [\text{S}]\mathbb{E}^+ \quad (\text{A.2})$$

where \mathbb{E}^\pm are vectors containing all the wave amplitudes into and out of each port. Note that due to equation (2.10), magnetic waves relate to the scattering parameters as

$$\mathbb{H}^- = \begin{bmatrix} -1 & 0 \\ 0 & 1 \end{bmatrix} [\text{S}] \begin{bmatrix} 1 & 0 \\ 0 & -1 \end{bmatrix} \mathbb{H}^+ \quad (\text{A.3})$$

that is, the magnetic field gains a negative sign when reflected whereas the electric field does not.

If the network related to the S-parameters is reciprocal, the S-matrix will be symmetric^[13], i.e.

$$[\text{S}] = [\text{S}]^\top \quad (\text{A.4})$$

and if the network is lossless, the S-matrix is unitary^[13], i.e.

$$[\text{S}][\text{S}]^\dagger = \mathbb{I} \quad (\text{A.5})$$

where \dagger denotes the conjugate transpose.

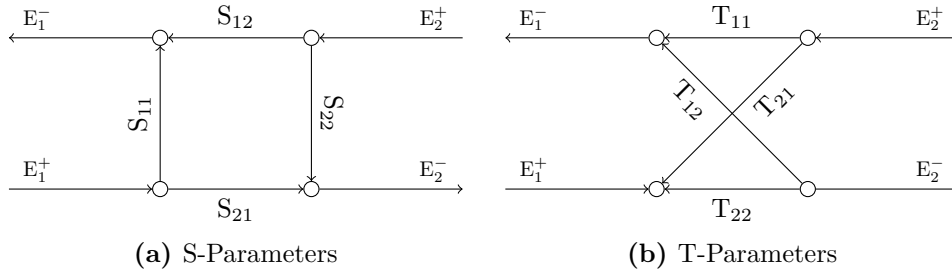


Figure A.1: Signal flow graphs of the two types of scattering parameters.

A.2 T-Parameters

The transmission parameters (T-parameters) are similar to the S-parameters and are typically only defined for two-ports. Whereas the S-parameters relate the incident waves to the waves leaving the ports, the T-parameters relate the waves at one port to those at the other port. The T-parameters is less descriptive regarding the power flow of a component, but has the advantage of simply calculating the result of a network of cascaded components. The T-parameters are also represented by a matrix, the two-port T-matrix defined as

$$\begin{bmatrix} E_1^- \\ E_1^+ \end{bmatrix} = [\mathbf{T}] \begin{bmatrix} E_2^+ \\ E_2^- \end{bmatrix} \quad (\text{A.6a})$$

$$\begin{bmatrix} H_1^- \\ H_1^+ \end{bmatrix} = \begin{bmatrix} -1 & 0 \\ 0 & 1 \end{bmatrix} [\mathbf{T}] \begin{bmatrix} -1 & 0 \\ 0 & 1 \end{bmatrix} \begin{bmatrix} H_2^+ \\ H_2^- \end{bmatrix} \quad (\text{A.6b})$$

Figure A.1b shows the signal flow graph for two-port T-parameters. Note that if two two-ports were cascaded, E_2^\pm of the first network would equal E_1^\mp of the second. The equivalent T-matrix for two cascaded components with T-matrices T_a and T_b respectively is therefore given as

$$T_{equiv} = T_a T_b \quad (\text{A.7})$$

which obviously holds for longer cascade chains as well.

In order to find the T-parameters from two-port S-parameters, simply re-arrange equation (A.2), collect the terms and identify the T-parameters. The S-parameters can be found from the T-parameters analogously. The resulting conversion is then

$$S_{11} = \frac{T_{12}}{T_{22}} \quad T_{11} = -\frac{\det([\mathbf{S}])}{S_{21}} \quad (\text{A.8a})$$

$$S_{12} = \frac{\det([\mathbf{T}])}{T_{22}} \quad T_{12} = \frac{S_{11}}{S_{21}} \quad (\text{A.8b})$$

$$S_{21} = \frac{1}{T_{22}} \quad T_{21} = -\frac{S_{22}}{S_{21}} \quad (\text{A.8c})$$

$$S_{22} = -\frac{T_{21}}{T_{22}} \quad T_{22} = \frac{1}{S_{21}} \quad (\text{A.8d})$$

Then through identification, it follows that the T-matrix of a reciprocal 2-port has $\det([T]) = 1$ and that for a lossless 2-port the following holds

$$T_{12} = \det([T])T_{21}^* \quad (\text{A.9a})$$

$$|T_{11}| = |T_{22}| \quad (\text{A.9b})$$

$$|T_{12}| = |T_{21}| \quad (\text{A.9c})$$

$$|T_{11}|^2 = |T_{12}|^2 + 1 \quad (\text{A.9d})$$

$$|\det([T])| = 1 \quad (\text{A.9e})$$

Note how for reciprocal lossless two-ports $T_{12} = T_{21}^*$ which corresponds well with the idea that the diagonal components correspond to the transmission through the two-port.

A.3 Generalized S- and T-Parameters

This thesis uses a relation between waves at the ports of a network similar to the S-parameters, however also taking into account sources within the network independent of the ports. These parameters are on the form

$$\begin{bmatrix} E_1^- \\ E_2^- \end{bmatrix} = [S] \begin{bmatrix} E_1^+ \\ E_2^+ \end{bmatrix} + \mathbb{A} = \begin{bmatrix} S_{11} & S_{12} \\ S_{21} & S_{22} \end{bmatrix} \begin{bmatrix} E_1^+ \\ E_2^+ \end{bmatrix} + \begin{bmatrix} A_1 \\ A_2 \end{bmatrix} \quad (\text{A.10})$$

where \mathbb{A} represents the independent interior sources. These parameters may also be related to a form of generalized T-parameters on the form

$$\begin{bmatrix} E_1^- \\ E_1^+ \end{bmatrix} = [T] \begin{bmatrix} E_2^+ \\ E_2^- \end{bmatrix} + \mathbb{B} = \begin{bmatrix} T_{11} & T_{12} \\ T_{21} & T_{22} \end{bmatrix} \begin{bmatrix} E_2^+ \\ E_2^- \end{bmatrix} + \begin{bmatrix} B_1 \\ B_2 \end{bmatrix} \quad (\text{A.11})$$

where, using the same method as before, $[T]$ and \mathbb{B} can be calculated from $[S]$ and \mathbb{A} as

$$[T] = \begin{bmatrix} -\frac{\det([S])}{S_{21}} & \frac{S_{11}}{S_{21}} \\ -\frac{S_{21}}{S_{22}} & \frac{S_{21}}{S_{21}} \end{bmatrix} \quad (\text{A.12a})$$

$$\mathbb{B} = \begin{bmatrix} 1 & -T_{12} \\ 0 & -T_{22} \end{bmatrix} \mathbb{A} \quad (\text{A.12b})$$